



UNIVERSITAT DE
BARCELONA

Pathophysiology of immune-related complications in Lysinuric Protein Intolerance

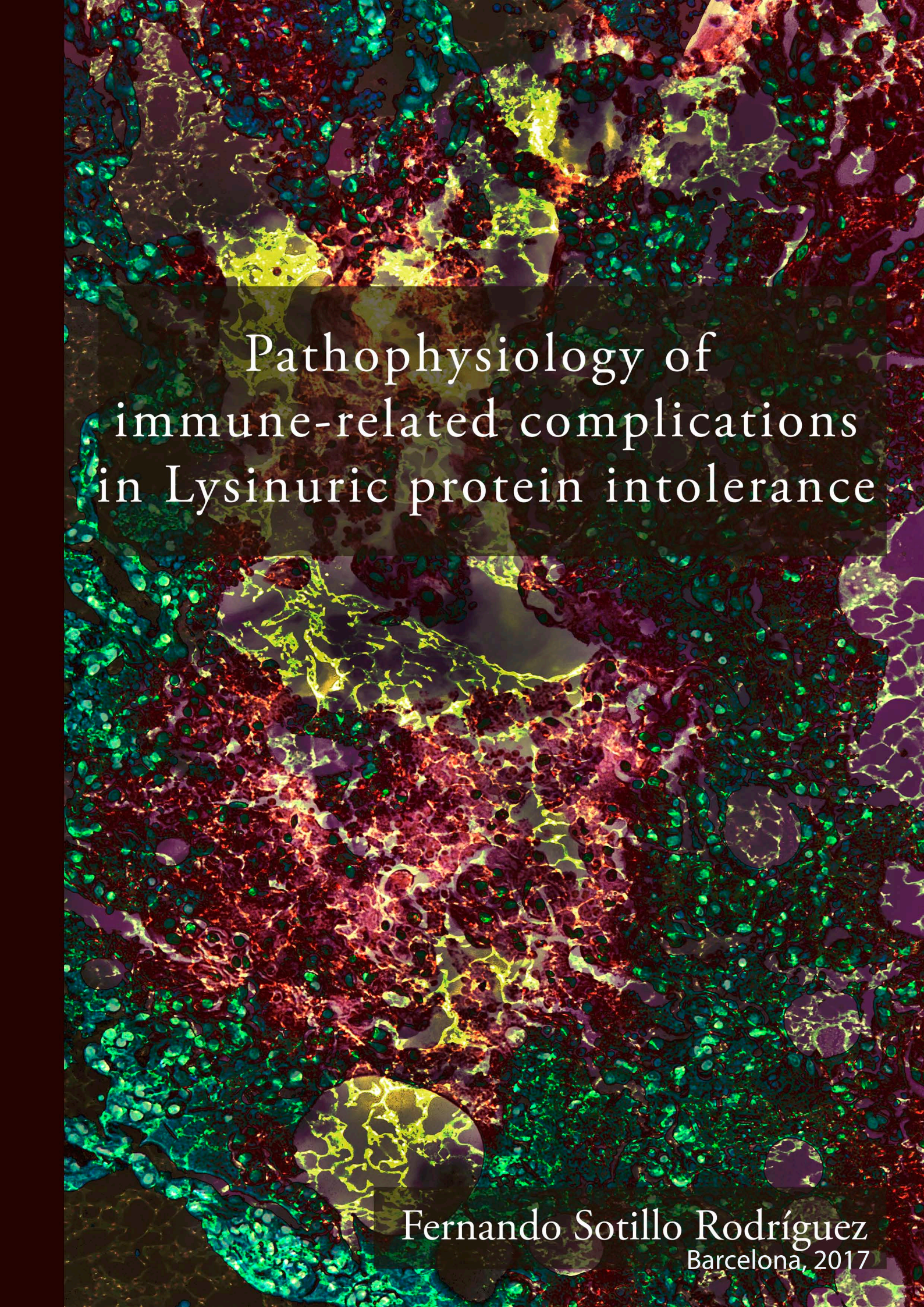
Fernando Sotillo Rodríguez



Aquesta tesi doctoral està subjecta a la llicència **Reconeixement- NoComercial – SenseObraDerivada 3.0. Espanya de Creative Commons.**

Esta tesis doctoral está sujeta a la licencia **Reconocimiento - NoComercial – SinObraDerivada 3.0. España de Creative Commons.**

This doctoral thesis is licensed under the **Creative Commons Attribution-NonCommercial-NoDerivs 3.0. Spain License.**

A complex fluorescence microscopy image of tissue, likely showing cellular structures and protein localization. The image features a dense network of green and red signals, with bright yellow-green areas indicating specific protein expression or interactions. The overall appearance is highly detailed and colorful, typical of immunofluorescence staining.

Pathophysiology of
immune-related complications
in Lysinuric protein intolerance

Fernando Sotillo Rodríguez
Barcelona, 2017



UNIVERSITAT DE
BARCELONA



INSTITUT
DE RECERCA
BIOMÈDICA

Universitat de Barcelona

Facultat de Farmàcia i Ciències de l'alimentació

Programa de Doctorat en Biomedicina

Pathophysiology of immune-related complications in Lysinuric Protein Intolerance

Memoria presentada por **Fernando Sotillo Rodríguez**

para optar al título de doctor por la Universitat de Barcelona

Directores

Doctorando

Manuel Palacín

Susanna Bodoy

Fernando Sotillo

Barcelona, Diciembre 2017

A mi familia,
por el apoyo,
por la educación.

Quiero agradecer a...

Manuel y Susanna, Susanna y Manuel, mis dos codirectores. Tan diferentes y tan necesarios. Pasión y realismo, la pizarra llena de flechas y la fulla amb el que s'ha de fer, del "si esto no se puede hacer, no habríamos descubierto América" al "si sortís tot el que fem, publicaríem un Nature cada mes". Muchas gracias por la tremenda oportunidad que me habéis dado, por todo lo que me habéis enseñado y por todo lo que me habéis transmitido. No solo me habéis hecho descubrir lo maravillosa que es la ciencia, también he aprendido que lo importante no es como empieza sino como acaba, que lo concreto te conduce hasta lo general y que toda buena historia se compone a base de pequeñas piezas. De verdad, gracias.

Sara, compañera de tesis para la eternidad. De hecho, no me puedo imaginar una compañera mejor que tú. Contigo hemos bebido, hemos leído, he aprendido, he disfrutado, pero sobre todo, hemos rajado! Ha sido brutal tenerte al lado estos años. Y si hablamos de rajar, ahí están las dos gurús, las dos maestras, Aida y Alba, criminal equipo titular.

El resto de Palacines, los defensores de la estructura. Por un lado Albert y su templanza para adaptarse a quién tenga al lado, desde Ana hasta Paloma pasando por Elena. Y por el otro la dulce Paola, Joana, dempeus sempre y Ekaitz. Y por supuesto, importantísima, la última invitada al LPI team, Judith; espero que además de a preparar aminoácidos, hayas aprendido que lo importante no es hablar mucho, si no hablar bien ;) (ya estabas suficientemente preparada como para poder hacer el máster en Madrid).

Los Zorranos por su ayuda y compañía, Saska, Maribel, Montse, David, Manu, Yuli y muy especialmente a JP. JP y Jordi (al becario también) porque sin él sería un poco menos JP, y el lab un auténtico caos. También a Olga, Natalia Molner y Natalia Plana. Y cómo no a Jordi Durán, el MVP del TAC.

Patrizia, Álvaro, Sonia, Pablo, Eric, Iris y Clara porque no habría llegado al IRB de no haber pasado por el IDIBELL. Y al IDIBELL no habría llegado de no haber pasado por El 12, así que también gracias a Julia (por el enchufe) y a Ana (por el relevo).

Al Mossack (y a algunos no Mossack) por convertir cada coñazo en pura carcajada, por tantos años, por tantos momentos. A Bea por la pedazo de portada. Al bueno de Dani Fransi, pilar fundamental desde Leuven y a Isa, pilar fundamental desde el tuto, que después de ser Villarriba, han pasado a ser familia. I per descomptat a l'Ester, que és més que família, és companya, és mestra, és suport, és consell... en definitiva, és el que calgui en cada moment.

... a todos vosotros, por todo ello, GRACIAS. Un pedacito de esta tesis es vuestro.

AM	Alveolar macrophages
APC	Allophycocyanin
Arg	Arginine
ATII	Alveolar epithelium type II cells
BALF	Bronchoalveolar lavage fluid
BFU-E	Burst-Forming Unit Erythroid
BH4	Tetrahydrobiopterin
BMDM	Bone Marrow Derived Macrophages
bp	Bairs Pairs
CFU-E	Colony-Forming Unit Erythroid Cells
DAMP	Damage-Associated Molecular Patterns
DAPI	4',6-diamidino-2-phenylindole
DC	Dendritic Cells
EPO	Erythropoietin
FACS	Fluorescence-Activated Cell Sorting
FAD	Flavine-Adenine Dinucleotide
FC	Fold Change
FDR	False Discovery Rate
FITC	Fluorescein isothiocyanate
FMN	Flavin Mononucleotide
FSC	Forward Scatter
Gln	Glutamine
GM-CSF	Granulocyte Macrophage Colony-Stimulating Factor
GSEA	Gene Set Enrichment Analysis
His	Histidine
HLH	Hemophagocytic lymphohistiocytosis
HSC	Hematopoietic stem cells
IFN	Interferon
IHC	Immunohistochemistry
IRE	Iron Responding Elements
IRP	Iron Responding Proteins
KO	Knock Out
Leu	Leucine
LPI	Lysinuric Protein Intolerance
LPS	Lipopolysaccharide
Lys	Lysine
LysM	Lysozime 2 promoter
MAEA	Macrophage-erythroblast attacher
MAS	Macrophage activation syndrome

MCH	Mean Corpuscular Hemoglobin
M-CSF	Macrophage Colony-Stimulating Factor
MCV	Mean Corpuscular Volume
Met	Methionine
NK	Natural Killer
NLR	NOD-like Receptors
NO	Nitric Oxide
NOS	Nitric Oxide Synthase
OHT	4-hydroxytamoxifen
Orn	Ornithine
PAP	Pulmonary Alveolar Proteinosis
PAPMP	Pathogen-Associated Molecular Patterns
PBS	Phosphate Buffer Saline
PCA	Principal Components Analysis
PCR	Polymerase Chain Reaction
PE	Phycocerythrin
Perls'	Perls' Prussian Blue staining
PRR	Pattern Recognition Receptor
PS	phosphatidylserine
qRT-PCR	quantitative Real Time Polymerase Chain Reaction
RBC	Red Blood Cells
ROS	Reactive Oxygen Species
RPM	Red Pulp Macrophages
rpm	revolutions per minute
RT	Room Temperature
SCF	Stem Cell Factor
SIRS	Systemic Inflammatory Response Syndrome
SLE	Systemic lupus erythematosus
SPF	Specific Pathogen Free
SSC	Side scatter
TF	transferrin
TFR	Transferrin receptor
TGF	Transforming Growth Factor
TLR	Toll-like Receptors
TNF	Tumor necrosis factor
TPO	Thrombopoietin
UBC	Ubiquitin C
UTR	Untranslated Regions
WT	Wild Type
β-ala	β-alanine

TABLE OF CONTENT

TABLE OF CONTENT	9
INTRODUCTION	13
Amino acid transport and disease	15
<i>Heteromeric Amino Acid Transporters</i>	15
<i>Transport of cationic amino acids</i>	16
Lysinuric Protein Intolerance	20
<i>Pulmonary Alveolar Proteinosis</i>	25
<i>Pulmonary Alveolar Proteinosis in Lysinuric Protein Intolerance:</i>	27
<i>Hemophagocytic lymphohistiocytosis</i>	29
<i>Hemophagocytic lymphohistiocytosis in Lysinuric Protein Intolerance</i>	31
Macrophages	32
<i>Principles of immunity</i>	32
<i>Amino acid control of immunology</i>	33
<i>Macrophage populations</i>	34
<i>L-Arginine metabolism in macrophages</i>	36
<i>Nitric Oxide Synthases</i>	37
<i>Nitric Oxide in Lysinuric Protein Intolerance</i>	38
<i>Arginase 1</i>	39
Iron metabolism	40
<i>Erythropoiesis</i>	41
<i>Iron transport and storage</i>	42
<i>Iron metabolism in macrophages</i>	45
OBJECTIVES	49
METHODS	54
Animals	57
<i>Metabolic cages</i>	58
<i>Slc7a7^{-/-} mouse model:</i>	60
<i>Genotyping:</i>	62
Protein protocols	64
<i>ELISA</i>	64
<i>Membrane purification and protein extraction</i>	65
<i>Western Blot</i>	66
Gene expression	67
<i>RNA extraction</i>	67
<i>RT-PCR</i>	71
<i>qRT-PCR</i>	71
<i>Microarray</i>	75
Isolation of murine macrophages	77

<i>Alveolar macrophages</i> -----	78
<i>Splenic Red Pulp macrophages</i> -----	78
<i>Bone Marrow Derived Macrophages</i> -----	80
Histology and cytology-----	82
<i>Histology</i> -----	82
<i>Cytology</i> -----	84
Non-heme iron tissue quantification-----	84
In vitro assays -----	84
<i>Nitric Oxide</i> -----	84
<i>Erythrophagocytosis Assay</i> -----	85
Erythropoiesis analysis-----	86
RESULTS-----	87
Previous results of the group-----	89
Immune-related complications in LPI -----	93
<i>Slc7a7^{-/-} mouse model develops Pulmonary Alveolar Proteinosis</i> -----	93
<i>Slc7a7^{-/-} mouse model develops Hemophagocytic lymphohistiocytosis</i> -----	99
<i>Slc7a7^{-/-} mouse model suffers defective erythropoiesis</i> -----	103
<i>Macrophages accumulate abnormally iron in LPI</i> -----	104
<i>Slc7a7^{LysM^{-/-}} mouse model</i> -----	107
<i>Molecular characterization of Slc7a7^{-/-} red pulp macrophages</i> -----	113
<i>In vitro experiments: effect of LPI metabolic environment and erythrophagocytosis</i> -----	123
DISCUSSION-----	129
CONCLUSIONS-----	141
APPENDIX I-----	145
APPENDIX I. Heatmap of Nrf2 target genes.-----	147
BIBLIOGRAPHY -----	149

INTRODUCTION

Amino acid transport and disease

Proteins account for up to 30% of the human diet in western societies. Approximately 300g of protein are absorbed every day and only the equivalent of 10g appears as fecal nitrogen. After the digestion of proteins, peptides and amino acids are efficiently absorbed in enterocytes of the small intestine. Maximum amino acid and peptide absorption activity takes place mainly in the proximal jejunum, but other parts of small intestine also show this capacity. Inside enterocytes, peptides are hydrolyzed in amino acids, and together with those directly absorbed, they are released into the bloodstream and then delivered to all the tissues of the organism. Amino acids serve cells multiple functions, being used for protein synthesis, energy production and as precursors for different bioactive molecules. To avoid waste of these valuable molecules, kidney's epithelial cells filter unbound amino acids and reabsorb them. The proximal tubule of the kidney nephron is the major site of nutrient reabsorption with 95 to 99% of efficiency. (Broër and Stefan, 2008). As a consequence of malfunctioning of amino acid transport, different inherited diseases have been described. Hartnup disorder (OMIM 234500, first described in 1956), as the result of defective tryptophan transport due to mutations in B0AT1, cystinuria (OMIM 220100, first described in 1810), characterized by defective transport of arginine, lysine, ornithine and cysteine and due to rBAT and/or b^{0,+}AT mutations, or lysinuric protein intolerance (LPI, OMIM 222700, first described in 1965) where transport of cationic amino acids is impaired due to γ^+ LAT1 mutations, are just some examples.

Heteromeric Amino Acid Transporters

Heteromeric Amino Acid Transporters (HATs) are a family of amino acid transporters expressed in the plasma membrane (especially in epithelial cells of kidney and intestine) and mediate the transport of several amino acids across the membrane. HATs are composed by two subunits, a heavy and a light one. The light subunit acts as the catalytic part conferring amino acid transport specificity to the complex (Reig *et al.*, 2002). On the other hand, the heavy subunit acts as a chaperone and is responsible for the holotransporter to reach plasma

INTRODUCTION

membrane. Nine different light subunits (*SLC7A5* to *SLC7A13*) have been identified while only two heavy subunits (*SLC3A1* and *SLC3A2*) are known. rBAT (*SLC3A1*) associates exclusively with b⁰⁺AT (*SLC7A9*) and Agt1 (*SLC7A13*). On the other hand, the other known heavy subunit 4F2hc/CD98 (*SLC3A2*) dimerizes with the following six different light subunits: LAT1, γ⁺LAT2, γ⁺LAT1, LAT2, asc1 and xCT (*SLC7A5*, 6, 7, 8, 10 and 11 respectively). The last light subunit (asc-2, *SLC7A12*) seems to interact with yet unknown heavy subunit. The other members of SLC7 family, *SLC7A1* to *SLC7A4* are monomeric transporters that not belong to HATs family and share less than 25% amino acid identity to the light subunit of HATs. All HATs members, with the exception of asc isoforms, are obligatory exchangers with 1:1 stoichiometry (Palacín *et al.*, 2004). They differ in amino acid selectivity transport and/or in tissue specificity.

Transport of cationic amino acids

Cationic amino acids, besides of protein synthesis, are involved in some essential metabolic processes. Thus, their transport becomes fundamental to maintain a correct homeostasis. For instance, arginine is crucial for ammonia detoxification, as it is intermediary of the urea cycle. In addition, arginine is the sole substrate of Nitric Oxide Synthases (NOS) for nitric oxide (NO) production. NO has been identified as a cellular signaling molecule involved in many physiological processes such as vasodilation or immune activation (Bogdan, 2001). Another example of the relevance of cationic amino acids transport is that lysine is an essential amino acid (cannot be synthesized *de novo*). As it can be obtained exclusively from external sources, a proper transport becomes vital.

Cationic amino acids are transported through four different transport systems, summarized in Table 1. They differ in their affinity for cationic amino acids, in their dependence on sodium and in their specificity to transport neutral amino acids in exchange with the cationic ones

INTRODUCTION

SYSTEM	NA ⁺ -DEPENDENCE	SUBSTRATES
γ⁺L	negative for AA ⁺ positive for AA ⁰	Lys, Arg, Orn Leu, Met, Gln, His
b^{0,+}	negative	Lys, Arg, Orn, Cystine
γ⁺	negative	Lys, Arg, Orn, His
B^{0,+}	positive	AA ⁰ , AA ⁺ , β-Ala

Table 1. Transport systems for cationic amino acids. Amino acids are presented by the three letters code. AA⁰, basic amino acids. AA⁺ cationic amino acids.

- γ⁺L system:

the first functional characterization of the γ⁺L transport system was done in human erythrocytes (Devés, Chavez and Boyd, 1992). The affinity of this system depends on the type of neutral amino acids and cations present in the medium. Trans-stimulation experiments proved that the exit of radioactive lysine was stimulated by sodium in presence of extracellular neutral amino acids (except tryptophan) (Deves and Angelo, 1996) (Table 1, Figure 1). Substrates exit is dependent on the presence of extracellular substrates (Chillarón *et al.*, 1996), thus γ⁺L system behaves as an obligatory exchanger.

All members of this system belongs to HATs family. It is composed by two light subunits γ⁺LAT1 and γ⁺LAT2, both associated to 4F2hc. The highest expression of γ⁺LAT1 is found in the basolateral membrane of epithelial cells in kidney and intestine, but it is also present in peripheral blood leukocytes, lung, placenta and spleen (Torrents *et al.*, 1998). Its relevance may be higher in kidney, because it is where citrulline is converted to arginine and released into the blood to supply the rest of the organism. Nevertheless by simple arginine supplementation in diet, increased the expression of *Slc7a7* in the jejunum of pigs compared to a control group with no arginine supplementation, depicting its crucial role in the absorption of arginine (Yin *et al.*, 2014). Regarding disease involvement, mutations in γ⁺LAT1 lead to a rare disease called Lysinuric protein intolerance (Torrents *et al.*, 1999). Moreover polymorphisms in *SLC7A7* have been associated with risk of glioma, suggesting a role in the etiology of this type of cancer (Fan *et al.*, 2013). The γ⁺LAT2 system, in contrast, is widely expressed in epithelial and non-epithelial cells, mainly in the brain, testes and parotid gland, although weaker signals are also found in the small intestine, kidney and heart. Mouse *Slc7a6*

INTRODUCTION

cdNA showed 92% sequence identity with the human one (Bröer *et al.*, 2000). Its physiological role is still not completely understood.

- $b^{0,+}$ system:

Members of $b^{0,+}$ system also belong to the HATs family. This system is formed by only one light subunit, $b^{0,+}$ AT which associates with rBAT heavy chain. It mediates high affinity transport of cystine and cationic amino acids, and low efficient exchange of neutral amino acids (Chillarón *et al.*, 1996) (Table 1, Figure 1). It is expressed at the brush border of small intestine enterocytes and of proximal tubule kidney epithelial cells. It is the main apical reabsorption system of cystine in kidney and mutations in either subunit are responsible of cystinuria. Hyperexcretion of cysteine and cationic amino acids is a typical finding in cystinuria patients. In addition, high concentration of cysteine in urinary tract often causes recurrent formation of renal stones (Strologo *et al.*, 2002). Current cystinuria classification defines as cystinuria type A when the causative mutation occur in rBAT, type B when the mutation are found in $b^{0,+}$ AT, and AB when one mutation is found in each gene. Combinations of genetic mouse models revealed that cystinuria shows a digenic inheritance, and that half dose of both subunits of the transport system $b^{0,+}$ allows the appearance of the urolithiasis phenotype (Espino *et al.*, 2015).

- γ^+

The transporters members of this family are known as Cationic amino acid transporters (CATs). They are monomeric transporters and do not belong to HATs family. They are integral glycoproteins of membrane, formed by 14 transmembrane segment. The members of this family are CAT1, CAT2A, CAT2B and CAT3. CAT2A and 2B are splicing isoforms that differ in 42 amino acids. There is a fourth member, CAT4 which shares low identity with the other members of the family and which amino acid transport activity has not been demonstrated (Sperandeo *et al.*, 1998).

CAT1 shows a wide tissue expression. Its expression is highly regulated at transcriptional, post-transcriptional and post-translational level, being modulated by many signals such as hormones, cytokines or growth factors. For the majority of cells, CAT1 seems to be the main arginine importer, and it is strongly expressed in highly proliferative cells and tumor cells. CAT1 ablation is perinatally lethal in mouse, leading to severe anemia with defective hematopoiesis and causing death on the day of birth (Perkins *et al.*, 1997).

CAT2A and CAT2B show different substrate affinity and different abundance in tissue expression. CAT2A shows lower substrate affinity and it is mainly expressed in liver. On the

INTRODUCTION

other hand, CAT2B shows higher affinity for the substrate and it has been localized in lung, testis and stimulated leukocytes (MacLeod, 2009). CAT2 knock out (KO) mouse models are viable and do not present apparent phenotypical abnormalities. However, CAT2 deficient animals showed higher susceptibility than wild type when infected with *Schistosoma mansoni* and *Toxoplasma gondii* suggesting a critical role for CAT2 in regulating host immune responses (Thompson *et al.*, 2008).

CAT3 is widely expressed in the mouse embryo, but seems to be confined to brain in the adult. In humans it has been also found in other tissues such as thymus and mammary gland (Closs *et al.*, 2006)

- $B^{0,+}$ system:

This system comprises only one transporter named $B^{0,+}AT$. It is the only cationic sodium-dependent transporter described (Table 1, Figure 1). It is a glycoprotein of 12 transmembrane segments encoded by SLC6A14. In human, its expression is abundant in the salivary gland, airway epithelial cells and sinus mucosa. It transports all neutral amino acids but its affinity differs for each one (Broër and Stefan, 2008).

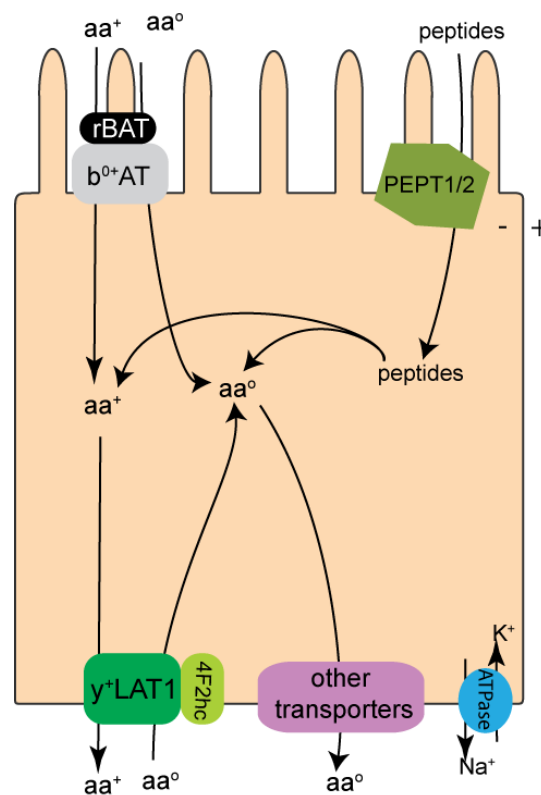


Figure 1. Schematic representation for transport of cationic amino acids in kidney/intestine epithelial cell. Cationic amino acids can enter the cell in exchange with neutral amino acids via rBAT- $b^{0,+}AT$. Small peptides can enter the cell via PEPT1 and 2 and then be degraded into single amino acids. Cationic amino acids can exit the cell in exchange with neutral amino acids via y^+LAT1 -4F2hc.

Lysinuric Protein Intolerance

Lysinuric Protein Intolerance (LPI, OMIM 222700) is a rare autosomal disease caused by mutations in *SLC7A7* gene, which encodes for γ^+ LAT1 (Torrents *et al.*, 1999). LPI was first described in 1965 in three Finnish children as a metabolic inborn error characterized by protein intolerance and deficient transport of cationic amino acids (Perheentupa and Visakorpi, 1965). It presented high concentrations of lysine and arginine in urine and low urea in blood (Perheentupa and Visakorpi, 1965). The highest prevalence of LPI is found in Finland (1/60000) but also clusters of patients have been reported in Japan and Italy, and sporadic cases worldwide (Barilli *et al.*, 2010; Ko *et al.*, 2012; Mauhin *et al.*, 2017). Human *SLC7A7* consists of 10 exons and 11 introns and it was mapped on chromosome 14q11.2 (Mykkänen *et al.*, 2000). More than 50 different mutations in *SLC7A7* have been described worldwide in LPI patients, comprising missense, nonsense, deletions, insertions, polymorphisms and splicing mutations (Palacín, Borsani and Sebastio, 2001). All the Finnish LPI patients described share the same founder mutation in *SLC7A7*: a splice site mutation 1181-2A→T which leads to a 10bp frame shift deletion in the cDNA (Mykkänen *et al.*, 2000). In Japan it has also been described a founder mutation effect. All LPI patients studied from the geographic region of northern Japan, shared the same mutation (Noguchi *et al.*, 2016). Studies in Finnish patients confirmed the autosomal inheritance of the disease and the lack of symptoms in heterozygote individuals (Norio *et al.*, 2008).

The co-expression of γ^+ LAT1 with 4F2hc in *Xenopus laevis* oocytes leads to the formation of a heteromeric amino acid transporter that mediates the exchange of cationic amino acids with neutral amino acids plus sodium (Torrents *et al.*, 1998). Although the highest expression of γ^+ LAT1 is found at the basolateral membrane of epithelial cells in the renal tubules and small intestine (Palacín, Borsani and Sebastio, 2001), *SLC7A7* mRNA is also found in peripheral blood leukocytes, lung, placenta and spleen (Torrents *et al.*, 1998). Focusing on leukocytes, the highest expression of *Slc7a7* in mice is mainly found in macrophages (Figure 2) (immgen.org, biogps.org). Among the different populations of macrophages analyzed in mouse, those with the highest *Slc7a7* expression are red pulp macrophages > microglia > small intestine lamina propria macrophages (Figure 2). Among B cells, also populations from spleen and peritoneal cavity show a considerable expression of *Slc7a7* (Figure 2).

INTRODUCTION

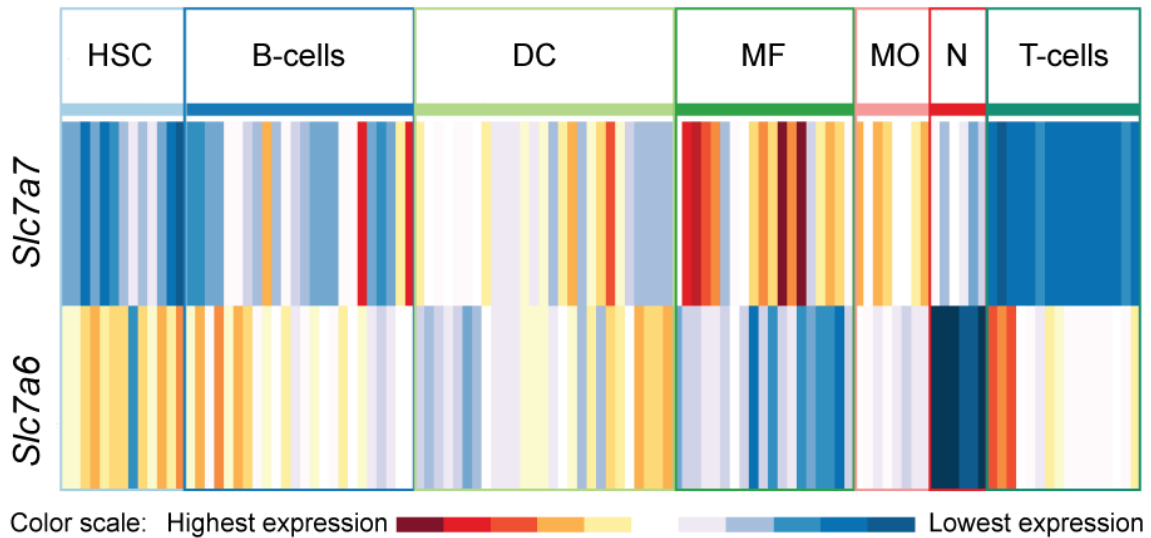


Figure 2. Comparison of γ^L transporters expression in key leukocytes populations. HSC: hematopoietic stem cells; DC: dendritic cells; MF: macrophages; MO: monocytes; N: neutrophils. Image modified from My GeneSet of the Immunological Genome Project (immgen.org).

As a result of mutations in γ^L LAT1, LPI patients show hyperexcretion of lysine, arginine and ornithine, especially lysine, in urine, and poor intestinal absorption of cationic amino acids. The deficient intestinal absorption in LPI patients together with the deficit in renal reabsorption, lowers their plasma concentration of cationic amino acids and their body pools become depleted. Sometimes the concentration of any or some of these amino acids in plasma can be found within the normal age-sex adjusted ranges of the patient (Mauhin *et al.*, 2017). Moreover a large-scale amino acid profile done with 26 Finnish LPI patients showed that in addition to cationic amino acids, tryptophan, tyrosine, leucine, methionine, valine and phenylalanine were also significantly decreased compared to controls. In contrast, the levels in plasma of homocitrulline, citrulline, beta-aminoisobutyric acid, glutamic acid, glycine, aspartic acid, proline and serine were significantly increased in the patients. The authors suggested that the amino acid imbalance found may be affecting the TCA cycle and thus energy production in LPI patients. This study also revealed an altered lipid profile in LPI patients, suggesting an intensified lipolysis that may induce hepatic steatosis and fibrosis in patients (Kurko *et al.*, 2015).

Clinical symptoms of LPI appear after weaning. Decreased plasma arginine and ornithine, urea cycle intermediaries (Figure 3), drive a secondary defect of the urea cycle leading to hyperammonemia crisis after rich protein ingestion that can cause coma and seizures. Chronic hyperammonemia can be diagnosed by functional analyses which cover ammonia cycle during along one day, analyzing ammonia in plasma samples taken before and one hour after each meal. Besides, orotic aciduria and characteristic amino acid profiles should be also present

INTRODUCTION

(Figure 3). Also vomiting and diarrhea are frequent symptoms in LPI patients. Because of this, LPI patients develop spontaneous aversion to protein meals. This leads to an inadequate nutrition status that results in malnourishment and failure to thrive. LPI patients commonly show pallor, poor muscle tone and sparse hair due to the deficient nutrition. Also osteopenia with delayed bone age and frequent bone fractures are common in LPI patients (Ogier de Baulny, Schiff and Dionisi-Vici, 2012a). Mental development is usually normal except in those patients that have developed recurrent hyperammonemia crisis. The fault in the urea cycle in LPI is less severe than in other conditions where the urea cycle enzymes are defective.

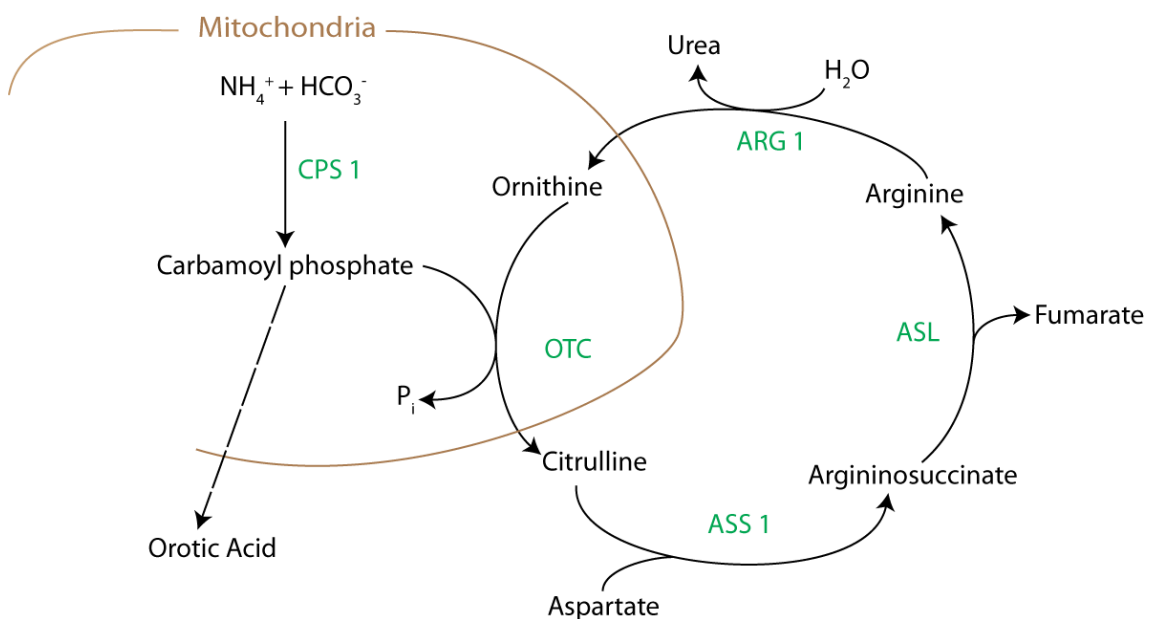


Figure 3. Schematic representation of the urea cycle. CPS1: carbamoyl-phosphate synthase; OTC: ornithine carbamoyltransferase; ASS1: argininosuccinato synthase; ASL: argininosuccinato lyase; ARG1: arginase 1;

Classical treatment of LPI patients includes citrulline supplementation, which is not transported through γ^+LAT1 and is converted to arginine and ornithine, overcoming thus the urea cycle malfunctioning (Sebastio, Sperandeo and Andria, 2011). Also a diet with a low protein content and statins are commonly used for LPI treatment. L-citrulline is a neutral amino acid that is transported through other different transporters than γ^+LAT1 , thus LPI patients are able to absorb it normally. It can be converted first into argininosuccinate by the argininosuccinate synthase (ASS1) and then into arginine by argininosuccinate lyase (ASL) (Figure 3), providing thus intermediaries to the urea cycle and improving its functioning in the patients. Improvement of urea cycle decreases hyperammonemia and then it also results in

INTRODUCTION

improvement of the nutrition status of patients. Nevertheless, L-citrulline supplementation does not correct the low lysine concentration. As lysine is an essential amino acid, its deficiency cannot be corrected by the administration of any other amino acid.

However LPI is a more complex multi organ disease and patients not only develop the mentioned hallmarks of LPI but also a wide range of complications related to immune and hematologic dysfunctions. Such complications comprise pulmonary alveolar proteinosis (PAP), anemia, hemophagocytic lymphohistiocytosis (HLH), systemic lupus erythematosus (SLE) or glomerulonephritis among others. In addition, improper response in front of viral infections (varicella) (Lukkarinen *et al.*, 1998) or recurrent infection of common bacteria have been reported in LPI patients. Regarding the immune related complications, wide variability has been described in LPI patients. This variability is found as much in the type as in the severity of the complications. In addition there is no correlation between the genotype and phenotype. Even patients with same mutations developed different complications. Also the prevalence among these complications is widely different. For instance, hepatosplenomegaly is extensively developed (Ogier de Baulny, Schiff and Dionisi-Vici, 2012a) whereas for SLE only some sporadic cases have been described (Kamoda *et al.*, 1998; Aoki *et al.*, 2001). Lysine scarce together with the protein restricted diet used for the treatment, has been suggested as a possible cause of the hematologic findings in LPI patients (Katriina Parto *et al.*, 1994).

Disruption of proper macrophage function (homeostasis and activation) seems to be crucial in the development of immune-related complications in LPI, however, the molecular mechanisms remain elusive. Some studies have been conducted trying to elucidate the role of γ^+ LAT1 in macrophages (Rotoli *et al.*, 2004; Barilli *et al.*, 2010, 2012; Kurko *et al.*, 2015). γ^+ L activity system has been shown to be the main driver of arginine transport in human monocytes from healthy subjects at steady state (Barilli *et al.*, 2010) and after interferon stimulation (Rotoli *et al.*, 2004). Similar results were obtained for alveolar macrophages from healthy subjects, whereas in fibroblasts arginine transport was equally mediated by γ^+ and γ^+ L systems. As a matter of fact, arginine transport was clearly diminished in monocytes and alveolar macrophages (AM) from LPI patients, but not in fibroblasts (Barilli *et al.*, 2010). This fact can be explained by the expression of both different transporters. *SLC7A7* showed the highest expression among all transporters of γ^+ and γ^+ L systems in human monocytes (Rotoli *et al.*, 2004), and its expression in AM was about 2-fold higher than *SLC7A6*. In contrast, *SLC7A7* expression was essentially absent in fibroblasts while *SLC7A6* expression was clearly detected, meaning that γ^+ L system in fibroblast is basically represented by γ^+ LAT2 (Barilli *et al.*, 2010). As Granulocyte Macrophage colony-stimulating Factor (GM-CSF) signaling pathway is essential for

INTRODUCTION

the correct maturation of AM, monocyte-to-macrophage differentiation using GM-CSF for 6 days was evaluated between LPI patients and healthy volunteers. Comparable differentiation between LPI and healthy monocytes was observed as revealed the expression of LPLA2, a phospholipase selectively expressed in AM, PPARY, a key mediator of surfactant catabolism in AM, and PU.1, a master regulator of AM differentiation by GM-CSF. No differences were found in the expression of these markers between LPI and control cells (Barilli *et al.*, 2010). Also by using this type of cells and polystyrene latex beads, decreased phagocytosis was reported in LPI macrophages (Barilli *et al.*, 2012).

More recently in the largest study done with LPI monocyte-derived macrophages, it has been shown an aberrant response of macrophages from LPI patients after Toll-like receptor (TLR) 4, TLR9 and TLR1/2 stimulation (Kurko *et al.*, 2015). Stimulation with unmethylated CpG DNA motifs (CpG) led to an increase in expression of *SLC7A7* in both control and LPI macrophages. CpG directly stimulates TLR9 signaling pathway, involved in bacterial and viral defense. After CpG stimulation, LPI macrophages showed a clear disability to secrete interferon (IFN) α compared to control macrophages. In addition, macrophages were also stimulated with lipopolysaccharide (LPS) and Pam₃CSK₄ to assess TLR4 and TLR1/2 response respectively. In both cases LPI macrophages showed an increased cytokine secretion compared to control ones. IL-1RA, IL-12, TNF α were the cytokines that came out as significantly expressed from a 26 cytokine panel. The same panel was used to measure cytokines in plasma. In this case CXCL8, CXCL9 and CXCL10 came out significantly increased in plasma from LPI patients compared to controls. Overall, these results depict an aberrant immunological response of macrophages in LPI (Kurko *et al.*, 2015).

The huge phenotypic variability together with the poor genetic correlation in patients and the lack of a viable animal model for human LPI, have impaired the advances in the understanding of LPI immune-related complications. Sperandeo *et al.* attempted to generate a mouse model for LPI by retroviral gene trapping (Sperandeo *et al.*, 2007). It resulted in a mouse model with a *Slc7a7* null allele as demonstrated the Northern blot analysis of *Slc7a7*^{-/-} fetuses. The genotyping of 606 pups revealed ratios of genotypes inconsistent with Mendelian inheritance: 28.4% of WT, 68.6% of heterozygotes and 3% of *Slc7a7* null homozygotes. Only two *Slc7a7* null homozygotes mice survived, and were kept with a low protein diet and citrulline supplementation. They showed growth retardation compared to wild type littermates. The older animal survived for 25 months without signs of the disease. After 25 months diet was changed to normal protein diet without citrulline supplementation, and the animal presented rapid weight loss, hypotonia and tremors, dying finally 15 days later. Both animals showed

INTRODUCTION

elevated urinary excretion of cationic amino acids and hyperammonemia. Fetuses at day 16.5 and pups were examined both showing a developmental delay and a smaller size. Cationic amino acid concentrations were measured in amniotic fluid at day 16.5 and no differences were found among the samples of the three different genotypes. This finding excluded the possibility that the development delay was due to the lack of cationic amino acids availability for the fetus. Nevertheless, down-regulation at mRNA and protein level of insulin-like growth factors (*Igf*) 1 and 2 was found in fetal livers of *Slc7a7* null fetuses compared to wild type ones. This downregulation was even more accentuated in the smallest *Slc7a7* null embryo. In contrast, the two *Slc7a7* null animals that survived did not showed down-regulation of these two growth factors. In addition, *Slc7a7* null fetuses showed a dysregulation of the binding proteins (*Igfbp*) ligands for *Igf*-1 and 2. *Igfbp*-1 was down-regulated whereas *Igfbp*-2 and 6 were up-regulated compared to wild type fetal livers. Hence, this results can be a possible explanation of the intrauterine growth restriction undergone by *Slc7a7* null fetuses. Moreover, micro-array based gene expression analysis in intestine and liver of the two *Slc7a7* null adults, revealed the dysregulation of more than 400 and 500 transcripts respectively. The Gene Ontology (GO) analysis revealed that the transport category was the most enriched one both in intestine and liver. Transport category was the most enriched one for up- and down-regulated genes, evincing that it was the most dysregulated one.

Pulmonary Alveolar Proteinosis

Pulmonary alveolar proteinosis (PAP) is a rare disorder in which proteinaceous material accumulates within the alveoli. It occurs in three clinical forms: congenital, secondary or acquired (Trapnell, Whitsett and Koh, 2003). The congenital form comprises a group of inherited diseases that includes mutations in surfactant proteins B (MIM 265120) and C (MIM 610913), in lipid transporter ABCA3 (MIM 610921), as well as in both α and β chains of the GM-CSF receptor (MIM 300770, MIM 614370). Secondary form is associated with conditions that impair the functioning of alveolar macrophages (AM) or conditions that reduce the number of this cell population. Such conditions can be hematologic cancers, inhalation of inorganic dusts, pharmacologic immunosuppression and certain infections. Finally, acquired PAP, also known as idiopathic, is the most common form accounting for around 90% of the cases. It is currently described as an autoimmune disorder that targets Granulocyte

INTRODUCTION

Macrophage colony-stimulating Factor (GM-CSF) and its signaling pathway (Trapnell, Whitsett and Koh, 2003).

All forms of PAP are characterized by surfactant accumulation inside alveoli and by a foamy shape of alveolar macrophages. Alveoli are the basic units for gas exchange process and due to the enormous surface area they represent, the surface tension at the air-water interface is too high to allow this process (Agassandian and Mallampalli, 2013). Lung surfactant is an essential component that allows gas exchange by reducing surface tension. Surfactant is comprised by approximately 90% lipid, of which phosphatidylcholine is the principal one, and the other 10% are four surfactant proteins (SP-A, SP-B, SP-C and SP-D). Synthesis and secretion of functional surfactant is exclusively done by alveolar epithelium type II cells (ATII). For surfactant clearance three different pathways have been described: uptake and recycling/catabolism by ATII, uptake and catabolism by AM and transport from alveoli up to bronchial tree (Goss, Hunt and Postle, 2013).

In PAP diagnosis, high-resolution computed tomography (HCRT) shows patchy, ground-glass opacifications with superimposed interlobular septal and intralobular thickening, a pattern commonly referred to as “crazy paving”. Though not specific for PAP, the extent and severity of these radiographic findings correlates with the degree of impairment in pulmonary function as measured by spirometry or arterial blood gas analysis. Bronchoalveolar lavage fluid (BALF) of PAP patients has a milky opaque appearance. Foamy and enlarged AM as well as an increased number of lymphocytes are frequently found in BALF preparations from PAP patients when analyzed in bright field microscope. Lung histology is the gold standard for PAP diagnosis. Usually lung parenchyma structure is conserved. Lymphocytic infiltrations and fibrotic lesions are also usually found. Alveoli are found filled with a material that stains with periodic acid-Schiff (PAS) and that is resistant to diastase treatment. This PAS positive material is also found within the AM in some PAP forms. After immunohistochemistry (IHC) against surfactant proteins, this accumulated material shows high content of these proteins (Trapnell, Whitsett and Koh, 2003).

Moreover some genetic mouse models have revealed that an aberrant activation of alveolar macrophages can also lead to a spontaneous development of PAP. An increased alternative polarization (M2) of alveolar macrophages has been shown to result in PAP in mice. This is the case of mice that overexpress the closely related cytokines Il-13 (Homer, Zheng and Chupp, 2002) or Il-4 (Ikegami *et al.*, 2000) in lung, and the knock out mouse model for Bach2 transcription factor (Nakamura *et al.*, 2013). In the later study, *Bach2* came out as a novel

INTRODUCTION

transcriptional repressor of M2 activation in macrophages. On the other hand, restricted overexpression of T-bet transcription factor in T-cells, leads to an uncontrolled classic (M1) polarization of AM that also results in PAP in *T-bet^{tg/tg}* animals (Iriguchi *et al.*, 2015).

Pulmonary Alveolar Proteinosis in Lysinuric Protein Intolerance

One of the most life threatening complications in LPI is the respiratory involvement (Barilli *et al.*, 2012). Both male and female LPI patients with lung involvement have been described in Finland (Parto *et al.*, 1993; K Parto *et al.*, 1994; Tanner *et al.*, 2017), Italy (Dirocco *et al.*, 1993; Santamaria *et al.*, 1996, 2004, Barilli *et al.*, 2010, 2012), France (Valimahamed-Mitha *et al.*, 2015; Mauhin *et al.*, 2017), Canada (Douda *et al.*, 2009) and China (Zhang and Cao, 2017). LPI cases complicated with PAP are summarized in Table 2. Regarding these studies lung involvement appears to be frequent in LPI patients, where 58.6% of the studied patients developed some kind of lung complication, and specifically PAP, was reported in the 37.6% of patients. These studies also reflect the variability in clinical presentation and course of lung disease in LPI. The lung involvement described in LPI patients ranges from fibrosis and interstitial lung densities with subclinical symptoms until pulmonary hemorrhages and PAP development with fatal respiratory insufficiency.

INTRODUCTION

Number of LPI patients	LPI patients with PAP	Comments	Reference
2	2	Recombinant GM-CSF improved PAP resolution in one case	Zhang and Cao, 2017
4	4	Recombinant GM-CSF improved PAP resolution in two cases	Tanner <i>et al.</i> , 2017
14	10	LPD+Cit didn't affect respiratory symptoms. Corticosteroids for MAS didn't improved respiratory symptoms	Valimahamed-Mitha <i>et al.</i> , 2015
3	1	Two remaining patients also developed lung complications	Barilli <i>et al.</i> , 2012
1	1	Recombinant GM-CSF treatment satisfactory	Barilli <i>et al.</i> , 2010
1	1	Recombinant GM-CSF treatment no improvement	Douda <i>et al.</i> , 2009
1	1	Recombinant GM-CSF failed. Lung-heart transplant failed.	Santamaria <i>et al.</i> , 2004
9	1	All the remaining patients although asymptomatic, showed lung involvement by HRCT	Santamaria <i>et al.</i> , 1996
8	1	Other four patients had lung complications	Parenti <i>et al.</i> , 1995
3	?	All three patients presented interstitial lung disease	Dirocco <i>et al.</i> , 1993
31	3	Almost all patients had other lung complications or immune complications	Parto <i>et al.</i> , 1993

Table 2. Reported cases of LPI patients complicated with PAP. GM-CSF: Granulocyte-macrophage colony stimulating factor. HRCT: high-resolution computed tomography

The main putative candidates for lung disease in LPI are AM as postulated by Parto *et al.*, 1994. In that study, authors analyzed alveolar cells collected by BAL and lung specimens obtained at autopsy from four LPI patients that had developed acute irreversible respiratory insufficiency. Three of them had developed PAP and the other one, pulmonary interstitial and intra-alveolar cholesterol granulomas. The subjects used as controls for this study were five patients matched for sex and age and diagnosed of allergic alveolitis, rheumatoid arthritis, pleuritic and asbestos exposure two of them. Multilamellar structures in BAL fluid of the three LPI patients with PAP, as well as within the AM, were found. The mean area of AM of one patient was bigger than the control ones, and two patients showed an increased ratio of lymphocytes/macrophages in BAL fluid. Furthermore, the AM from LPI patients showed iron inclusions. Also measurable iron amounts could be found in AM from control patients, however the mean ratio of iron/chlorine in LPI macrophages was 2.79 ± 3.48 whereas the respective ratio in control AM was 0.41 ± 0.53 ($p < 0.01$) (K Parto *et al.*, 1994).

Another case of LPI patient who developed PAP, did not show improvement after two whole lung lavages. The patient was treated with human recombinant GM-CSF but did not show neither improvement (Santamaria *et al.*, 2004). Despite his monocytes and granulocytes

INTRODUCTION

expressed correctly GM-CSF receptor β -chain, no improvement could be observed because the treatment was discontinued after 8 days due to side effects. As the respiratory conditions got worst, it was decided to perform lung transplantation. After surgery patient did well, no rejection was observed. 18 months after transplantation the patient went to hospital due to a severe Epstein Barr pneumonia. The high resolution computed tomography scan and transbronchial biopsy revealed signs of PAP. Because of PAP reappeared following lung transplantation, the authors hypothesized that PAP in LPI could be caused by deficient hematopoietic-origin cells. Even though, presence of antiGM-CSF autoantibodies could not be excluded. In addition, three more cases of PAP in LPI were treated with GM-CSF with different outcomes. A Canadian LPI patient (Douda *et al.*, 2009) who developed PAP was treated during three months with GM-CSF with no side effects, but the boy's respiratory deterioration continued. The second one, an Italian boy, was treated during 7 consecutive days followed by 7 days off (total of 6 cycles), to avoid side effects, and the respiratory conditions improved (Barilli *et al.*, 2010). Finally, a 6 year old girl was treated twice a day with GM-CSF at 5 μ g/kg. The respiratory condition improved notably after three months of treatment (Zhang and Cao, 2017).

Hemophagocytic lymphohistiocytosis

Exists a set of clinical entities that share a common immunopathologic condition known as cytokine storm. Sepsis, hemophagocytic lymphohistiocytosis (HLH), macrophage activation syndrome (MAS) and systemic inflammatory response syndrome (SIRS) comprise this group of cytokine storms. The designation of these clinical entities generally comes from the underlying cause of the disease. Thus, sepsis is the one originated by bacterial infection, HLH by malignancy or genetic origin, MAS as a rheumatologic disease and SIRS is idiopathic or drug induced. The common features that all these syndromes share are: massive inflammatory response, elevated serum cytokine levels, multiorgan system disease, hemophagocytic macrophages and often, death. However, the cytokines that predominate in these syndromes may differ. For instance while TNF- α predominates in sepsis, IFN- γ is the predominating one in HLH and MAS (Behrens *et al.*, 2011).

HLH can occur as familial or as sporadic cases. In both cases HLH may be triggered by a variety of events that disrupt immune homeostasis. MAS and HLH closely resemble and may develop

INTRODUCTION

together. In addition both are characterized by excessive activation and proliferation of macrophages and CD8⁺ T cells (Grom and Mellins, 2010). The genetic inheritance of familial HLH has revealed that it is caused by abnormalities in the perforin-mediated granule exocytosis of natural killer (NK) and CD8⁺ T cells, which is in agreement with the reduced cytotoxic activity displayed by these cells in patients. Perforin is a protein expressed in natural killer cells NK and CD8⁺ T cells that makes holes in the membrane of their target cells. Mutations in perforin 1 (*PRF1*), syntaxin 11 (*STX11*), syntaxin binding protein 1 (*STXBP1*) and munc13-4 (*UNC13D*) have been identified to prone for HLH. In addition, mutations in *LYST*, *RAB27A* and *AP3b1* combine this predisposition to HLH with clinical manifestations of albinism and variable degrees of other immune dysfunctions (Jessen *et al.*, 2013). The excessive activation and infiltration of macrophages, NK and T lymphocytes results in the mentioned cytokine storm and the development of the syndrome. Due to this loss of immune homeostasis, patients usually present hepatosplenomegaly, prolonged fever and cytopenia. In addition, increased levels of biochemical markers such as ferritin, triglycerides, soluble CD25 as well as increased phagocytosis in various tissues are also diagnostic criteria for HLH diagnosis (Jessen *et al.*, 2013).

It has been proposed that continuous stimulation of CD8⁺ T cells by infected antigen presenting cells would results in the cytokine production, but this process would never end due to the disability of CD8⁺ T cells to release cytotoxic granule and then lysate their target cells, leading to the sustained hyper inflammatory response. However, defects in granule exocytosis are often absent in MAS (Behrens *et al.*, 2011). In addition, perforin-related mutations seem to be not enough to trigger HLH and, as revealed mouse models, and exogenous infections are also required (Jensen 2013). It was shown that in absence of viral infection, continued CpG-Tlr9 activation was sufficient to produce a MAS-like syndrome in mice. The development of this syndrome was IFN γ dependent. However, dendritic cells, but not CD8 lymphocytes nor NK cells, were characterized as the responsible population of the increase in IFN γ production. In addition, Il-10 was described as a negative modulator of the severity of the disease. Mice with repeated CpG-Tlr9 stimulation developed a milder phenotype than those which CpG administration was combined with anti-Il-10r. Indeed, increased hemophagocytosis was only observed after Il-10 blockade. Thus, Il-10 was proposed to be a good candidate responsible of the variability found for MAS and HLH in patients (Behrens *et al.*, 2011).

Hemophagocytosing macrophages characterization has been another focus of research in HLH and MAS. They have been described to show a M2-like polarization profile (Grom and Mellins,

INTRODUCTION

2010; Canna *et al.*, 2014). Increased expression of the scavenger receptor CD163 was constantly found in hemophagocytes, while positive expression of CD206 (*MRC1*) or CD64 (*FCGR1A*) was found only in some cases (Canna *et al.*, 2014).

HLH diagnosis can be done by molecular characterization of mutations in HLH-associated genes. Children should show homozygosity or compound heterozygosity. By contrast, in adults with clinical findings of HLH heterozygosity may be sufficient for the diagnosis of suspected HLH. Additionally, HLH diagnosis can be affirmative if patients fulfill five of the following findings (Jessen *et al.*, 2013):

- Fever
- Splenomegaly
- Cytopenia in at least two lineages
- Hyperferritinemia
- High soluble CD25 concentration
- Hypertriglyceridemia and/or hypofibrinogenemia
- Hemophagocytosis in spleen, bone marrow or lymph nodes
- Low/absent natural killer activity

Hemophagocytic lymphohistiocytosis in Lysinuric Protein Intolerance

HLH is another complication that arises in some LPI patients, and that has been reported in LPI patients from different ethnic groups (Yoshida *et al.*, 1995; Duval *et al.*, 1999; Güzel-Ozantürk *et al.*, 2013; Ouederni *et al.*, 2017). HLH in LPI has been reported in different forms, however, usual traits of HLH in LPI are persistent elevated ferritin and lactate dehydrogenase in serum, intermittent hemophagocytosis in bone marrow and spleen and absence of fever. Hepatosplenomegaly is also frequently reported. LPI patients suffering from HLH do not show profound immunodeficiency, and in addition to macrophages, other myeloid precursors are actively involved in hemophagocytosis. This combination of traits seems to be specific of HLH in LPI compared to other forms of HLH such as the familial one (Duval *et al.*, 1999; Gordon *et al.*, 2007; Ogier de Baulny, Schiff and Dionisi-Vici, 2012a; Ouederni *et al.*, 2017).

Macrophages

Principles of immunity

Immunity comprises the innate system and the adaptive system. Innate immunity is considered to appear phylogenetically previous than adaptive immunity and it constitutes the first line of defense against common bacterial infections and other pathogens. Basically, it is carried out by myeloid-origin cells. Its protective strategy is based in the expression of generic receptors that are able to recognize different components commonly shared by different pathogens. The collection of pathogen molecules that are recognized, are collectively known as pathogen-associated molecular patterns (PAMP). Some examples of PAMP are bacterial lipopolysaccharide (LPS), viral double stranded RNA or unmethylated CpG motifs. In addition, these cells can also detect signals of tissue damage known as damage-associated molecular patterns (DAMP). The receptors that allow detection of PAMP and DAMP are known as pattern recognition receptor (PRR). Some examples of PRR described are the family of Toll-like receptors (TLR), NOD-like receptors (NLR) and other scavenger receptors. This recognition allows triggering an inflammatory response to avoid pathogen's proliferation, to clear dead cells or remove potential harmful substances. Phagocytosis of invading pathogens or dying cells is part of the inflammatory response, and it is carried out by specialized phagocytic cells, such as macrophages, neutrophils, monocytes and dendritic cells (DC). Phagocytosis can be mediated by the Fc receptors in the case of opsonized particles or by a wide spectrum of scavenger receptors. The inflammatory response also includes the release of chemokines and cytokines that recruit and activate other cells, amplifying thus the immune response (Janeway *et al.*, 2001).

Nevertheless, the innate system is not large enough to recognize all possible pathogens. Then, vertebrates have evolved the adaptive immune system. Adaptive immunity is mediated by lymphoid-origin cells that express immunoglobulins and T cell receptors. Both of them are inherited as gene segments formed by the variable (V), diversity (D) and joining (J) segments, each encoding a part of the variable region of immunoglobulins and T cell receptors. These segments are irreversibly joined by DNA recombination giving a stretch of DNA that encodes a complete variable region. The VDJ rearrangement occurs in progenitors of B and T cells, and is mediated by RAG1 and RAG2 (Litman, Rast and Fugmann, 2010). It allows generating specificity for almost unlimited number of antigens with a limited number of gene segments.

INTRODUCTION

By this mechanism, each cell generates unique genes and thus expresses unique receptor specificity. For the initiation of adaptive immunity response, phagocytic cells are also important. Phagocytic cells, especially dendritic cells, after ingestion of pathogens or pathogen particles are activated becoming antigen-presenting cells. Then, they move to the lymph nodes and stimulate lymphocytes, initiating the adaptive response (Janeway *et al.*, 2001).

However this evolved system of recognition of almost infinite antigens implies an important risk; the erroneous recognition of self-molecules as foreign, and the self-reaction against them. When this miss-recognition occurs, autoimmune disorders arise. To avoid it, regulatory mechanisms that finely controls the immune response have evolved (Grohmann and Bronte, 2010).

Amino acid control of immunology

A proposed mechanism for immune regulation is amino acid auxotrophy. It has evolved as a controlling mechanism that can modulate the production of antimicrobial effectors or shape the response of T-cells (Murray, 2015). Specially, two amino acids seem to be crucial for this regulatory mechanism: arginine and tryptophan. In the case of tryptophan, higher vertebrates express three enzymes with the capacity to catabolize it: two isoforms of indoleamine 2,3-dioxygenase (IDO1, IDO2) and tryptophan 2,3-dioxygenase (TDO). In the case of arginine, its catabolic enzymes are the three isoforms of NOS and the two isoforms of Arginase (ARG1, ARG2). Interestingly both IDO isoforms as well as NOS2 and ARG1 isoforms are induced by inflammatory cues such as cytokines (McGaha *et al.*, 2012), while there seems to be no catalytic enzymes for other amino acids induced in the same way (Murray, 2015).

An example of immune regulation by these mechanisms has been shown for IDO1-expressing DCs, which can exert immunosuppression by preventing T-cell proliferation (Munn *et al.*, 2005). Similarly, it has been shown how in a tissue-specific manner, Arg1-expressing macrophages also restricted T-cell proliferation (Murray, 2015).

IDO1 expression is strongly induced by IFN γ via STAT1 and IRF1 dependent mechanism. TGF β has also been shown to induce IDO1 expression via non-canonical NF κ B activity (McGaha *et al.*, 2012). However, the IDO1's induction pattern exerted by these two molecules is strikingly different. In DCs, IFN γ promotes a rapid hyperexpression of IDO1 tending to return to basal levels over the time, while the hyperexpression of IDO1 induced by TGF β is only appreciable at longer time periods. IFN γ induction promotes high and quick catalytic activity of IDO1. On the

INTRODUCTION

other hand, after TGF β stimulation, IDO1 becomes phosphorylated in its immune-based inhibitory tyrosine motifs (ITIMs), mediating intracellular signaling events in a self-sustaining feed-forward loop that leads to durable immunoregulatory effects. In addition, Mondanelli and colleagues demonstrated how the catabolic induction of Arg1 by TGF β in DCs is in turn, mandatory for IDO1 activity, drawing thus a link for both regulatory systems (Mondanelli *et al.*, 2017).

Nevertheless not only pathways involving tryptophan and arginine depleting enzymes have been reported in the regulation of immunology. Also amino acid transport has been shown to play a role in the control of immunity. This is the case of LAT-1 (*SLC7A5*) that belongs to the HATs family and which mediates the exchange of tryptophan and tyrosine with neutral amino acids. LAT-1 was revealed as essential for metabolic reprogramming and clonal expansion of T-cells after antigen presentation (Sinclair *et al.*, 2013). T-cells respond to antigen presentation by up-regulating the expression of LAT-1, promoting the entrance of neutral amino acids, which in turn leads to up-regulate the machinery necessary for proliferation and differentiation (via cMyc and mTORC1). Moreover, LAT-1 has been recently involved in pathogenesis of psoriasis by $\gamma\delta$ T cells in skin (Cibrian *et al.*, 2016). Tryptophan is the metabolic precursor of ligands that activate AhR transcription factor. AhR regulates the expression of IL22 in T_H17, which in turn activates STAT3 in keratinocytes, increasing epidermal proliferation and differentiation, affecting this way psoriasis development.

Macrophage populations

Macrophages are part of the mononuclear phagocyte system. They mainly consist in two classes: tissue resident macrophages and infiltrating macrophages. Infiltrating macrophages can only be found in tissues during or after pathologic conditions (Hashimoto *et al.*, 2013). The origin of infiltrating macrophages is the subset of circulating monocytes known as inflammatory monocytes. This subset of monocytes is defined as CX₃CR^{low} Gr1⁺ in mice, and would be the homologs of human CD14⁺ monocytes (Geissmann, Jung and Littman, 2003). However the origin of most resident macrophages has been challenged during the last decade. There was proposed that the subset of murine monocytes CX₃CR^{high}Gr1⁻ could be the precursors of tissue resident macrophages because they are able to extravasate and persist into non inflamed tissues (Geissmann, Jung and Littman, 2003). Nevertheless, genetic fate mapping studies revealed that tissue resident macrophages express markers that correspond to embryonic origin (Yona *et al.*, 2013; Gomez Perdiguero *et al.*, 2014). This fact is in clear

INTRODUCTION

controversy with the idea that tissue resident macrophages develop from adult monocytes or adult hematopoietic stem cells. Indeed, further studies demonstrated that monocyte contribution to tissue resident macrophages is minimal (Guilliams *et al.*, 2013; Hashimoto *et al.*, 2013), or even absent in the case of microglia (Yona *et al.*, 2013), in steady state. Thus, tissue resident macrophages are populations that originate mainly from the yolk sac and that are able to self-renew under basal state conditions. Nevertheless monocytes and bone marrow-derived cells can also contribute to these subsets for instance in pathological states. The contribution rates vary among tissues and situations (Haldar *et al.*, 2014; Perdiguero and Geissmann, 2015).

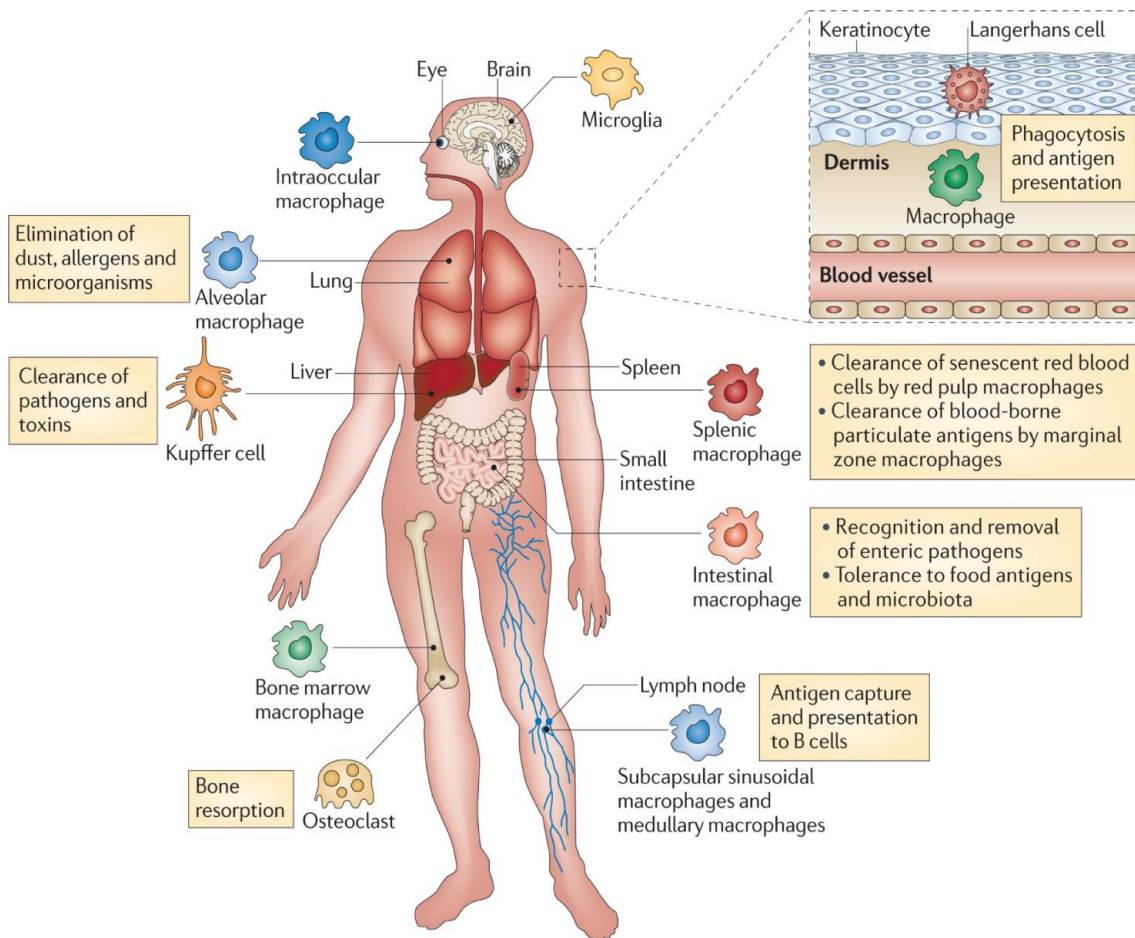


Figure 4. Homeostatic function of tissue resident macrophages. Schematic representation of subsets of tissue resident macrophages and their homeostatic functions. Among these tasks, phagocytosis, immune surveillance and antigen presentation are the most common ones. Figure taken from (Murray and Wynn, 2011).

Examples of tissue-resident macrophages are alveolar macrophages, liver's Kupffer cells, microglia, osteoclasts or splenic red pulp macrophages. These populations of macrophages constantly surveil their surroundings for signs of tissue damage or pathogen invasion. However, they also perform important homeostatic tasks of the specific tissue (Murray and

INTRODUCTION

Wynn, 2011). Tissue resident macrophage populations differentiate each other in terms of gene expression and functionality. Indeed, they can be distinguished by different combinations of surface markers (Becher *et al.*, 2014) and important homeostatic functions have been described for every tissue resident macrophage population (Murray and Wynn, 2011). The homeostatic tasks of macrophages depend on the tissue needs and they are essential for the correct functioning of the tissue (Figure 4). Some examples of the collection of different functions performed by tissue resident macrophages are surfactant recycling by alveolar macrophages, recycling of senescent red blood cells by splenic red pulp macrophages or bone resorption by osteoclasts.

Macrophages are well known by performing a primary immune response. By the use of mainly bone marrow derived macrophages (BMDM) and inflammatory peritoneal macrophages *in vitro*, it has been described two theoretical states of polarization of macrophages: classical and alternative. Classical (M1) activation induced by LPS (or other TLR activators) and IFN γ . M1 macrophages would be in charge of the defence of the host from bacteria, viruses and protozoa. On the other hand, alternative (M2) activation is mainly induced by IL13 and IL4 although other cytokines such as IL10 can also induce the M2 polarization. M2 macrophages have been related to wound healing, resolution of inflammation and helminthic defence. Nevertheless, this experimental polarization *in vitro* can hardly reproduce what actually happens *in vivo*, where a much complex combination of factors and cues stimulates macrophages shaping their responses (Murray, 2015).

L-Arginine metabolism in macrophages

Arginine is required by macrophages to proliferate and to generate a proper response when they become activated. Arginine is used differently in these two processes. While in proliferation arginine is mostly used for protein synthesis, in activation it is used to generate NO and citrulline (in classical activation) or ornithine and spermine (in alternative activation). Also the arginine transport differs in these two processes. In BMDM from mice in basal conditions and M-CSF-induced proliferation, arginine transport is mainly mediated by γ^+L system. While after BMDM activation γ^+ system drives the majority of arginine uptake, through the up-regulation of CAT2 transporter (Yeramian *et al.*, 2006). The induction of this transporter is independent of the availability of extracellular arginine. For proliferation arginine is mainly

INTRODUCTION

used for protein synthesis, while activated macrophages catabolize arginine through different pathways. In classical activation arginine is predominantly catabolized by iNOS into NO and citrulline, while in alternative activation, arginine is mainly converted into ornithine and polyamines by Arginase 1. In addition, macrophages express a truncated form of the urea cycle that allows them to generate arginine from citrulline by the action of Argininosuccinate synthase (Ass1) first and Argininosuccinate lyase (Asl) in a second step (Qualls *et al.*, 2012).

Nitric Oxide Synthases

L-Arginine is also the substrate for the family of NOS enzymes. NOS in mammals are dimers that require the presence of the cofactors calmodulin, tetrahydrobiopterin (BH₄), heme, flavine-adenine dinucleotide (FAD) and flavin mononucleotide (FMN) for their complete activity. Three different isozymes for NOS have been described. They share 50% of homology, are coded by three different genes and differ in their tissue expression and regulation. *NOS1*, also known as neuronal NOS (nNOS) is expressed prevalently in neuronal tissue. *NOS2*, also known as inducible NOS (iNOS) is present in various cell types of the immune system. Finally *NOS3*, the endothelial NOS (eNOS) is mainly found in endothelial cells (Bronte and Zanovello, 2005). Despite of their names, their expression is not restricted to those tissues and they can be found in a wide variety of cell types. nNOS and eNOS are expressed constitutively and their activity is regulated primarily by elevation of Ca²⁺ fluxes in the cell and subsequent binding to calmodulin. On contrary, iNOS activity is basically regulated by *de novo* protein synthesis and stability of iNOS mRNA and protein. Once active, it acts in a Ca²⁺ independent manner (Bogdan, 2001). NOS enzymes catalyze the oxidation of L-Arginine to generate L-Citrulline and NO. Two domains are found in these enzymes that mediate this reaction. The amino-terminal oxygenase domain transfers electrons donated by the conversion of NADH to NADP through FAD and FMN until the carboxy-terminal reductase domain. Calmodulin is required for the electron transport. The carboxy-terminal reductase domain utilizes the cofactors BH₄ and heme to catalyze the oxidation of arginine with oxygen (Bronte and Zanovello, 2005).

iNOS has been widely reported to have a crucial role in immune cells. Through the production of NO it promotes cytotoxic activity to pathogen clearance. iNOS induction can be driven by cytokines and microbial components. IFN γ , α and β and microbial products such as LPS or CpG

INTRODUCTION

have been shown to be inducers of iNOS in mouse systems. IFN γ together with LPS elicit dimerization of STAT1, which through its phosphorylation triggers a signal cascade that involves NF- κ B, MyD88 as well as other factors. This cascade results in a transcriptional up-regulation of iNOS. The crucial role of STAT1 and NF- κ B in iNOS activation has been also demonstrated in cells from human origin, although significant differences with mouse exist. For instance, such is the case of human AM, which lack the expression of NOS2 mRNA and protein (Bogdan, 2015).

However NO has a signal transducer role in addition to its antipathogenic effect. Its production can be also induced by other hormones and metabolic products different than the mentioned cytokines and bacteria components. This is the case of erythropoietin (EPO) that blocks the expression of iNOS by preventing the binding of NF- κ B to its promoter. In addition, other factors such as some miRNAs, hypoxia or reactive oxygen species (ROS) have also been shown to have an impact in iNOS regulation (Bogdan, 2015).

Another mechanism of control of iNOS activity that is of special interest in this thesis is the one exerted by the availability of extracellular arginine, despite sufficient intracellular arginine availability. It is known as the L-arginine paradox. Extracellular arginine regulates iNOS expression in macrophages and astrocytes. Upon cytokine stimulation, iNOS mRNA increases independently of the extracellular arginine concentration, however, both iNOS protein levels and subsequent NO produced were strictly dependent on the extracellular arginine concentration (El-Gayar *et al.*, 2003; Lee *et al.*, 2003).

Nitric Oxide in Lysinuric Protein Intolerance

Historically, nitric oxide (NO) production has been a major concern in LPI physiopathology. L-arginine is the substrate of the three nitric oxide synthase (NOS) isoforms (NOS1, 2 and 3) for NO production. The three isoforms catalyze the same reaction, the conversion of L-Arginine in NO and L-Citrulline. Aberrant NO production in LPI macrophages have been pointed as a putative cause of immune-related complications of LPI (Sebastio, Sperandeo and Andria, 2011; Ogier de Baulny, Schiff and Dionisi-Vici, 2012a). This hypothesis relies on the rational that the lack of γ^+ LAT1 would be reducing the export of arginine outside the cell, thus in such situation the inducible nitric oxide synthase (iNOS, NOS2) would have more available substrate and the production of NO would be increased, producing aberrant macrophage activation. In this

INTRODUCTION

scenario, treatment of citrulline supplementation would raise up even more the trapped intracellular arginine producing a worsening of the immune-related complications.

Different results can be found in the literature regarding NO in LPI patients. In all the studies, NO was measured as nitrites, its derivative form found in plasma. On one hand, Kamada *et al.* reported a decreased concentration of circulating NO, and recovery to control levels after arginine infusions, in one Japanese patient (Kamada *et al.*, 2001). In the same way, Kayanoki *et al.* also reported decreased concentration of NO derivatives in another LPI patient and arginine infusion recovered his NO levels to the basal ones compared to control subjects (Kayanoki *et al.*, 1999). On the other hand, other studies have reported the contrary in Italian (Mannucci *et al.*, 2005) and Finnish (Kurko *et al.*, 2015) patients. Manucci *et al.* found increased NO derivatives in plasma of three LPI patients. Of note, NO levels in one of those patients returned to normal values after resolution of cutaneous lesions and improvement of immunological abnormalities. Kurko *et al.* in a study where a total of 26 LPI patients and 19 healthy controls were compared, found that the nitrite levels were slightly but significantly increased in patients compared to controls (Kurko *et al.*, 2015).

In vitro studies with primary cultured cells from LPI patients have neither revealed results pointing in the same direction. Primary fibroblasts from LPI patients showed an increased production of NO compared to controls (Mannucci *et al.*, 2005). On the contrary, monocyte derived macrophages from LPI patients showed decreased NO levels (Kurko *et al.*, 2015). In both *in vitro* assays mentioned, the production of NO was assessed in non-stimulated cells and the expression of iNOS was not detected, then the production of the NO measured would be attributable to one of the constitutive NOS isoforms rather than to iNOS.

Arginase 1

Arg1 expression in macrophages has been classically linked to wound healing and anti-helminth response. In M2 activation IL13 and IL4 activate the transcription factor STAT6, which in turn binds to an Arg1 enhancer and cooperates with other transcription factors producing an overexpression of Arg1. However, Arg1 function has been shown also to have a regulatory effect on the inflammatory response. For example, Arg1 lacking mice infected with *Schistosoma mansoni* suffered a lethal T cell-associated immunopathologic non-resolving

INTRODUCTION

inflammatory response. It has been suggested that macrophages expressing Arg1 may be depleting arginine locally, preventing then T-cell proliferation (Murray, 2015).

Moreover, this local arginine depletion by Arg1 expressing macrophages has been suggested that also could serve to limit NO production by iNOS expressing macrophages. Arg1 and iNOS when co-expressed in the same cell, virtually compete for the same substrate, arginine. As explained above, extracellular arginine rather than intracellular, has been shown to regulate iNOS expression. Thus Arg1 competing with iNOS for substrate and depleting arginine from milieu can extent as a regulator of iNOS activity. In addition, Arg1 can block iNOS translation from mRNA (Murray, 2015). Indeed some pathogens take advantage from this mechanism. Two examples of them are *Helicobacter pylori* and *Leishmania spp*, which are able to express arginases. By this way, they consume and thus deplete arginine from milieu, limiting NO production and improving their survival and proliferation (Grohmann and Bronte, 2010). Moreover, the intracellular bacteria *Mycobacterium bovis*, have been shown to induce Arg1 host expression. This results in a host self-induced depletion of arginine, reducing then the NO production capacity of host's macrophages and dampening the bacteria killing power. This mechanism is TLR-STAT6 dependent, meaning that Arg1 is a key component of the bacteria strategy to survive in NO producing cells. Mice lacking Arg1 expression restricted to macrophages showed an advantage in bacteria killing terms compared to WT animals (El Kasmi *et al.*, 2008). All this data reinforce the idea that Arg1, at least in macrophages, has a regulatory role in limiting NO production.

Iron metabolism

Iron itself or as a component of heme and iron-sulfur clusters is essential for many cellular processes and metabolic pathways such as oxygen transport, cellular respiration and DNA synthesis. However, the bulk of iron in a human adult body is found as part of heme in the hemoglobin of erythrocytes. Thus, abnormalities in iron metabolism commonly result in anemia-related diseases. Iron deficiency is the most common form of anemia representing a global health problem. Iron-deficiency anemia is usually defined as microcytic (reduced volume of erythrocytes) and hypochromic (reduced hemoglobin per erythrocyte). On the other hand, iron overload is also detrimental. The most common forms of iron overload in western societies are hereditary diseases, affecting the iron sensor genes such as *HFE*, *TFR2*, *HAMP* and *HJV* or disrupting hematopoiesis, resulting in hemochromatosis and thalassemia respectively (Muckenthaler *et al.*, 2017).

Erythropoiesis

Erythropoiesis is the process by which erythroid progenitors proliferate and differentiate into reticulocytes. During this process, hematopoietic stem cells (HSC) become burst-forming unit erythroid (BFU-E), and progress to colony-forming unit erythroid cells (CFU-E) (Muckenthaler *et al.*, 2017). Erythroids become reticulocytes by losing their nuclei, which then move into the bloodstream giving lastly the mature RBC (Figure 5). Erythrocytes represent the most common cell type in adult blood. Bone marrow provides a niche for the constant production of new erythrocytes. This niche consists of endothelial cells of the vascular system, stromal cells, osteoblasts and hematopoietic cells. It provides a network that supports direct cell-cell contact and exposure to growth factors, cell adhesion molecules and cytokines. Stem cell factor (SCF), thrombopoietin (TPO), GM-CSF or IL3 are some the cytokines that erythroid precursor are responsive to. SCF seems to be especially relevant in the earliest erythroid precursors. SCF binds to its receptor, KIT, a tyr-kinase that signals through several pathways. At subsequent stages SCF acts synergistically with EPO in the proliferation and development of the erythroid precursors. The new cells enter the circulation as reticulocytes, and in human beings it takes about one week until they complete their maturation process. Mature erythrocytes have a certain deformability degree, have a small size (6-8µm) and have a biconcave shape. These characteristics confer them a perfect surface for gas exchange and allows their flow through microcapillaries in the tissues (Dzierzak and Philipsen, 2013).

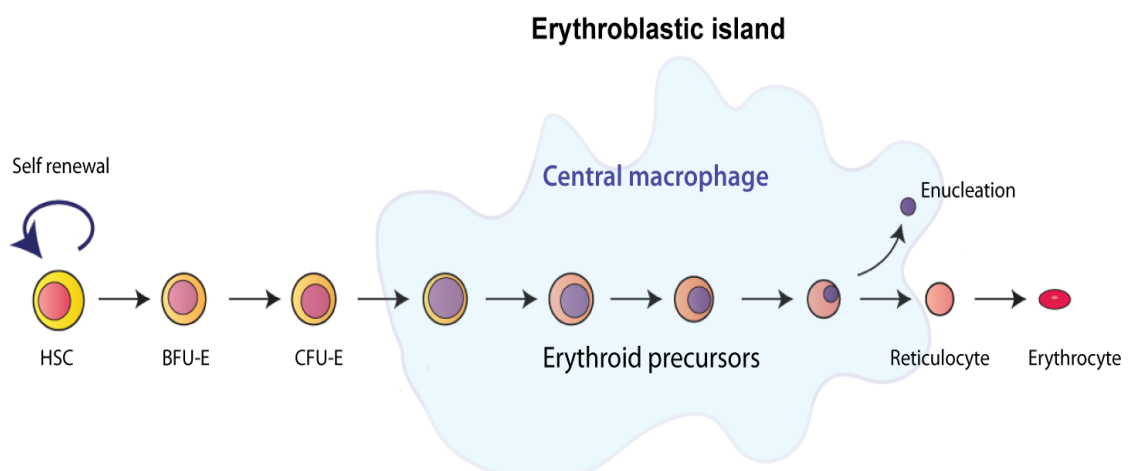


Figure 5. Erythropoiesis. Schematic representation of erythropoietic process. Figure modified from (Dzierzak and Philipsen, 2013).

INTRODUCTION

Last steps of erythroid differentiation take place in the erythroblastic islands. It consists in a central macrophage (also known as nurse macrophage) surrounded by differentiating erythroid progenitors. The nuclei expelled by erythroblasts during the end of their maturation process are rapidly phagocytosed by the central macrophage (Figure 5). Contact interactions between the central macrophage and the erythroblasts, as well as between the erythroblasts and the extracellular matrix are essential for the terminal differentiation of the erythroblasts. An illustrative example of the proteins that mediate these interactions is the macrophage-erythroblast attacher (MAEA), which is expressed in the surface of both type of cells and is essential for the correct maturation and enucleation of erythroblasts. Also a role for cell signaling between erythroblasts has been described. Erythroid precursors express CD95 (FAS) death receptor along the differentiation process. However only mature cells express CD95 ligand (FASL) but these cells are insensitive to FAS signaling. On the contrary, immature cells undergo proapoptotic processes in response to FASL. Thus it stops progression along the differentiation process of some of the immature cells. The apoptotic cells are cleared very efficiently by macrophages. A decreased survival rate is a hallmark of many inherited anemias. Also 50% of rheumatoid arthritis patients develop anemia, and treatment with antibodies blocking the death signal TNF α improves the anemia and reduces the number of apoptotic erythroid progenitors in the bone marrow (Dzierzak and Philipsen, 2013). The expression of the surface proteins that mediate these interactions in the erythroid progenitors is dynamical along the differentiation process. A good example of this is CD44, a receptor for hyaluronic acid that mediates cell-cell and cell-matrix interactions. The expression of CD44 has been shown to decrease along with the size as the erythroid precursors move forward in the differentiation process (Chen *et al.*, 2009).

Iron transport and storage

Erythropoiesis has extremely high iron requirements to sustain hemoglobin synthesis; more than 2/3 of body iron is used in hemoglobin (Sebastiani, Wilkinson and Pantopoulos, 2016). It is estimated that, in an adult human being, around 20-25 mg of iron per day are needed for hematopoiesis. However, only 1-2 mg of iron per day is absorbed in the gut. Then, this iron demand is basically covered by the iron obtained from the recycling of senescent red blood cells (RBC), done by macrophages. Dietary absorbed iron is tightly regulated and depends on

INTRODUCTION

body iron needs. It usually just compensates for iron losses or for increases in iron demand, as can happen during pregnancy (Muckenthaler *et al.*, 2017). Dietary iron absorption needs to transport iron through both basolateral and apical membranes of enterocytes. The iron transport across the apical membrane is mediated by DMT1 (*SLC11A2*) while the transport across the basolateral membrane is mediated by ferroportin (FPN, *SLC40A1*) (Figure 6).

Hepcidin regulates iron transfer from macrophages, hepatocytes and enterocytes to circulation. It is mainly secreted by the liver and promotes ferroportin internalization and degradation predominantly in lysosomes (Nemeth *et al.*, 2004). Hepcidin is regulated basically by the transcription of its gene, *HAMP*. It is induced by hyperferremia, cytokines such as IL-6 and TLR-4 activation. On the other hand, repression of *HAMP* transcription can occur as a response to hypoferremia, anemia, tissue hypoxia and some hormones (Soares and Weiss, 2015). Liver is able to store iron and can act as an iron buffer. Indeed liver by the secretion of hepcidin, transferrin and many other proteins is a central regulator of iron levels in the organism. In addition, in conditions of heightened erythrocyte elimination liver assumes a central role by recruiting monocyte-derived macrophages to perform this task (Theurl *et al.*, 2016). Moreover, in situations of increased hemolysis, hepatocytes secrete haptoglobin and hemopexin to counteract the toxic effects of free hemoglobin and heme respectively. The complex hemopexin-heme is removed from circulation through CD91 (*LRP1*) (Hvidberg *et al.*, 2005), while the haptoglobin-hemoglobin one, is recognized and cleared by CD163. Both CD91 and CD163 receptors are mainly expressed by macrophages.

Free iron has potent toxic effects, and to avoid its toxic effects there exist a collection of proteins that regulate its uptake, storage and transport. Iron responding proteins (IRP) and iron responding elements (IRE) system is a mechanism to regulate the levels of some proteins involved in iron metabolism. The IREs are highly conserved hairpin structures of 25-30 nucleotides, and they constitute binding sites of IRPs (1 and 2). IREs are placed in the 3' UTR or in the 5' UTR, and depending on its position they serve as stabilizers mRNA elements (3' UTR) or as a translation control elements (5' UTR) (Wilkinson and Pantopoulos, 2014). On the other hand, IRPs are cytosolic proteins that recognize and bind to IREs. In situations of cellular iron scarce, IRPs bind to IREs and regulate the transcription/degradation of those mRNAs. Transferrin receptor (TFR) and ferritin can be taken to illustrate this regulatory mechanism. TFR mRNA contains 5 IREs in its 3'UTR while both ferritin chains (H and L) contain a single IRE at their 5'UTR. Under conditions of limiting cellular iron, IRPs bind to ferritin IRE (5' UTR) inhibiting their transcription and to TFR IRE (3'UTR) stabilizing and protecting mRNA from

INTRODUCTION

degradation. This coordinated response increases cellular iron availability, by priming the uptake and preventing the storage.

Iron is mainly transported by transferrin (TF) and internalized by the binding of transferrin to TFR (Figure 6). Prior to be exported, iron needs to be oxidized from Fe^{2+} to Fe^{3+} so that can be bound to TF. There are three known multi-copper oxidases that mediate this reaction: ceruloplasmin (in circulation), hephaestin (in cell membrane) and zyklopen (in placenta) (Zhang and Enns, 2009). Deficiency of ceruloplasmin and hephaestin causes both in human and mice iron retention and anemia. Once iron is bounded to TF it can be transported to erythroid cells to sustain their demand in erythropoiesis. TF- Fe^{2+} binds to TFR and this complex is internalized by endocytosis in developing RBC. Iron is released from the complex thanks to the acidic environment of the endosome. Then iron is reduced by STEAP3 and transported to the cytosol by NRAMP1 (*SLC11A1*). The complex TF-TFR is recycled to the membrane where they dissociate. The freed iron forms an iron pool in the cytoplasm that can be utilized for incorporation to proteins, stored within ferritin molecules or exported to the extracellular space through ferroportin. This cycle of iron acquisition has been demonstrated to be crucial for erythroid cells, cardiomyocytes, muscle cells and dopaminergic neurons (Muckenthaler *et al.*, 2017).

Iron storage is mainly done by ferritin (Figure 6). Ferritin is a multimeric protein composed by 24 heavy (FTH) and light (FTL) monomers. FTH subunits have ferroxidase activity, thus ferritin converts Fe^{2+} and stores it as Fe^{3+} (Soares and Weiss, 2015). It is mainly an intracellular storage protein, however it can also be detected in cerebrospinal fluid, synovial fluid and plasma. Serum ferritin is considered as one acute phase reactant, and an increase in its levels may indicate inflammation. It is mainly secreted by macrophages. Ferritin secretion is regulated by IRP2, and specific ablation of IRP2 in macrophages, but not in hepatocytes, caused a decrease in serum ferritin levels. Nevertheless, IRP2 ablation ubiquitously caused higher serum ferritin level than macrophage specific ablation, denoting that macrophages are not the only cells that secrete serum ferritin (Dunja, Hentze and Galy, 2009). In serum it has been used in diagnostics to estimate body iron levels; low ferritinemia correlates with low body iron stores, whereas high serum ferritin correlates with elevated body iron stores, thus it is widely accepted that serum ferritin correlates with body iron storage. However, that serum ferritin reflects iron status of macrophages rather than whole body iron status seems to be more accurate (Cohen *et al.*, 2010).

INTRODUCTION

Ferroportin is the only mammalian non-heme iron exporter identified to date. The first ferroportin characterization was in zebrafish. Zebrafish mutants for ferroportin (*weh*) suffer from hypoferremia that causes hypochromic anemia and progressive decrease of erythroid cells. Its iron exporter function was corroborated in a *Xenopus* oocyte system. The highest ferroportin expression was detected by northern blot in placenta, kidney, spleen, liver (human) and specifically in duodenum within the large intestine (mouse) (Donovan *et al.*, 2000). Patients carrying mutations in *SLC40A1* present hemochromatosis type IV (OMIM 606069). This hereditary disease shows an autosomal dominant transmission. Elevated serum ferritin levels, low transferrin saturation and mild iron-deficient anemia are common laboratory traits found in these patients (Franchini, 2006).

Iron metabolism in macrophages

The main homeostatic task of the splenic red pulp macrophages (RPM) is recycling iron from senescent or damaged red blood cells (RBC) to sustain erythropoiesis' iron demand. In some extent also bone marrow macrophages (BMM) and liver's Kupffer cells can perform this task too (Haldar *et al.*, 2014; Nairz *et al.*, 2015). When RBC become aged they cannot undergo apoptosis due to their lack of nuclei, however they undergo some changes in their cell membrane composition that allow macrophages to recognize and engulf them. A well-known example of these changes is the display of phosphatidylserine (PS). PS is usually present in the inner leaflet of the cell membrane, but when it flips at the outer membrane, it is recognized by macrophages as an "eat-me" signal. This signal is used by both apoptotic cells and aged RBC (Boas, Forman and Beutler, 1998). PS is recognized by TIM4, which is expressed by macrophages at the cellular membrane (Miyanishi *et al.*, 2007), promoting the phagocytosis of the cells showing PS at the outer leaflet of the membrane. In addition to TIM4, Stabilin 1 and 2 have been also shown to recognize PS and mediate the engulfment of cell corpses and aged RBCs by macrophages (Park *et al.*, 2008, 2009). By contrast, a "do not eat me" signal expressed by many cells including healthy RBCs is CD47. It is recognized by SIRP α in RPM and DC preventing the phagocytosis signal (Oldenborg *et al.*, 2000). However, it has been also demonstrated that aged RBC have the capacity to bind thrombospondin-1 through a conformational change in CD47 enabling then their phagocytosis (Burger *et al.*, 2012). Nevertheless, a variety of receptors have been described to be involved in erythrophagocytosis. Among them we can find the scavenger receptor CD36. More specifically,

INTRODUCTION

CD36 seems to play a relevant role in the recognition of erythrocytes parasitized by *Plasmodium falciparum* (McGilvray *et al.*, 2000). Another receptor involved in the phagocytosis of apoptotic cells is CD14. Although initially it was described to recognize bacterial structures, nowadays it is well known that it also recognizes structures from apoptotic cells (Gregory, 2000). Another scavenger receptor involved in erythrophagocytosis is CD163; this receptor is mainly expressed by macrophages and recognizes the complex hemoglobin-haptoglobin complex, as mentioned above (Kristiansen *et al.*, 2001). It is highly expressed by erythrophagocytosing macrophages and it is a marker for hemophagocytic disorders such as HLH. The role of scavenger receptor A (known as *SR-A* in humans, *Msr1* in mice) is not well understood. However mice deficient for this receptor are not as efficient as wild type littermates in clearing aged RBCs from circulation (Theurl *et al.*, 2016). Although not strictly restricted to erythrophagocytosis, parabiosis studies identified the transcriptomic changes occurring in actively phagocytic macrophages (A-Gonzalez *et al.*, 2017). This study revealed that the transcriptomic profile of phagocytic macrophages differs between the various tissue-resident macrophages populations. Although not a receptor, downregulation of *I11b* is a common trait found in the phagocytic macrophages from all the tissues studied (intestine, spleen and bone marrow). Also upregulation of *Cd163* and *Timd4* seem to be conserved markers of phagocytosis among the different tissue-resident populations analyzed. However, interestingly, overexpression of *Mrc1*, another scavenger receptor, seems to be characteristic of phagocytic macrophages from intestine and bone marrow, but not for the splenic ones (A-Gonzalez *et al.*, 2017).

The engulfed erythrocytes are degraded in the phagolysosome. Hemoglobin is split into heme and the globin chains. Heme is transported through HRG1 (*SLC48A1*) to cytosol where it is degraded by hemoxigenases (*HMOX1,2*) into iron (Figure 6), bilirubin and CO. Alternatively, heme can also be exported outside the cell through the feline leukemia virus, subgroup C, receptor (*FLVCR*). Mice with *flvcr* ablation developed severe anemia and lack definitive erythropoiesis (Keel *et al.*, 2008). In addition, ionic iron can move into the cytoplasm through Nramp1 (Nairz *et al.*, 2015). A pool of labile iron is generated, and iron can be then used for the different cellular processes needed, and then it can be also exported to the extracellular milieu through ferroportin or it can be stored within ferritin (Figure 6).

Heme activates the molecular program that allows macrophages to metabolize iron by two independent pathways: 1) by promoting Bach1 degradation via proteasome, heme allows SpiC expression and subsequently its target genes. Among the targets of SpiC genes such as *Hmox1*, *Slc40a1*, *Blvrb*, or *Slc7a11* have been identified (Haldar *et al.*, 2014). Furthermore, the

INTRODUCTION

activation of this pathway allows RPM to acquire a complete differentiation state, a fact that was shown in *Spic*^{-/-} mouse model, where there was an almost complete absence of this cell population (Kohyama *et al.*, 2009). Indeed, it was demonstrated that heme promotes the differentiation into RPM of a subpopulation of cells considered as monocytes. This supports the idea that monocytes, in some extent can contribute to RPM population (Haldar *et al.*, 2014). SpiC expression was also found in BMM and in liver, the other tissues were tissue-resident macrophages also show a higher capacity of iron metabolism. 2) In parallel, by the degradation of Keap1, it ceases the inhibition to Nrf2 and allows the binding of the latest to ARES-containing genes such as *Hmox1*, *Slc40a1*, *Slc48a1* or *Fth* (Marro *et al.*, 2010).

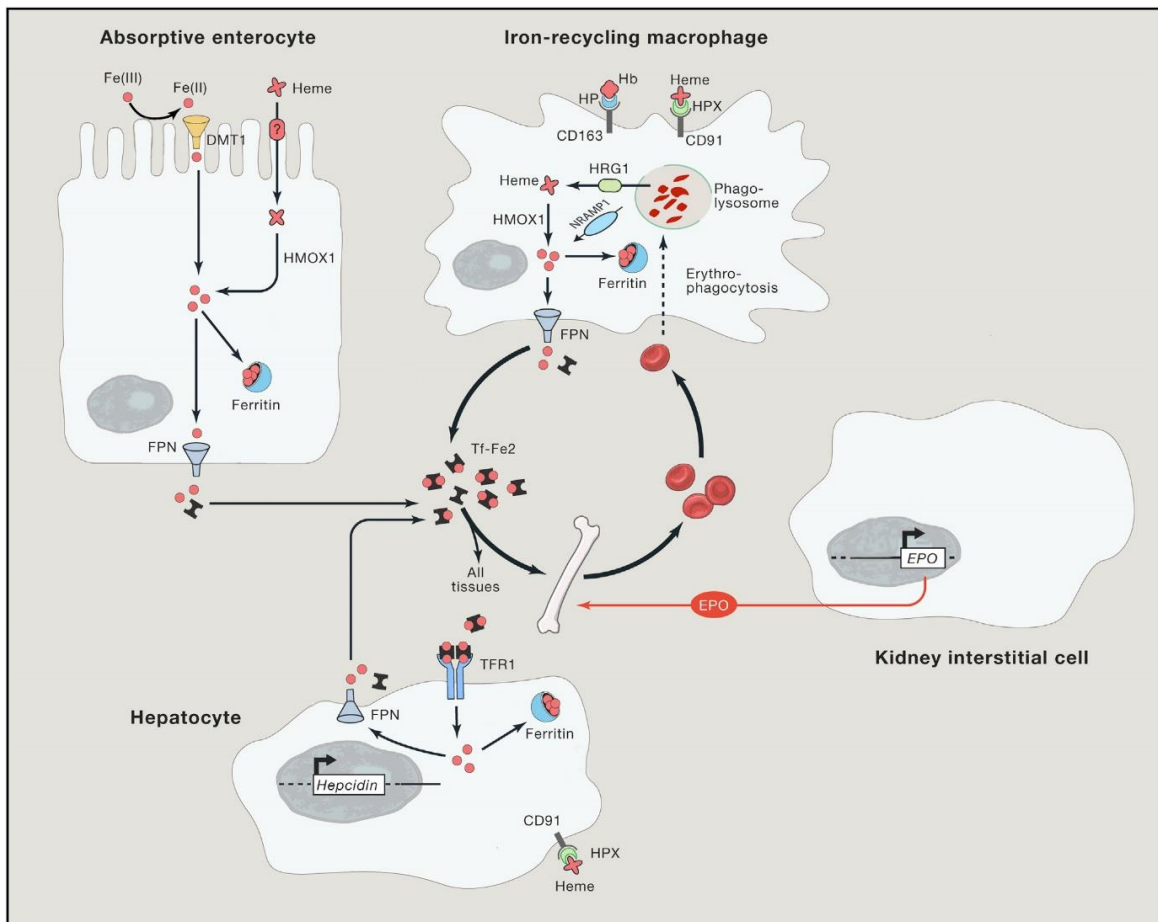


Figure 6. Systemic iron homeostasis. Enterocytes uptake iron via DMT1. It is transported into the bloodstream via FPN and delivered to all tissues bound to Tf. It is mainly used for hemoglobinize newly synthesized RBCs. Specialized tissue macrophages engulf aged or damaged RBCs. Iron from engulfed RBCs is recycled by degrading heme via HMOX1. Iron can be stored in ferritin or delivered again to blood via FPN. Hepatocytes sense iron levels and trigger hepcidin response to regulate them. Hepatocytes can also store iron within ferritin to buffer iron levels. Kidney epithelial cells can also sense iron and oxygen deficiency and release EPO to stimulate erythropoiesis. Adapted from (Muckenthaler *et al.*, 2017).

INTRODUCTION

Iron handling by macrophages is also relevant for their immune function. Several data from clinical studies and infection models showed that macrophage iron overload interferes with their antipathogenic response (Nairz *et al.*, 2017). Iron is an essential nutrient for both mammals and microorganisms, and the general strategy to fight extracellular infections is iron retention by macrophages leading to hypoferrremia. This is mainly achieved by the induction of mechanisms of iron uptake and iron retention. Indeed, iron overload or iron supplementation in the host make the outcome of some infections worse. Conversely, in the case of intracellular pathogens, the strategy is to release iron and induce hyperferrremia.

Macrophages in response to LPS can produce small amounts of hepcidin reducing thus iron export (Theurl *et al.*, 2008). However sustained iron retention requires the input of other mechanisms, such as ferroportin repression induced by $\text{INF}\gamma$. $\text{INF}\gamma$ also induces NO production by iNOS, which in turns exerts regulatory actions of iron metabolism proteins in macrophages, promoting iron export and limiting iron retention. NO modulates binding activity of IRPs to their target IREs in genes, as is the case of ferritin which expression is reduced in the presence of NO (Weiss *et al.*, 1993). Nevertheless there is a negative regulatory feedback loop between iron and NO. When intracellular iron increases, iNOS translation is repressed promoting then iron retention (Weiss *et al.*, 1994). Furthermore, NO itself acts as a regulatory signal for some iron-related proteins. This is the case of ferroportin, which expression is enhanced in presence of NO via Nrf2 transcription factor. Indeed, *Nos2^{-/-}* mice showed iron accumulation in macrophages due to decreased ferroportin expression (Nairz *et al.*, 2013). In addition, other cytokines such as IL-4, IL-10 and IL-13 induce intracellular iron uptake and retention (Soares and Weiss, 2015). Other molecules with iron binding capacity that seem to have a role in iron trafficking during infection are lactoferrin and lipocalin (*Lcn2*). Lactoferrin is expressed in many tissues and its principal duty is to bind iron and restrict it to microbes. Moreover lactoferrin modulates activation and proliferation of NK cells, lymphocytes and macrophages. Lipocalin is a peptide secreted by activated macrophages that can bind iron-laden bacterial siderophores and deliver them to macrophages through the lipocalin receptor (*Slc22a17*), limiting thus iron acquisition by bacteria (Soares and Weiss, 2015). Lipocalin receptor recognizes both lipocalin iron free and iron laden molecules and can thus mediate bidirectional iron transport (Nairz *et al.*, 2015).

OBJECTIVES

OBJECTIVES

Although the metabolic component of LPI has been widely studied, and consequently specific treatments are currently in use, the molecular mechanisms behind the immune and hematologic complications in LPI are still poorly understood. In addition, a possible relationship between the metabolic and the immune components of the disease has not been addressed to date. To face these challenges, our group has generated the first conditional mouse model that targets *Slc7a7* during the adulthood (*Slc7a7^{-/-}*). Thus, the objectives of this thesis are:

1. To characterize the phenotype developed by the *Slc7a7^{-/-}* mouse model, in order to validate it as a useful animal model to study LPI.
2. To determine whether the metabolic component of LPI has an impact on the immune complications.
3. To unravel the molecular mechanisms that drive the immune complications in LPI.

METHODS

Animals

All mice models used in this thesis were bred at Parc Científic's animal facility, which fulfills the government regulations on the use of experimentation animals. All protocols involving animals were reviewed and approved by the Parc Científic's Animal Experimentation Ethics Committee and by the corresponding Department of Generalitat de Catalunya. Experiments were carried out in accordance with animal welfare laws, with the highest scientific, humane, and ethical principles.

The Parc Científic's animal facility is a Specific Pathogen Free (SPF) installation where mice are kept under controlled conditions that ensure their defined health status and maintain an environment that is free of certain infectious organisms that are pathogenic and can interfere with research objectives. It is important to note that an SPF status indicates that mice have been tested and determined to be free of certain pathogens but not necessarily free of all pathogens that can affect the species.

All mice used during this thesis were C57BL/6J (strain C57BL, substrain 6 from Jackson Laboratory, standard abbreviation B6); the most widely used inbred strain in research. Although transgenic animals were done using different strains, at the time of starting this work all mice were already in pure genetic background (more than 12 backcrosses).

Mice were maintained in a 12h light-dark cycle (light from 6 am to 6 pm) and temperature and humidity-controlled room. Like most commonly used laboratory animals, mice are nocturnal so in the dark cycle of the facility is when their activity is the highest. Working after 6pm should be avoided since alterations on the photoperiod could cause reproduction or behavioral problems. There are other factors, such as loud noise, too many different people handling the animals or strong odors that may also alter mice's biological rhythms.

Until the beginning of the experiments, or unless stated, mice were housed in cages placed in ventilated racks, fed with standard chow and had access to drinking water *ad libitum*. Animals were fed with two different standard chow depending on their developmental stage. RM3 diet (Special Diet Services) (22.4% protein) was supplied from the after-weaning period until the age of two months, then it was changed for RM1 diet (Special Diet Services) (14.8% protein) for the adulthood. According to current legislation, the number of adult animals in one cage should never be higher than 5. Female mice can be separated and housed together anytime during their life in order to maximize number of animals per cage and minimize space used, but care has to be taken when housing together adult males. Even though mice are not

aggressive towards other species, humans included, and their instinctive reaction is to escape, towards other male mice they become territorial and hostile, leading to fights and bites that can badly damage the animals. Young males at weaning day can be housed together even if they come from different littermates, but after one month-old it is strongly recommended not to do so. Notwithstanding, aggressions may occur within littermates and, therefore, the aggressor -the only one in the cage without wounds- has to be separated into a new cage.

LPI was induced by changing the standard chow with tamoxifen diet TAM400/CreER (Envigo) for one week with. Afterwards, tamoxifen diet was changed for a low protein diet (Research Diets, D06111601) (8% casein), and animals were kept with this diet until they were sacrificed for experiments. For the group of treated animals, L-citrulline (C7629-100mg., Sigma) was supplemented in the water drink (1g/L).

Metabolic cages

For the collection of urine and feces of mice metabolic cages were used. This sort of cages are specially designed to allow separate collection of urine and feces from mice, as well as controlling the water and food intake. The principle of a metabolic cage (**Figure 7**) is to house individually a mouse in an enclosure with a wire grid floor (**Figure 7**), which is wide enough so feces and urine are not retained. The upper-chamber is made of smooth, gnaw-proof polycarbonate, transparent to admit total room light. Mice have access to water and food (**Figure 7**). A collection tube is placed below the drinking bottle in order to collect possible water that may leak from the bottle and, thus avoid wrong water intake measurements or dilution of urine collected. For proper separation of samples, the cage is designed so that the urine slides down the funnel and is redirected to the urine collector by a ring placed at its end, and feces are collected simply by gravity into another container.

As a general procedure, mice were housed individually in these cages for 4 days, with the first day (day 1) as an adaptation period to the new environment. Samples from the first 24 hours were not analyzed. For analysis, urine from 2nd, 3rd and 4th day was collected. 50 µl of thymol 10% in isopropanol were added to urine collector tubes to preserve the sample. Appropriate chow (standard or low protein) was powdered and passed through a sieve. Mice, chow, water, feces and urine were weighed daily, as well as collection tubes and funnels were changed every day. All procedures concerning the metabolic cages (sample collection and weights) were done always between 10 – 12am to obtain reliable 24-hours data. Metabolic cages were

placed in a separate room from the animal room but maintaining the light-dark cycles and climate conditions.

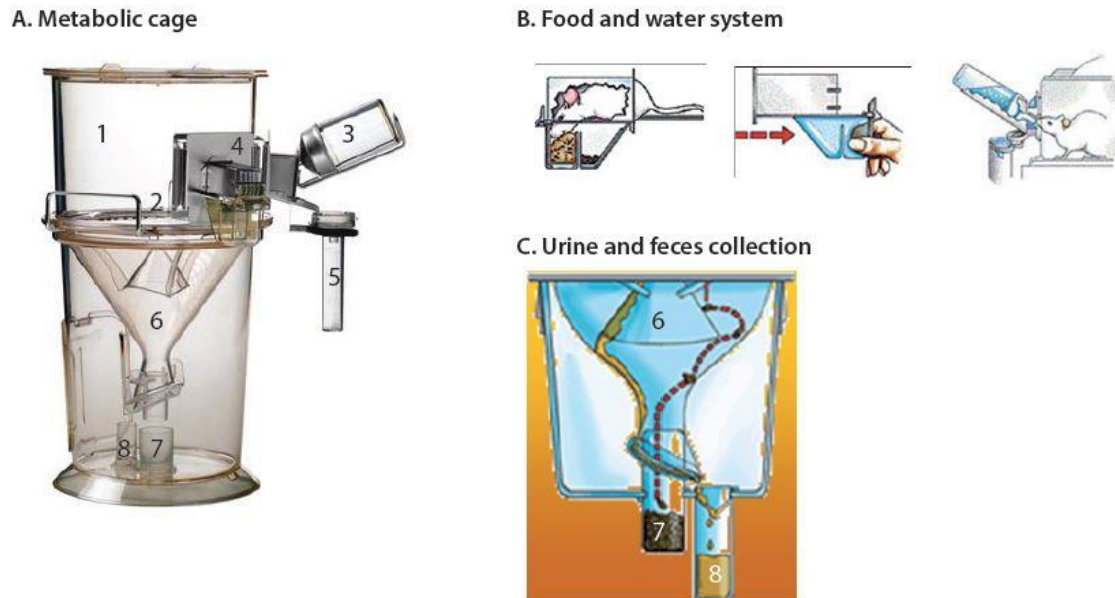


Figure 7 Metabolic cages components. A. Metabolic cage. 1. Living space. 2. Grid. 3. Drinking water bottle. 4. Feeder chamber with food drawer. 5. Water collection tube for leaks. 6. Collection funnel. 7. Feces collection tube. 8. Urine collection tube. B. Food and water system. To access the food chamber, the animal has to enter it through a trap door, so no food can be spilled in the cage. C. Urine and feces collection. The collection funnel is coated with a silicone that allows urine slip and prevents feces from sticking, assuring the correct separation of samples.

Routinely, animals were sacrificed for experiments in CO₂ chambers or by cervical dislocation. Obtaining of different tissues of interest was done according to a standard necropsy protocol, using sterile material (forces, scissors, gauzes), cleaned with water and soap and with ethanol 70% between animals. When needed, tissues were weighed using a precision balance and afterwards, tissues were snap frozen in liquid nitrogen and then stored at -80°C until further use for RNA or protein extraction, fixed in PFA for histological analysis or freshly processed for cell sorting or primary cultures.

Blood collection was usually done by intracardiac puncture. Before proceeding, EDTA 0,2M was passed through 1 mL syringes with 25G needle several times in order to “coat” the syringe with EDTA to prevent coagulation of the blood when collecting sample. Blood was collected into Microvette EDTA-tubes CB300 (Sarstedt). For hematologic analysis 200µl of blood were separated. Hemogram was done using Abacus JuniorVet (Diatron) device. For plasma collection, blood was centrifuged for 10 minutes 3000rpm 4°C and plasma was separated and frozen at -80°C.

Slc7a7^{-/-} mouse model:

As explained in the introduction, *Slc7a7* null mice is perinatally lethal. To overcome this problem and be able to model human LPI a new inducible mouse model was generated, *Slc7a7*^{-/-} mouse model. This mouse model was generated by GenOway (Lyon, France).

The mouse *Slc7a7* gene is located on chromosome 14 and extends on around 46 kb. Mouse *Slc7a7* gene is composed of 12 exons, separated by 11 introns ranging between 201 and 34688 bp (Figure 8). The open reading frame encodes for a 510 amino acid polypeptide. The translation initiation site is located in exon 4 and the stop codon is located in exon 12 (Figure 8).

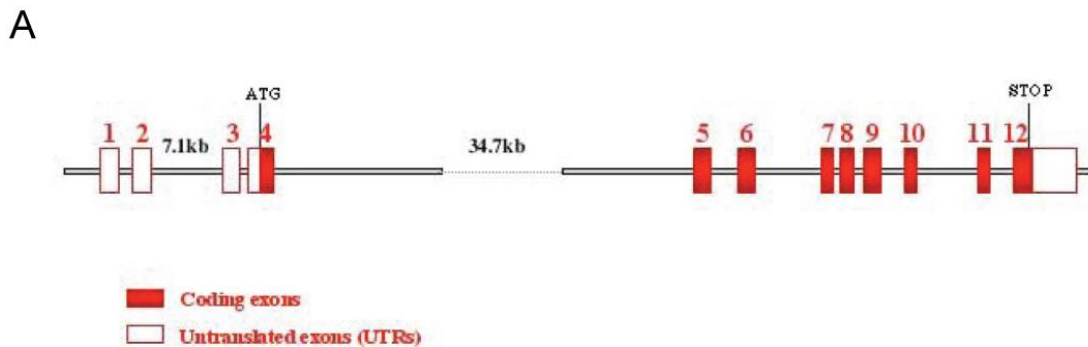


Figure 8 Schematic representation of the genomic organization of murine *Slc7a7* gene. Diagram is not depicted in scale. Dotted line represents uncharacterized sequences. Closed line corresponds to the intronic sequences. White boxes represent untranslated regions (5' and 3' UTRs).

Exons 3 and 4 were targeted to produce *Slc7a7*-loxP (Figure 9). The conditional ablation of *Slc7a7* gene was further achieved by breeding the animals with different Cre-expressing lines, and taking advantage of the Cre-lox technology, allowing the location and timing of gene expression to be closely regulated. In this thesis we generate two different Cre specific mice lines: *Slc7a7*^{LysM^{-/-}}, specific for some myeloid populations, and *Slc7a7*^{-/-} with Cre-UBC promoter, ubiquitously expressed in all cells after tamoxifen induction. For the conditional expression of Cre recombinase, Cre-ERT2 mouse line was used (B6.Cg-Tg(UBC-cre/ERT2)1Ejb/2J, The Jackson Laboratory, stock #008085). The Cre-ERT2 fusion protein consists of Cre recombinase fused to a triple mutant form of the human estrogen receptor; which does not bind its natural ligand (17 β -estradiol) at physiological concentrations but will bind the synthetic estrogen receptor ligands 4-hydroxytamoxifen (OHT) and, with lesser sensitivity. Restricted to the cytoplasm, Cre-ERT2 can only gain access to the nuclear compartment after exposure to OHT. Cre

recombinase-mutated estrogen receptor fusion protein is expressed under the control of the human Ubiquitin C (UBC) promoter (Cre_UBC). When these Cre-ERT2 mice are bred with mice containing a *loxP*-flanked sequence of interest, tamoxifen-inducible, Cre-mediated recombination will result in deletion of the flanked sequences in widespread cells/tissues. This Cre-ERT2 transgenic mouse line was generated via lentitransgenesis (Lois *et al.*, 2002); a self-inactivating lentiviral vector was designed with the human ubiquitin C (UBC) promoter sequence upstream of a Cre-ERT2 fusion gene (Cre recombinase fused to a G400V/M543A/L544A triple mutation of the human estrogen receptor ligand binding domain). Cre-ERT2-expressing lentivirus were microinjected into the perivitelline space of one-cell zygotes (129SvEv;C57BL/6 mixed genetic background). Morula and blastocyst stage embryos were implanted into pseudopregnant recipient mice. A founder with a single-copy integrant expressing high levels of Cre-ERT2 was chosen to establish the Cre-ERT2 lentitransgenic mouse line.

The general strategy for *Slc7a7* ablation is summarized in Figure 9. An additional step of *in vivo* excision of the Neomycin cassette was performed in order to avoid putative interferences of the Neomycin cassette with the *Slc7a7* promoter. The resulting chimeras were bred with C57Bl/6J WT mice in order to generate a pure line of excised mice. This extra breeding gave rise to three pure flp-excised heterozygous male mice. These animals were further backcrossed with C57Bl/6J animals until obtain a pure C57Bl/6J genetic background.

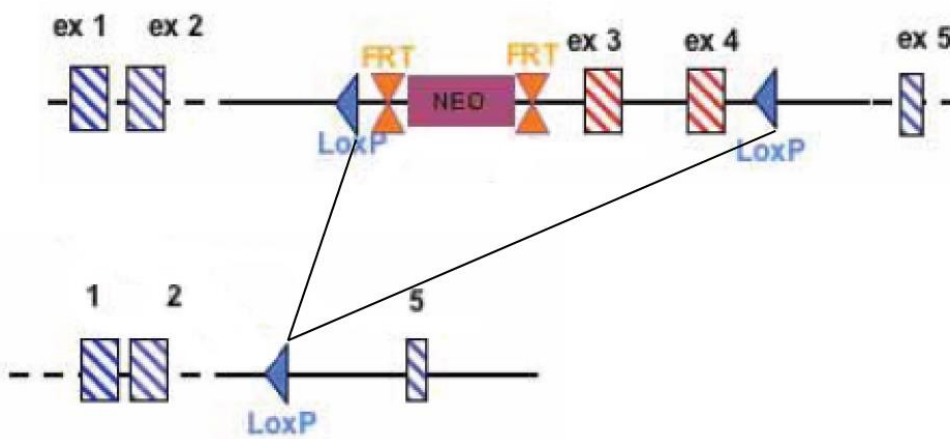


Figure 9 Schematic representation of the *Slc7a7*^{-/-} generation strategy. The exons are represented by boxes while line represent intronic sequences. In red are the targeted exons and in blue the rest of exons.

Additionally, a macrophage-specific KO mouse model was also needed. This new model was generated by breeding *Slc7a7-loxP* animals with a line that carried the Cre recombinase under

the Lysozyme 2 (*Lyz2*) promoter (*LysM*) (Clausen *et al.*, 1999). *LysM_Cre* animals were kindly relinquished by Prof. Angel Nebreda (B6.129P2-*Lyz2*^{tm1^(cre)/fo}/J, The Jackson Laboratory, stock #004781) . Although *LysM* expression has been shown to be shared between activated macrophages, monocytes and granulocytes and to be absent in some tissue resident macrophages (Hume, 2011), *LysM_Cre* mice are widely accepted as a macrophage-specific KO mouse model.

Genotyping:

Mice were genotyped by standard Polymerase Chain Reaction (PCR). DNA was extracted from tail or ear biopsies, digested and analyzed by regular PCR.

- Extraction of Genomic DNA from mouse tails:

Tails were digested with proteinase K (20mg/ml) at 55°C with shaking at 550rpm overnight prior to DNA extraction. After 15 minutes centrifuge at 13200 rpm and supernatant discard, 500µl of isopropanol were added. Tubes were twirled several times until “jellyfish DNA” formation, and centrifuge for 3 minutes at 13200 rpm. Supernatant was discarded, and 500µl of 70% EtOH were added to precipitate DNA. After 3 minutes centrifuge at 13200 rpm, tubes were air dried and afterwards resuspended in 200µl of mQ water.

Slc7a7^{-/-} genotyping:

Multiplex PCR is done to amplify loxP sites and Cre at the same reaction.

- Primers:

11857flp-SPE1: 5'- GGAGATTCCTGATCGAGCACCTTCTTATCAC -3'

11858flp-SPE1: 5'- GCTTTGTATTGCTTTTCCATTCCCAGATACC -3'

AF-Cre1: 5'- CGGTCGATGCAACGAGTGATGAGG -3'

AF-Cre2: 5'- CCAGAGACGGAAATCCATCGCTCG -3'

- PCR:

Reagent	Volume (μ l)	Cycles	Temperature	Time
DNA	1.5	1	95°C	5'
Primer 11857flp-SPE1 (10 μ M)	0.5	35	95°C	30''
Primer 11858flp-SPE1 (10 μ M)	0.5		60°	30''
Primer AF-Cre1 (10 μ M)	0.25		72°C	30''
Primer AF-Cre2 (10 μ M)	0.25			
dNTP	0.5	1	72°C	3'
Buffer 10x DNA polymerase	2.5	1	4°C	∞
H ₂ O mQ	19.125			
DNA polymerase (Biotools)	0.125			

Table 3. PCR conditions for *Slc7a7*LoxP sites and Cre recombinase.

PCR results were ran in 2% agarose gel for 45 minutes 100V.

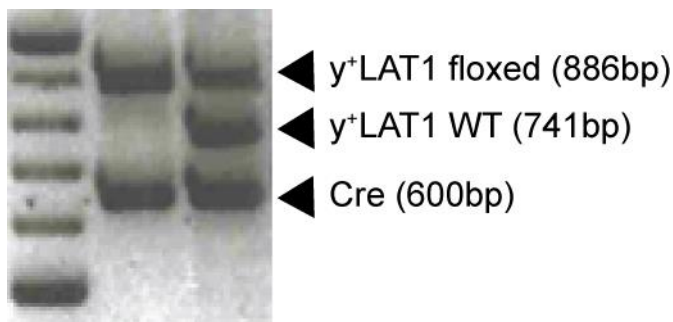


Figure 10. Genotyping PCR products. First lane is ladder. Second and third lane depict all the possible bands. The band meaning together with molecular weight are also shown.

Slc7a7^{LysM^{-/-}} genotyping:

Two different PCR are carried out. The first reaction is the same reaction that for *Slc7a7*^{-/-} genotyping, aimed to identify the floxed alleles and the expression of the Cre recombinase. By contrast, the second reaction is aimed to check whether Cre recombinase is under the LysM (*Lyz2*) promoter. For the second reaction three different primers are used. One forward primer that anneals with the LysM promoter. One reverse primer that also anneals within the LysM promoter. And finally a second reverse primer that anneals within the Cre recombinase. By this strategy depending whether the animals express the LysM_Cre or not, two PCR products or only one, respectively, are obtained.

- Primers:

LysM_Forward: 5'- CTTGGGCTGCCAGAATTTCTC -3'

LysM_WT_Reverse: 5'- TTACAGTCGGCCAGGCTGAC -3'

LysM_Cre_Reverse: 5'- CCCAGAAATGCCAGATTACG -3'

- PCR:

Reagent	Volume (μ l)	Cycles	Temperature	Time
DNA	1.5	1	95°C	4'
LysM Forward (10 μ M)	0.5	35	95°C	30''
LysM Cre Reverse (10 μ M)	0.5		60°C	30''
LysM WT Reverse (10 μ M)	0.5		72°C	30''
dNTP	0.5	1	72°C	3'
Buffer 10x DNA polymerase	2.5	1	4°C	∞
H ₂ O mQ	19.125			
DNA polymerase (Biotools)	0.125			

Table 4 PCR conditions for Cre recombinase to determine the specific LysM promoter.

PCR results were ran in 2% agarose gel for 45 minutes 100V.

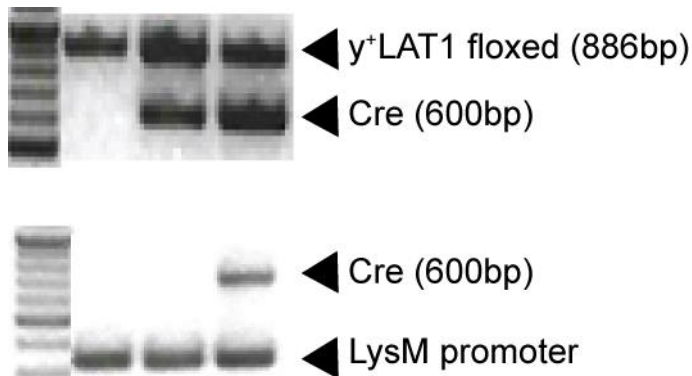


Figure 11 Genotyping PCR products. First lane is ladder. Up: result of the first PCR. LoxP sites and Cre expression are detected. Down: result of the second PCR. LysM promoter is detected. Second, third and fourth lane depict all the possible bands. The band meaning together with molecular weight are also shown.

Protein protocols

ELISA

Protein levels in mouse plasma of ferritin were quantified by an *in vitro* enzyme-linked immunosorbent assay (ELISA) kit, Ferritin (FTL) Mouse ELISA Kit (Abcam). In this assay, anti-ferritin antibodies have been adsorbed to the surface of polystyrene microtiter wells. Samples

are incubated in the wells to allow the ferritin present in the sample to react and hence form complexes with the anti-ferritin antibodies. Then secondary antibodies conjugated with horseradish peroxidase (HRP) are added. Finally, by the addition of a chromogenic substrate the amount of the enzyme bound in complex is measured with a spectrophotometer (450nm), and the quantity of ferritin present in the sample is proportional to the absorbance registered. To do this test, plasma samples were diluted 1:20, using 12.5 of plasma (in duplicates) for each mouse.

Protein levels in mouse plasma of Il-6 were also quantified by ELISA, using the Il6 (Mouse) ELISA Kit (Abnova). The assay principle is the same as the described for ferritin. Absorbance was also measured at 450nm. In this case, samples were not diluted and 100µl of plasma were directly incubated in the wells.

Protein levels of γ⁺LAT1 and ferroportin were quantified by western blot. As both proteins are membrane proteins, in order to enhance their detection membrane purification was performed.

Membrane purification and protein extraction

Material:

Membrane extraction buffer: Hepes 25mM, EDTA 4mM, Sucrose 250mM; pH 7.4.

Protease Inhibitor Cocktail Set III, Animal free, Calbiochem (#535140).

Mini-BeadBeater 24, Cell Disrupter, BioSpec Products Inc.

Ceramic beads, Laboratorios Conda (#13114-325).

Microfuge tubes polypropylene 1.5ml, Beckman Coulter.

Complete cell fractionation kit, Promokine (PK-CA577-K268).

From mouse tissues:

Frozen tissues were added to membrane extraction buffer plus protease inhibitor cocktail at a working dilution of 1:1000. Then tissues were disrupted for 2 cycles of 30 seconds $2.5 \cdot 10^3$ oscillations/minute with cell disrupter device. Then supernatant was collected and centrifuged for 10 minutes 10^4 rpm 4°C. Cell debris were discarded and supernatant was collected and ultracentrifuged for 1 hour at 55.000 rpm 4°C in TLA-55 rotor in Optima XLS centrifuge

(Beckman Coulter). Pellets were resuspended in membrane extraction buffer plus protease inhibitor. Routinely, half of a kidney was resuspended with 200ul of buffer.

From cultured BMDMs:

Cells were scraped and collected in cold PBS. Then centrifuged for 5 minutes at 1500 rpm 4°C. Membranes purification and protein extraction were done with Membrane protein extraction kit following manufacturer instructions.

Western Blot

The general premise of this technique relies in that proteins in a mixture are separated by molecular weight using polyacrylamide gel electrophoresis and then are transferred to a membrane made of nitrocellulose or polyvinylidene difluoride. Immobilized proteins are specifically detected using the appropriate primary and secondary antibodies. Primary antibodies bind the protein directly and they are recognized by a modified secondary antibody, usually linked to a reporter enzyme or a fluorophore, that can be detected and its signal quantified.

In this thesis secondary antibody detection was done by chemiluminescent detection. The secondary antibodies used were linked to a HRP which in the presence of the appropriate substrate produces luminescence.

In all western blottings, actin was used as the reference protein to normalize the amount of target proteins.

First of all, samples of a known protein concentration have to be prepared. To measure protein concentration Pierce assay (ThermoFisher Scientific) was used. For γ -LAT1 detection, samples of 50 μ g of protein were prepared. For ferroportin detection, samples of 30 μ g of protein were prepared. Protein extracts were mixed with 4x protein loading buffer and H₂O up to 30 μ l. Samples were heated for 5 minutes at 95°C and centrifuged at maximum speed for 30 seconds. Supernatant was then loaded into the corresponding well.

Electrophoresis: samples were ran in 10% acrylamide gels using the Mini-PROTEAN 3 Electrophoresis System (Bio-Rad). 100V were set up until samples were packed and passed the stacking area, and 150V until samples arrived to the end of the gel.

Transfer: proteins were transferred from the gels into PVDF membranes Immobilon-P (Merck Millipore, # IPVH00010) using the Mini Trans-Blot Electrophoretic Transfer Cell (Bio-Rad). For

γ^+ LAT1 detection transfer was done for 90 minutes at 250mA 4°C. Ferroportin transfer was performed for 90 minutes at 100V room temperature (RT).

Blocking: for γ^+ LAT1 1h RT with PBS-milk 5%. For ferroportin 1 hour RT with TBST- milk 3%.

Primary antibody incubation: both primary antibodies are homemade rabbit anti-mouse antibodies. γ^+ LAT1 antibody was generated at Manuel Palacin's laboratory by Dr. Susanna Boday, while ferroportin antibody was generated at Günter Weiss' laboratory. All the western blots for ferroportin detection, were done with the help of Markus Seiffert.

In both cases, membranes were incubated over night at 4°C. γ^+ LAT1 antibody was diluted 1:750 in PBS-milk 5%. Ferroportin was diluted 1:1000 in TBST-milk3%. For internal normalization, in both cases commercial anti β -actin was used (1:10000 in PBS-milk 1%) (Sigma, A1978-200UL).

Secondary antibody incubation:

- γ^+ LAT1: donkey anti-rabbit diluted in PBS-milk 1% (1:6500) 1 hour RT
- Fpn1: donkey anti-rabbit diluted in TBST-milk 1% (1:6500) 1 hour RT
- β -actin: donkey-anti mouse diluted in PBS-milk 1% or TBST-milk 1% (1:12500) 1 hour RT

In the case of ferroportin antibody detection was then accomplished incubating the membranes with Amersham ECL Western Blotting detection Reagents (GE Healthcare), and the image obtained with ChemiDoc MP Imaging System (Bio-Rad). In the case of γ^+ LAT1, membranes were incubated with Luminata Classico Western HRP Substrate (Merck Millipore), and the image obtained with Amersham Hyperfilm ECL and Hyperprocessor Automatic Film Processor (GE Healthcare). For β -actin both reagents were used, depending on the studied protein.

Gene expression

Gene expression levels were determined by mRNA analysis. RNA is a very labile molecule that can be easily attacked by RNases. Therefore, working with RNA needs an extra care and attention to avoid its degradation. All solutions that get in contact with RNA should be RNase-free. Gloves, filter tips and sterile material is mandatory as well. Pipettes and working surfaces can be decontaminated with RNaseZap solution before starting experiments.

RNA extraction

Material:

TRIzol Reagent, Ambion, Life Technologies (#15596-018)

Mini-BeadBeater 24, Cell Disrupter, BioSpec Products Inc.

Ceramic beads, Laboratorios Conda (#13114-325).

PureLink RNA Mini Kit, Invitrogen, ThermoFischer Scientific (#12183018A)

DNase PureLink Kit, Invitrogen, ThermoFischer Scientific (#12185010)

Reverse Transcriptase SuperScript II (ThermoFisher Scientific) (#100004925)

From mouse tissues:

Frozen tissues were resuspended in 500 µl of TRIzol and homogenized by 2 cycles of 30" 2.5·10³ oscillations/minute with cell disrupter device. Samples were kept for 5' at RT and centrifuged for 10' at 12000g 4°C. Supernatant was placed into a fresh tube. 200µl of chloroform were added. Samples were mixed vigorously, centrifuged for 15' at 12000g 4°C and upper phase was isolated with a 25G needle. Equal volume of EtOH 70% RNase free was added, kept for 10' at RT and vortexed. Then 700µl were placed into a purification column of PureLink RNA Mini Kit, and RNA was purified following manufacturer's instructions. A DNase treatment step was included.

From mouse freshly isolated macrophages:

Cells were centrifuged for 5' at 1300rpm RT and resuspended in 300 µl TRIzol. Then same protocol as for mouse tissues was followed.

From cultured BMDMs:

Growth media was removed and washed twice with PBS. Then cells were collected in 300µl of PureLink RNA Mini Kit's lysis buffer. Equal volume of EtOH 70% RNase free was added, kept for 10' at RT and vortexed. Then 700µl were placed into a purification column of PureLink RNA Mini Kit, and RNA was purified following manufacturer's instructions. A DNase treatment step was included.

From sorted cells:

From low number of cells (from 1000 to 7000) RNA was isolated in the Genomic facility of IRB Barcelona using a protocol based on magnetic beads and Agencourt RNAClean XP Kit (Beckman Coulter #A63987). Library preparation and amplification were performed as described

previously by Gonzalez *et al.*, 2010 (Gonzalez-Roca *et al.*, 2010). Amplification was performed for 22 cycles (Figure 12) and purified using PureLink Quick PCR Purification Kit (Invitrogen) in Genomic facility of IRB Barcelona.

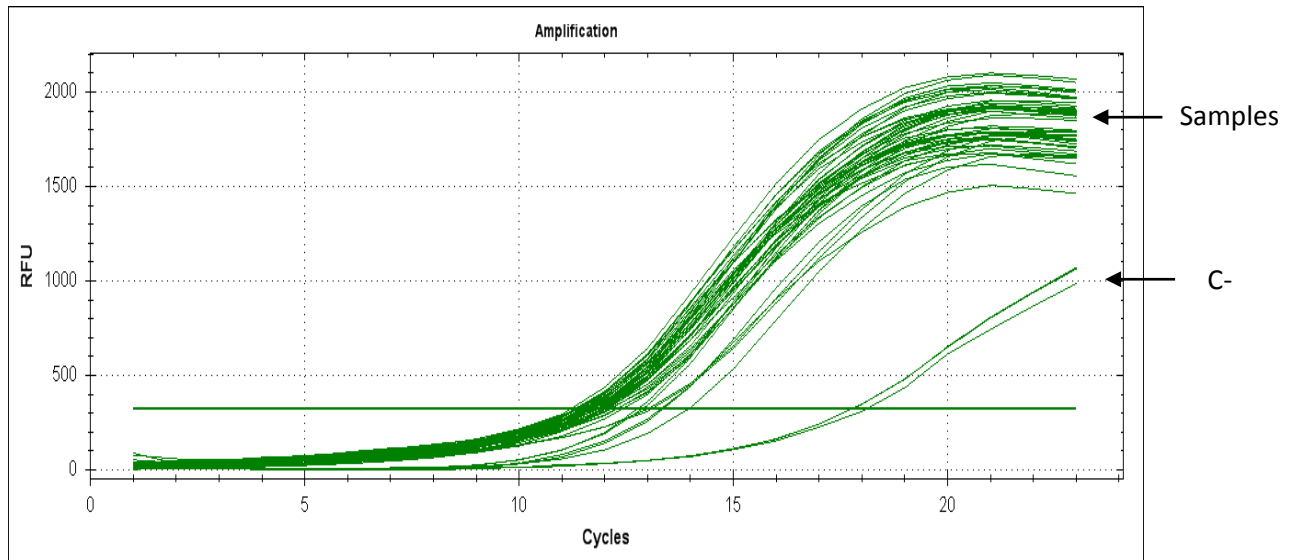


Figure 12 Representative image of CDNA amplification. All samples amplify in a similar way while the negative control (C-, no RNA) amplify many cycles after.

Quantification and integrity control:

RNA samples were quantified with NanoDrop ND-1000 (Figure 13) (ThermoFisher Scientific). The ratio of absorbance at 260nm and 280nm is used to assess the purity of DNA and RNA. A ratio of ~ 1.8 is generally accepted as “pure” for DNA; a ratio of ~ 2.0 is generally accepted as “pure” for RNA. If the ratio is appreciably lower in either case, it may indicate the presence of protein, phenol or other contaminants that absorb strongly or near 260nm. The absorbance ratio at 260nm and 230nm is used as a secondary measure of nucleic acid purity. The 260/230 values for “pure” nucleic acid are often higher than the respective 260/280 values. Expected 260/230 values are commonly in the range of 2.0-2.2. If the ratio is appreciably lower than expected, it may indicate the presence of contaminants which absorb at 230 nm.

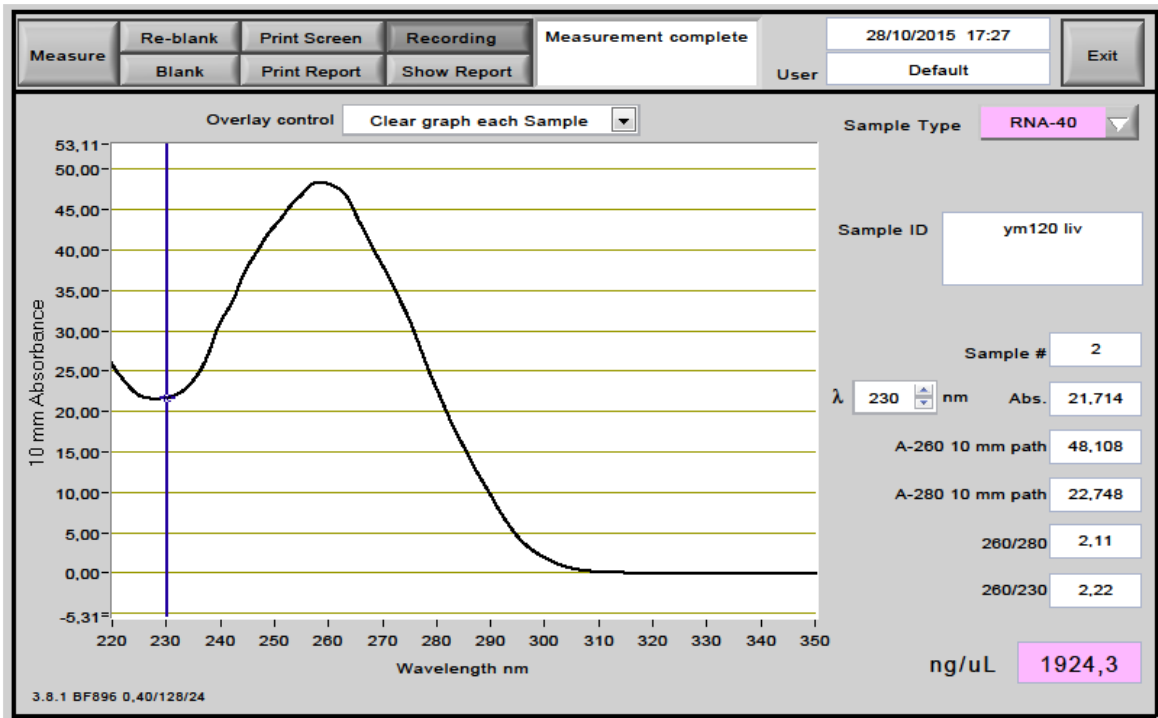


Figure 13. Representative image of Nanodrop RNA quantification. Sample concentration, absorbance peak and absorbance ratios 260/280 and 260/230 were taken into account.

Integrity of RNA samples obtained from mouse tissues or cultured cells was routinely checked up by running the samples in 1% agarose gel, 100V for 20 minutes. When RNA sample retains good integrity, two bands are clearly differentiated (Figure 14). When RNA sample is degraded, a smear is observed.



Figure 14. Representative image of RNA integrity test done with agarose gel. First lane is the ladder, second lane represents a good quality RNA sample and third lane represents a degraded RNA sample. 28s and 18s bands are marked.

Nevertheless, the integrity of the samples obtained from sorted cells was checked using the Agilent 2100 Bioanalyzer (Agilent Technologies). Samples are loaded in each well of this chip and are electrophoretically driven by a voltage gradient. During the chip run, dye molecules intercalate directly into RNA strands and these complexes are detected by laser-induced fluorescence. The software of the instrument translates this electrophoresis into gel-like images (bands) and electropherograms (peaks), comparing the ladder standard fragments to

the samples loaded and identifying ribosomal RNA peaks. At the end of the run, an RNA Integrity Number (RIN) is assigned to each sample on a scale of 1 to 10, being 1 the lowest and 10 the highest quality (Figure 15). This quality control becomes essential when high quality RNA is required (like high throughput gene expression assays).

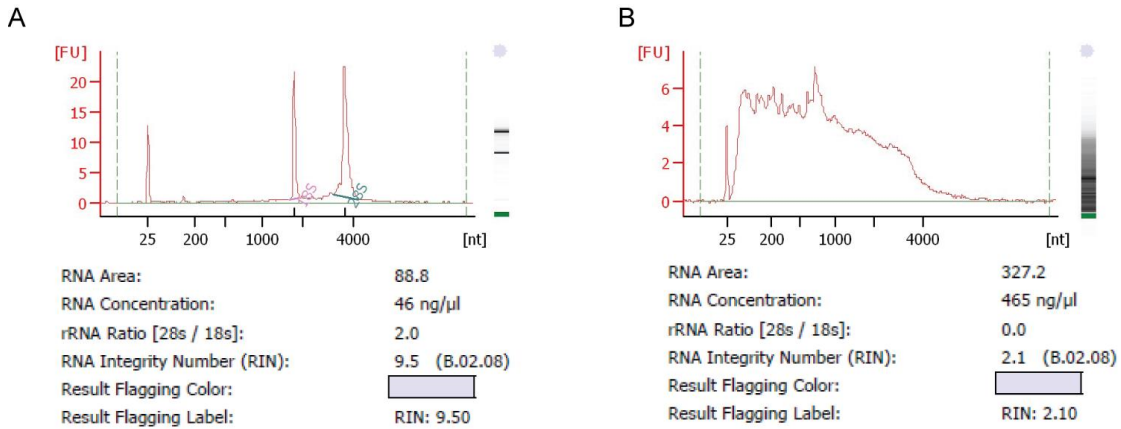


Figure 15. Representative image of RNA integrity test done with Bioanalyzer. A. exemplifies a good quality RNA sample. 18s and 28s peaks are well defined, consequently RIN gives 9.50. B. exemplifies a poor quality RNA sample. 18s and 28s peaks are not well defined, consequently RIN gives 2.10.

RT-PCR

cDNA from RNA samples were prepared by using SuperScript II technology. First, RNA samples were mixed with RNase free water and oligodT, and heated for 5 minutes at 65°C. Afterwards, a mix of buffer 5x, DTT, RNase inhibitor and dNTPs was added to samples. Then, samples were incubated for 50 minutes at 42°C. After the two initial minutes of incubation, 1ul of the enzyme was added. To stop reaction, enzyme was denatured by a step of 15 minutes at 70°C. Ideally, 1μg of RNA was used as template for cDNA generation. Sometimes samples did not reach this concentration so cDNA was done with less amount of RNA (depending on every specific experiment).

qRT-PCR

Usually, cDNA samples from sorted cells were diluted to 2ng/μl, while samples from cultured cells and mice tissues to 75ng/μl. mRNA quantity was measured by using Power SYBR Green PCR Master Mix (ThermoFisher Scientific, # 4367659) and analyzed in QuantStudio 6 Flex Real-Time PCR System (ThermoFisher Scientific). The expression levels were estimated by $2^{-\Delta\Delta Ct}$

method (Table 5). The gene expression for each individual sample was calculated based on the average of expression of all wild type samples. For the majority of experiments, β -actin was used as internal control for normalization. In the cases that other gene was used as internal control, it is indicated in the text.

Sample	Ct γ LAT1	Ct ACTB	Average Ct γ LAT1	Average Ct ACTB	Δ Ct γ LAT1	$\Delta\Delta$ Ct γ LAT1	$2^{(-\Delta\Delta$ Ct) γ LAT1
2652	17.357	13.687	16.807	13.358	3.450	1.327	0.399
	16.889	13.339					
	16.726	13.376					

Table 5. Exemplificative table for gene expression calculation.

Primers:

The pairs of primers used in this thesis have been either *de novo* designed or taken from an already published article. A complete list of the primers used, their target gene, sequence and design method are summarized in Table 6. In the case of primers taken from an already published article, sequence was confirmed to align with the desired gene by [BLAST](#). In addition, the melting curve was also checked to generate a unique peak.

In the case of *de novo* designed primers, first, the sequence of the gene was obtained from BLAST or [UCSC](#) genome browser. Then primers for the sequence were designed using Primer-BLAST tool or [Primer3](#). Some parameters were taken into account in order to choose the best primer pair: the product length should be around 200bp, the melting temperature should be between 57 and 60°C, G-C content should be between 40 and 55%, self complementarity between 1 and 3 and for self 3' complementarity, the optimum is 0. To test *in silico* self complementarity the Oligo Analysis Tool ([OAT](#)) was used. Finally, to test *in silico* the product amplified, the UCSC's tool In-Silio PCR was used.

Primer Name	Target Gene	Sequence	Design
y⁺LAT1 CreUBC FW	<i>Slc7a7</i>	TCAACAGCACCAAGTATGAAGTG	<i>de novo</i> designed
y⁺LAT1 CreUBC RV	<i>Slc7a7</i>	AGCCCAGATGACCAGTGAGA	<i>de novo</i> designed
my⁺LAT2-Fw	<i>Slc7a6</i>	CCTTGGCCATTGGGATTTCTAT	Martin <i>et al.</i> , 2006
my⁺LAT2-Rv	<i>Slc7a6</i>	ACAGCCACAGCGTCACTCTTATG	Martin <i>et al.</i> , 2006
mCAT1-Fw	<i>Slc7a1</i>	CTTGGACCAGTGCAAATGACG	Yeramian <i>et al.</i> , 2006
mCAT1-Rv	<i>Slc7a1</i>	TGATCCTGAGGCATGAGTGCA	Yeramian <i>et al.</i> , 2006
mCAT2-Fw	<i>Slc7a2</i>	GTGAAGAGGTTCCGGAATCCACA	Yeramian <i>et al.</i> , 2006
mCAT2-Rv	<i>Slc7a2</i>	CGTTAAAGCTGCAGA	Yeramian <i>et al.</i> , 2006
GM-CSFRa-Fw	<i>Csf2ra</i>	GAGTGACGTGCAGGAGGTTC	Nakamura <i>et al.</i> , 2013
GM-CSFRa-Rv	<i>Csf2ra</i>	TTCCTGTCAGTCACGTTGGG	Nakamura <i>et al.</i> , 2013
GM-CSFRbc-Rv	<i>Csf2rb</i>	AACATGACCTCTATCACCAG	Nakamura <i>et al.</i> , 2013
GM-CSFRbc-Fw	<i>Csf2rb</i>	GGAGTAGTAGTCTTCGTTTGTGA	Nakamura <i>et al.</i> , 2013
PU.1-Fw	<i>Spi1</i>	GATGCACGTCTCGATACTC	Nakamura <i>et al.</i> , 2013
PU.1-Rv	<i>Spi1</i>	TCATCTGAGCTCTGCTGGTG	Nakamura <i>et al.</i> , 2013
LPLA2-Fw	<i>Pla2g15</i>	GGGTAACCAGTTGGAAGCAAA	<i>de novo</i> designed
LPLA2-Rv	<i>Pla2g15</i>	TTGTCAATCCAGCAGTCAATGAT	<i>de novo</i> designed
PPARg-Fw	<i>Pparg</i>	TGTGAGACCAACAGCCTGAC	Nakamura <i>et al.</i> , 2013
PPARg-Rv	<i>Pparg</i>	TATCAGTGGTTCACCGCTTC	Nakamura <i>et al.</i> , 2013
Abcg1-Fw	<i>Abcg1</i>	GCCTACTACCTGGCAAAGACC	Nakamura <i>et al.</i> , 2013
Abcg1-Rv	<i>Abcg1</i>	AGCAGCGAACAGCACAAAAC	Nakamura <i>et al.</i> , 2013
Hepcidin Fw	<i>Hamp1</i>	TGCAACAGATACCACACTG	Galy <i>et al.</i> , 2013
Hepcidin Rv	<i>Hamp1</i>	CCTATCTCCATCAACAGAT	Galy <i>et al.</i> , 2013
Actin β Fw	<i>Actb</i>	GGTCATCACTATTGGCAACGA	Sala <i>et al.</i> , 2014
Actin β Rv	<i>Actb</i>	GTCAGCAATGCCTGGGTACA	Sala <i>et al.</i> , 2014
Spic Fw	<i>Spic</i>	TCCGCAACCCAAGACTCTTCAA	Haldar <i>et al.</i> , 2014
Spic Rv	<i>Spic</i>	GGGTTCTCTGTGGGTGACATTCCAT	Haldar <i>et al.</i> , 2014
HO1 Fw	<i>Hmox1</i>	ACATCGACAGCCCCACCAAGTTCAA	Sun <i>et al.</i> , 2002
HO1 Rv	<i>Hmox1</i>	CTGACGAAGTGACGCCATCTGTGAG	Sun <i>et al.</i> , 2002
CD163 Fw	<i>Cd163</i>	GCTAGACGAAGTCATCTGCACTGGG	Kovtunovych <i>et al.</i> , 2010
CD163 Rv	<i>Cd163</i>	TCAGCCTCAGAGACATGAACTCGG	Kovtunovych <i>et al.</i> , 2010
Marco-Fw	<i>Marco</i>	GGCACCAAGGGAGACAAA	Thelen <i>et al.</i> , 2010
Marco-Rv	<i>Marco</i>	TCCCTTCATGCCCATGTC	Thelen <i>et al.</i> , 2010
GAPDH	<i>Gapdh</i>	GCGGCACGTGATCCCA	<i>de novo</i> designed
GAPDH	<i>Gapdh</i>	CATGGCCTTCCGTGTTCTTA	<i>de novo</i> designed
Fpn1 Fw	<i>Slc40a1</i>	GTCGGCCAGATTATGACATTTG	Zhang <i>et al.</i> , 2011
Fpn1 Rv	<i>Slc40a1</i>	ATTCCAACCGGAAATAAAACCA	Zhang <i>et al.</i> , 2011
IL1b-FW	<i>Il1b</i>	AAGGAGAACCAAGCAACGACAAAA	<i>de novo</i> designed
IL1b-RV	<i>Il1b</i>	CTTGGGATCCACACTCTCCAG	<i>de novo</i> designed
Mrc1	<i>Mrc1</i>	CATCTTCGGGCCTTTGGAATA	Nakamura <i>et al.</i> , 2013
Mrc1	<i>Mrc1</i>	TGACCACTCTGCTGCTTTAG	Nakamura <i>et al.</i> , 2013
Msr1	<i>Msr1</i>	TGAACGAGAGGATGCTGACTG	<i>de novo</i> designed
Msr1	<i>Msr1</i>	TGTCATTGAACGTGCGTCAAA	<i>de novo</i> designed
Tim4	<i>Timd4</i>	GGCTCCTTCTACAAGAAACCACA	Miyanishi <i>et al.</i> , 2007
Tim4	<i>Timd4</i>	TCAGCTGTGAAGTGGATGGGAGA	Miyanishi <i>et al.</i> , 2007

Table 6. Primer list.

In the case of *Slc7a7* specific primers for *Slc7a7*^{-/-} were designed (y⁺LAT1 CreUBC FW, y⁺LAT1 CreUBC RV) (Figure 16). *LoxP* sites included exon 3 and 4 of *Slc7a7* gene. Exon 3 and the

beginning of exon 4 are non coding regions. Thus mRNA sequence was obtained and specific primers for the coding region of exon 4 were designed.



Figure 16. mRNA sequence of *Slc7a7* gene. Specific primers were designed to align within the coding region of the ablated exon 4.

Product length, G-C content and melting temperature, were within the desirable ranges. Then *In-Silico* PCR was done to predict the position of the product. As can be observed in Figure 17, the PCR product aligned with *Slc7a7*, corroborating the specificity of the primer pair.

UCSC In-Silico PCR

The sequences and coordinates shown below are from UCSC Genes, not from the genome assembly.

```
>uc007tvv.2 Slc7a7:272+501 230bp TCAACAGCACCAAGTATGAAGTG AGCCAGATGACCAGTGAGA
TCAACAGCACCAAGTATGAAGTGgctgctcagcagcagggccgacgatggc
tctgctctcggggatggggccagccagtcaggcgggagcaggcctcaactgaa
gaaggagatctccctgcttaatggcgtgtgtctcatagtggggaacatga
tcggctccggcatctttgtctcccctaagggtgtgtctcatgtacagtgcc
cttttggccTCTCACTGGTCATCTGGGCT
```

Figure 17. Result of the in-silico PCR for γ -LAT1 CreUBC primers. It can be observed that the PCR product aligns with *Slc7a7* gene.

Finally the complementarity of the primers was tested, and no conflicting complementarity was observed (Figure 18).

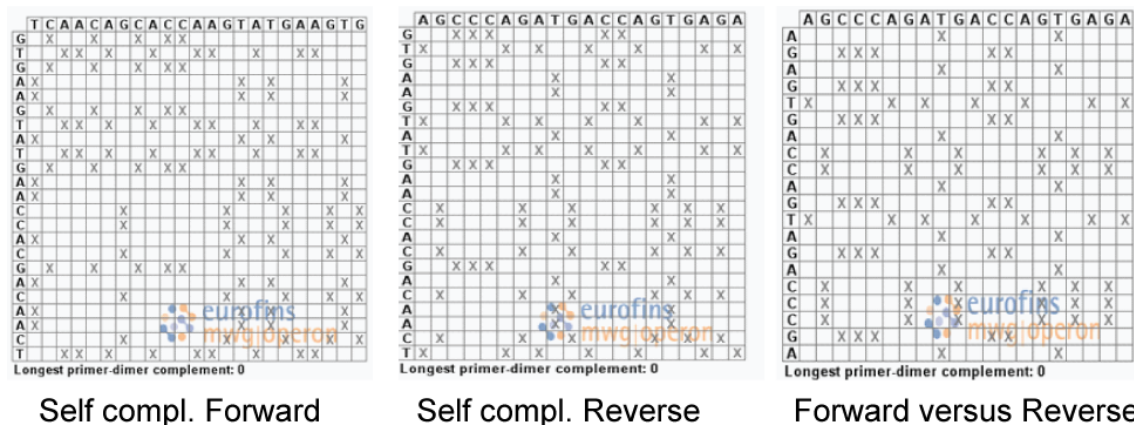


Figure 18. In-Silico self-complementarity test of γ -LAT1 CreUBC primers.

Microarray

This procedure was performed in the Genomics core facility and analyzed by Biostatistics core facility of IRB Barcelona. 8.5 ug of the cDNA from each sample were fragmented and labeling with GeneChip Mapping 250 K Nsp assay kit (Affymetrix) following the instructions of manufacturer. Finally, hybridization was performed using the GeneAtlas Hyb, Wash and Stain Kit for 3' IVT arrays. The complete protocol is summarized in Table7.

Samples ready to hybridize were denatured at 96°C for 10 min prior to incubation into Mouse MG-430 PM Array Strip, the Hybridization was performed for 16 h at 45 °C in the GeneAtlas Hybridization Oven (Affymetrix). Washing and Stain steps after hybridization were performed in the GeneAtlas Fluidics Station (Affymetrix), following the specific script for Mouse MG-430 PM Arrays. Finally, the arrays were scanned with GeneAtlas Scanner (Affymetrix) using default

parameters, and the generation of Cel files for bioinformatics analysis was done with GeneAtlas software (Affymetrix).

GEO format

Label:	biotin
Label protocol:	The indicated starting amount of total RNA was amplified using the TransPlex® Complete Whole Transcriptome Amplification Kit (Sigma; reference WTA2) and subsequently labeled using GeneChip Mapping 250 K Nsp Assay Kit (Affymetrix; catalog # 900766), according to manufacturer's instructions.
Hybridization protocol:	Affymetrix GeneAtlas Mouse MG-430 PM Array strip were hybridized with 8.5 ug of labeled, amplified dsDNA, washed, stained and scanned according to the protocol described in Affymetrix GeneAtlas Expression Analysis Manual.
Scan protocol:	Scanning was done on an Affymetrix GeneAtlas Scanner.
Description:	Gene expression data from X ng total RNA

Table 7. Summarized protocol for microarray experiment.

Microarray processing

Processing of microarray samples was carried out using packages *affy* (Gautier *et al.*, 2004) and *affyPLM* (Bolstad *et al.*, 2005) from R (R Core Team, 2016) and Bioconductor (Gentleman *et al.*, 2004). Raw CEL files were normalized using RMA background correction and summarization (Irizarry *et al.*, 2003). Standard quality controls were performed in order to identify abnormal samples (Gentleman, R., Huber, W., Carey, V., Irizarry, R. & Dudoit, 2005) regarding: a) spatial artefacts in the hybridization process (scan images and pseudo-images from probe level models); b) intensity dependences of differences between chips (MvA plots); c) RNA quality (RNA digest plot); d) global intensity levels (boxplot of perfect match log-intensity distributions before and after normalization and RLE plots); e) anomalous intensity profile compared to the rest of samples (NUSE plots, Principal Component Analyses). No sample was excluded for further analyses according to these quality control steps. Probeset annotation was performed using the information available in Affymetrix web page (Affymetrix Analysis Center. Netaffx. <https://www.affymetrix.com/analysis/index.affx>, accessed 03/13/2016).

Differential expression

A differential expression analysis was performed for *Slc7a7^{-/-}* and wild type comparisons using a linear model with empirical shrinkage (Smyth, 2004) as implemented in *limma* R package (Ritchie *et al.*, 2015). This model included the batch of scanning as covariate and the biological

replicate as random effect (Smyth, Michaud and Scott, 2005). Adjustment by multiple contrasts was performed by the Benjamini-Hochberg method (Benjamini and Hochberg, 1995).

Biological significance analysis

Pathway enrichment was assessed through the preranked version of Geneset Enrichment Analysis (GSEA) (Subramanian *et al.*, 2005). GSEA was applied to the ranking defined by the t-statistic of the differential expression analysis. Genesets derived from the KEGG pathway database (Kanehisa and Goto, 2000) and those annotated under Gene Ontology (GO) (Ashburner *et al.*, 2000) terms as collected in the *org.Mm.eg.db* R package (Ploner, 2015) were used for these analyses. Expression data was summarized to the gene level using the probesets showing the highest median absolute deviation within each gene.

Clustering and visualization

Gene expression of selected pathways were graphically represented in a heatmap using the *Heatplus* R package (Ploner, 2015) after centering and scaling the expression matrix gene-wise. Previously, expression data was summarized to the gene level using the most variable probeset mapping to the same gene (median absolute deviation). Genes and samples were clustered using the Ward agglomeration method and the correlation and euclidean distances, respectively.

Isolation of murine macrophages

Different populations of macrophages regarding their home tissue can be found. The diverse populations of tissue resident macrophages show different phenotypic and functional properties. The isolation and purification of the different macrophage populations varies regarding their anatomic localization. In this thesis alveolar macrophages, splenic red pulp and bone marrow derived macrophages were used.

Additionally, due to the low number of cells obtained by freshly isolation methods, a suitable *in vitro* model of differentiated macrophages was also needed. Cell culture techniques allow the growth of cells in a favorable artificial environment, providing good model systems for physiology and biochemistry studies. For this purpose, the most accepted model of *in vitro*

macrophages is the bone marrow derived macrophages (BMDM). This kind of cells were obtained directly from mechanical disaggregation of bone marrows of mice. Bone marrow derived macrophages were grown as adherent cultures and differentiated using appropriate culture medium. All procedures concerning cell culture were done under strict sterile conditions to prevent undesired contaminations.

Alveolar macrophages

Alveolar macrophages were isolated by performing bronchoalveolar lavages. Anesthetize animals were opened by the peritoneal cavity and sacrificed by bleeding through hepatic artery to avoid blood infiltration in lungs. Afterwards, thoracic cavity was opened carefully in order to keep lung intact and a small incision was done in the trachea in order to introduce the cannula (caliber 22). Once cannula was inside the trachea, trachea and cannula were tie together with black surgical silk (BBraun) to avoid the exit of the fluid.

Five 1ml aliquots of PBS were instilled per mice. Aliquots were recovered and combined resulting in a ~5ml final volume. This final volume was centrifuged for 10' at 400g 4°C. The liquid phase was discarded and the cell pellet was either used for cytospin preparations or for RNA extraction.

Splenic Red Pulp macrophages

RPM population was isolated by flow analytics cytometer sorting (FACS). The antibodies used to sort this population of cells were F4/80-PE, clone BM8 (BioLegend, #123109) (1:100), Cd11b-APC Cyan7, clone M1/70 (BD Pharmigen, #557657) (1:100) and Vcam1-FITC, clone 429 (BioLegend, #105705) (1:50), and the procedure was as follows:

1. Splenocytes extraction

Extract spleen and place it in a plate (60mm) with cold medium (PBS + 3%FBS, 6ml).

Disrupt spleen with the top of a syringe over a cell strainer of a 40µm (Falcon, #352340).

Collect it in a 15ml falcon.

Centrifuge 5' 1600rpm 4°C to remove media.

Discard supernatant and red pellet is resuspended in 5mL erythrocyte lysis buffer 1x (10x: NH_4Cl 1.7M; KHCO_3 120mM; EDTA 9mM; pH 7.3 4°C (adjust it with KOH), 5ml, weekly prepared). 5' RT in rotation.

Add 10ml PBS-FACS (PBS, 3% FBS, 2mM EDTA) to stop reaction.

Centrifuge 5' 1600rpm 4°C. Discard supernatant and resuspend pellet in 10ml of PBS-FACS 4°C and count cells in Neubauer's camera.

Prepare tubes or 96 well plates with 10^6 cells (controls), $\sim 7 \cdot 10^6$ cells (samples).

2. Blocking

Centrifuge 3' 300g 4°C.

Resuspend cells (10^6 in 100 μl of PBS-FACS 4°C). Adjust n° cells to volume.

Block with $\alpha\text{CD16/CD32}$ (BD Pharmigen, #553142) 3:100.

Incubate 15' 4°C (or 10' on ice).

Stop reaction adding 200 μl PBS-FACS and centrifuge 3' 300g 4°C.

3. Staining

Resuspend cells in PBS-FACS cold and add Ab mix.

Incubate 30' 4°C in darkness.

Stop reaction by adding 200 μl PBS-FACS and centrifuge 3' 300g 4°C.

Resuspend in 300 μl PBS-FACS and add 1 μl of DAPI to distinguish dead cells.

4. Sorting

Cell sorting was performed in BD FACSAria™ Fusion II (BD Biosciences).

Sorted cells were collected in 45 μl of lysis buffer (20 mM DTT, 10 mM Tris.HCl pH 7.4, 0.5% SDS and 0.5 $\mu\text{g}/\mu\text{l}$ proteinase K) for RNA extraction or in PBS for cytospin preparations. When collected for RNA extraction, immediately after their collection in lysis buffer, samples were incubated for 15' at 65°C and kept at -80°C until the RNA extraction.

Bone Marrow Derived Macrophages

Due to the elevated cost of recombinant M-CSF (recombinant murine M-CSF, Peprotech #315-02), depending on the sort of experiment BMDM were differentiated with recombinant murine M-CSF or with L-Cell supernatant. For preliminary trials and setting up experiments, BMDM differentiated with L-Cell were used. On the other hand, definitive experiments were carried out with BMDM differentiated with the recombinant cytokine. Based on the differentiation method, two different protocols were followed. For both protocols, mice's femur and tibia were peeled and kept in cold PBS until the primary culture room. Once in culture hood, sterilized tools were used and every step was done under the flow hood.

BMDM were differentiated for one week with DMEM, high glucose, pyruvate (Gibco, #41966029) (DMEM). For the amino acid-adjusted experimental conditions, DMEM without glutamine, lysine and arginine (Gibco, #A1443101) (DMEM-Arg) was used. Further supplementation with lysine (Sigma, #L5501), arginine (Sigma, #A5006) and citrulline (Sigma, #C7629) was done to set up the desired experimental conditions. The amino acid concentration found in the plasma of the mice as well as the amino acid concentration of the culture media is summarized Table 8.

(μM)	Plasma				Medium		
	WT with Cit	<i>Slc7a7</i> ^{-/-} with Cit	WT w/o Cit	<i>Slc7a7</i> ^{-/-} w/o Cit	DMEM	DMEM -Arg	FBS(μmol /100ml)
PSER	25.1	24.1	18.9	24.7			1.37
TAU	477.1	335.3	343.2	626.7			11.51
PEA	68.9	24.5	55.6	39.8			0.76
UREA	2177.5	2875.0	2623.6	3119.1			
ASP	30.6	19.6	8.6	13.0			6.95
THR	186.2	189.7	131.6	193.1	800	800	15.37
SER	139.0	144.6	92.8	139.2	400	400	29.36
ASN	39.8	61.4	37.8	56.0			49.38
GLU	56.1	56.8	32.7	56.6			67.58
GLN	591.3	839.5	507.1	1005.3	4000		49.38
SAR	59.2	729.4	296.9	379.3			
AAD	106.0	32.0	23.6	80.2			
GLY	211.4	210.7	155.3	244.9			64.17
ALA	518.3	451.4	313.7	528.5			92.46
CTR	71.9	119.2	49.0	84.1			10.3
AABA	7.1	12.1	7.0	9.0			
VAL	139.6	135.5	146.5	158.4	800	800	32.69
CYS	7.3	13.5	5.4	17.6			
MET	45.8	61.1	37.4	65.4	200	200	5.76
CYST	0.4	0.5	0.0	0.5	200	200	3.34
ILE	61.9	53.5	57.8	56.8	800	800	16.41
LEU	98.4	96.1	104.9	113.3	800	800	27.14
NLEU	75.8	98.6	86.2	97.7			
TYR	59.9	71.7	49.5	61.8	400	400	8.07
PHE	55.3	58.2	53.1	75.9	400	400	12.1
HOMOCYS	3.7	0.9	1.4	3.3			
GABA	189.4	73.6	59.2	73.1			
AMONI	110.4	114.4	84.4	425.6			
HLYS	4.6	1.7	0.4	0.5			
ORN	81.7	31.2	38.4	33.7			
LYS	253.5	159.2	464.6	196.2	800		20.1
1-HIS	6.9	1.7	3.1	2.9	200	200	6.43
ARG	47.9	31.1	39.1	20.7	400		8.48
HPRO	74.6	119.8	34.5	59.4			7.18
PRO	86.8	88.4	63.7	101.2			1.8

Table 8. Comparison for amino acid concentrations found in mice plasma and the different culture media used.

Murine recombinant M-CSF:

Bone marrows from each mouse were flushed with PBS+P/S (10%) into 50mL falcon using a 40µm strainer (Falcon, #352340). Pelleted cells were treated for 5' RT with RBC lysis buffer (R&D Systems, #WL2000). After stopping reaction with one volume of PBS+P/S, cells were resuspended in DMEM+P/S (10%)+FCS (10%)+M-CSF (50ng/ml) (Complete medium). 15 ml of complete medium per plate of 15 cm of diameter (Corning, #15430599) were used. Every two days medium was discarded and fresh complete medium was added.

L-cell supernatant:

Bone marrows from each mouse were flushed with DMEM. Cells were then, homogenized by passing 4-5 times through a 25-G needle. Cells were seeded in non-treated 15 cm plates (Clearline, #076060) with 30ml of Complete Medium (DMEM+30% L-Cell+10% FBS).

Generation of L-Cell supernatant:

0.5 10⁶ cells L929 (ATCC CCL1, NCTC clon 929), were placed in a 15 cm plate with 40ml DMEM +10%FBS +1% P/S. After 7 days of incubation, supernatants from every plate were collected, centrifuged for 5' 4°C 1500rpm, mixed and stored at -20°C in 50ml aliquots.

In order to check whether the batch is free of contamination, incubate a sample of 1-2ml at 37°C for a couple of days. It is also recommended to assess the biological efficiency of the supernatant. It can tested by doing a proliferation assay with BrdU.

Histology and cytology

Histology

Samples were fixed overnight at 4°C with neutral buffered formalin (HT501128-4L, Sigma-Aldrich). After fixation, bone tissue (femur) were washed with PBS 1x and decalcified with OSTEOSOFT® reagent (101728, Merck-Millipore) for 15 days at room temperature. All samples were embedded in paraffin. Paraffin-embedded tissue sections (2-3 µm in thickness) were air dried and further dried at 60 °C over-night, bone section were maintained at 60°C 48 hours (for iron special stain).

H&E and Special stainings

Paraffin-embedded tissue sections were dewaxed and stained with Haematoxylin eosin standard staining using a CoverStainer (Dako - Agilent), and Periodic Acid-Schiff (PAS) Stain Kit to identify surfactant (AR16592-2, Artisan, Dako, Agilent), Iron Stain Kit to identify iron pigments (AR15811-2, Artisan, Dako, Agilent) and Masson's Trichrome Stain Kit to identify collagen fibers and fibrin (AR17311-2, Artisan, Dako, Agilent) using the Dako Autostainer Plus (Dako, Agilent) following manufacturer procedures.

Immunohistochemistry stainings

Immunohistochemistry was performed using an Autostainer Plus (Dako-Agilent) for pulmonary surfactant-associated protein B (SP-B) and manually for F4/80 staining. Prior to immunohistochemistry, sections were dewaxed and therefore epitope retrieval was performed using Tris-EDTA buffer pH9 for 20min at 97°C using a PT Link (Dako, Agilent) or proteinase K ready to use (S3020, Dako, Agilent) for 5 min at room temperature (RT) for SP-B and F4/80 respectively. Washings were performed using the Wash Solution AR (AR10211-2, Dako, Agilent). Quenching of endogenous peroxidase was performed by 10 min of incubation with Peroxidase-Blocking Solution at RT (S2023, Dako, Agilent). Non-specific unions were blocked using 5 % of goat normal serum (16210064, Life technology) mixed with 2.5 % BSA diluted in wash buffer for 60 min at RT or 10 % of Normal Donkey serum (017-000-121, Jackson Immunoresearch) mixed with 2.5 % BSA diluted in wash buffer for 60 min at RT. For SP-B, the rabbit Anti-mature SP-B (WRAB-48604, Seven Hills Bioreagents) primary antibody was used at 1:1500 and incubated for 60 min at RT. The secondary antibody used was a BrightVision Poly-HRP-Anti Rabbit IgG Biotin-free, ready to use (DPVR-110HRP, Immunologic). For F4/80, the rat monoclonal Anti-F4/80, clone BM (14-4801-85, eBioscience) primary antibody was used at 1:100 (diluted in wash buffer with 5 % BSA) was incubated overnight at 4°C. The secondary antibody used was a Biotin-SP (long spacer) AffiniPure Donkey Anti-Rat IgG (H+L) (712-065-150, Jackson Immunoresearch) at 1:500 (in wash buffer) for 60' followed by amplification with Streptavidin-Peroxidase polymer at 1:1000 (S2438-250G, Sigma-Aldrich/Merck). Antigen-antibody complexes were revealed with 3-3'-diaminobenzidine (K346811, Dako), with the same time exposure (1 min). Sections were counterstained with hematoxylin (CS700, Dako, Agilent) and mounted with Mounting Medium, Toluene-Free (CS705, Dako, Agilent) using a Dako CoverStainer. Specificity of staining was confirmed by omission of the primary antibody or staining with rabbit IgG, polyclonal - Isotype control (ref: ab27478, Abcam) for F4/80 and SP-B, respectively.

Cytology

Preparations were done using Cytospin 4 (Thermo Fisher Scientific). Sorted red pulp macrophages were cytospun for 10' 10000 rpm. Suspension of AM were cytospun for 3' 600 rpm. Slides were air-dried for 30', fixed with CH₃OH for 30'' and stained with Quick Panoptic, a differential staining that allows distinguish the different blood cells (Química Clínica Aplicada, #993090) following manufacturer instructions. In the case of sorted red pulp macrophages, were also stained with Perls' Prussian blue as described for histology.

Image acquisition:

Brightfield images were acquired with were taken with Nikon E800 (Nikon) and Olympus DP72 (Olympus) or NanoZoomer-2.0 HT C9600 digital scanner (Hamamatsu) equipped with a 20X objective. All images taken with NanoZoomer were visualized with the NDP.view 2 U123888-01 software (Hamamatsu, Photonics, France), and with a gamma correction set at 1.8 in the image control panel of the NDP.view 2 U12388-01 software (Hamamatsu, Photonics, France). Areas of AM were calculated with ImageJ (Fiji).

Non-heme iron tissue quantification

2 to 3mm sections of freshly extracted tissues were weighted, quickly frozen in liquid nitrogen and stored at -80°C until iron determination. Non-heme iron quantification was done by Jorge Couso at Mayka Sanchez's lab following a modified protocol from Patel *et al.*, 2002.

In vitro assays

Nitric Oxide

For nitric oxide production of BMDMs assessment, 10⁵ cells per well were seeded in 96 wells plate and stimulated with LPS 100ng/ml (LPS from E.coli 055:B5, #L2880 Sigma) and IFN γ 50ng/ml (Preprotech #315-05) for different time points. The produced nitric oxide was measured in form of nitrate (soluble form) using the Griess Reagent System (Promega) or the Griess-Ilovay's nitrite reagent (Merck) by following the manufacturer instructions. Duplicates

were prepared for each sample. Absorbance was measured within 30' in a plate reader between 520nm and 550nm.

Erythrophagocytosis Assay

To test *in vitro* erythrophagocytosis, BMDM were co-cultured with erythrocytes to allow their engulfment. Erythrocytes were first labelled with a general membrane marker. After a co-incubation period of 2 hours, the non-engulfed erythrocytes are washed and macrophages are analyzed by FACS. So, macrophages with engulfed erythrocytes can be detected.

Material:

CellVue claret Far Red fluorescent cell Linker Midi Kit (MINCLARET-1KT, Sigma)

PKH26 Red Fluorescent Cell Linker Kit for general cell membrane labelling (PKH26GL-1KT, Sigma)

Erythrocyte labelling

Blood was collected in heparin tubes, centrifuged at 400g for 5', and plasma and buffy coat discarded. Erythrocytes were aged for 1 week at 4°C, and eventually stressed by being incubated for 20' at 48°C.

Stainings were diluted in diluent C (4:1000). Then, one part of erythrocytes was resuspended in the same volume of diluent C. The same volume of staining mix was added and incubated for 2' at dark. 20ml of DMEM-10%FCS to stop reaction were added, and sample were centrifuged at 400g for 5'. One wash with PBS wash done. Labeled-erythrocytes were then resuspended in sterile PBS.

Phagocytoses assay

10⁶ BMDMs were seeded in 6 wells plates 16h prior to experiment. 2h stimulation of BMDMs with LPS 100ng/ml was done prior to the addition of erythrocytes. Ten times the number of BMDM of erythrocytes were added, and co-incubated for 2h. Medium was discarded, cells were washed twice with PBS and RBC lysis step was done. Finally, cells were collected and analyzed by flow cytometry using CytoFLEX platform (Beckman Coulter).

Erythropoiesis analysis

Erythropoiesis in bone marrow of animals was analyzed by FACS. The percentages of the different erythroid precursors were assessed as described by Chen *et al.*, 2009 (Chen *et al.*, 2009). The antibodies used were CD44-APC, clone IM7 (BioLegend, #103011) (1:200), CD71-PE, clone C2 (BD Pharmingen, #553267) (1:800) and TER-119-FITC, clone TER-119 (BioLegend, #116205) (1:200).

Bone marrows from each mouse were flushed (25G needle) with PBS+P/S (10%) into 50mL falcon using a cell strainer of 40 μ m (Falcon, #352340). About 10⁶ of cells were used for each analysis. Cells were resuspended in 100 μ l of PBS-FACS and blocked with α CD16/CD32 (BD Pharmingen) 3:100 for 15' 4°C. To stop reaction 200 μ l PBS-FACS were added and centrifuge 3' 300g 4°C. Finally, cells were labeled by an incubation of 30' 4°C in darkness with the mentioned antibodies, add 1ul of DAPI and analyzed with CytoFLEX platform (Beckman Coulter). All procedure was done in 96 well plate.

RESULTS

“Dubium sapientiae initium”

René Descartes. (Attributed).

Previous results of the group

Since *null Slc7a7* mouse model is perinatally lethal (Sperandeo *et al.*, 2007), in collaboration with Professor G. Sebastio, our groups has generated a tamoxifen-inducible mouse model (*Slc7a7^{-/-}*). These animals deplete γ^+ LAT1 ubiquitously after tamoxifen induction. To address the effect of the metabolic hallmarks of LPI, two experimental groups of animals were established based on the treatment received: 8% protein diet (low protein diet, LPD) with and without citrulline. Both groups of animals were analyzed at the same time after tamoxifen induction (Figure 19). Most of the results presented in this section were obtained by Dr. Susanna Bodoy.



Figure 19. Schematic representation of the experimental strategy. Animals of 12 weeks of age were fed with tamoxifen diet for 1 week. After 1 week, tamoxifen was changed to 8% protein diet and one group of animals received citrulline (1g/L) in the water drink while the other group did not.

To validate the model we checked γ^+ LAT1 expression in kidney, intestine and bone marrow derived macrophages (BMDM), corroborating its ablation (Figure 20).

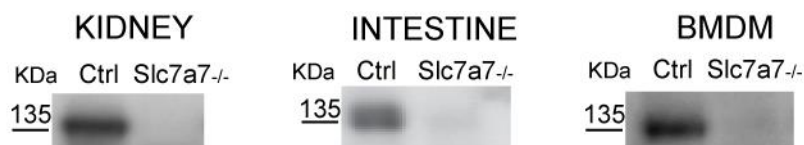


Figure 20. γ^+ LAT1 expression in kidney, intestine and bone marrow derived macrophages (BMDM). 50ug. of kidney, intestine and BMM membranes were loaded. A clear band at 135KDa corresponding to the heterodimer of γ^+ LAT1-4F2hc was observed in the Control (Ctrl) and it disappeared in the *Slc7a7^{-/-}* membranes.

We then assessed the viability of *Slc7a7^{-/-}* animals after the induction of LPI. 50% of *Slc7a7^{-/-}* mice which did not received citrulline died within the first month after tamoxifen induction, whereas most of the animals that received citrulline did not show survival problems for at least two months (Figure 21). Then, citrulline treatment clearly improved the severity of the disease.

RESULTS

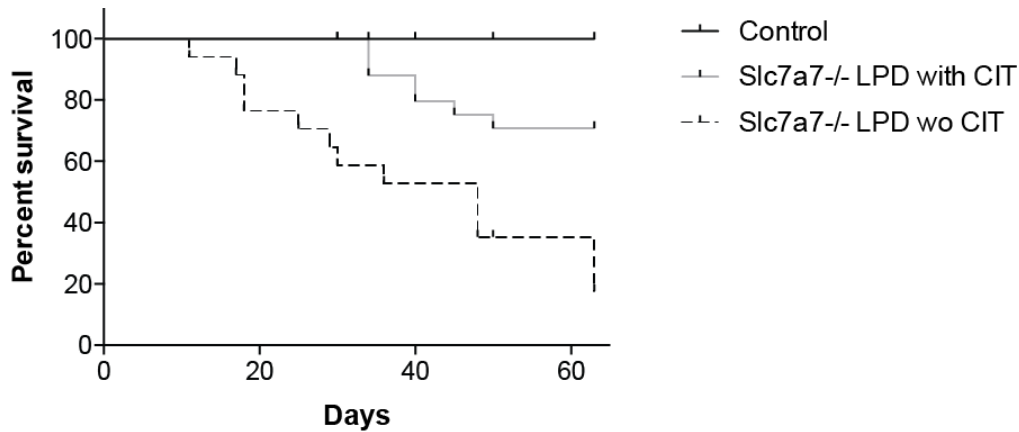


Figure 21. Survival curve of *Slc7a7*^{-/-} animals after tamoxifen induction. Citrulline supplementation (grey line) enhanced the survival rate of *Slc7a7*^{-/-} animals fed with 8% of protein diet versus *Slc7a7*^{-/-} without citrulline supplementation (dashed line). Black line represents wild type animals (*loxP* floxed Cre negative). Survival rate was monitored for 60 days with 15 animals per group.

Slc7a7^{-/-} mice suffered a severe loss of body weight, mainly explained by a reduction in the intake and by the dramatic loss of white adipose tissue (WAT) (Figure 22). The intake reduction is caused because of the discomfort generated by hyperammonemia, and consequently citrulline supplementation improved the intake of *Slc7a7*^{-/-} animals. In addition to the adipose tissue, spleen of *Slc7a7*^{-/-} mice also undergone a serious weight loss, whereas other tissues such as liver or kidney remained unaffected, indicating that the loss of tissue weight is specific for some tissues. Body, spleen and white adipose tissue weight loss were mitigated by citrulline supplementation (Figure 22).

RESULTS

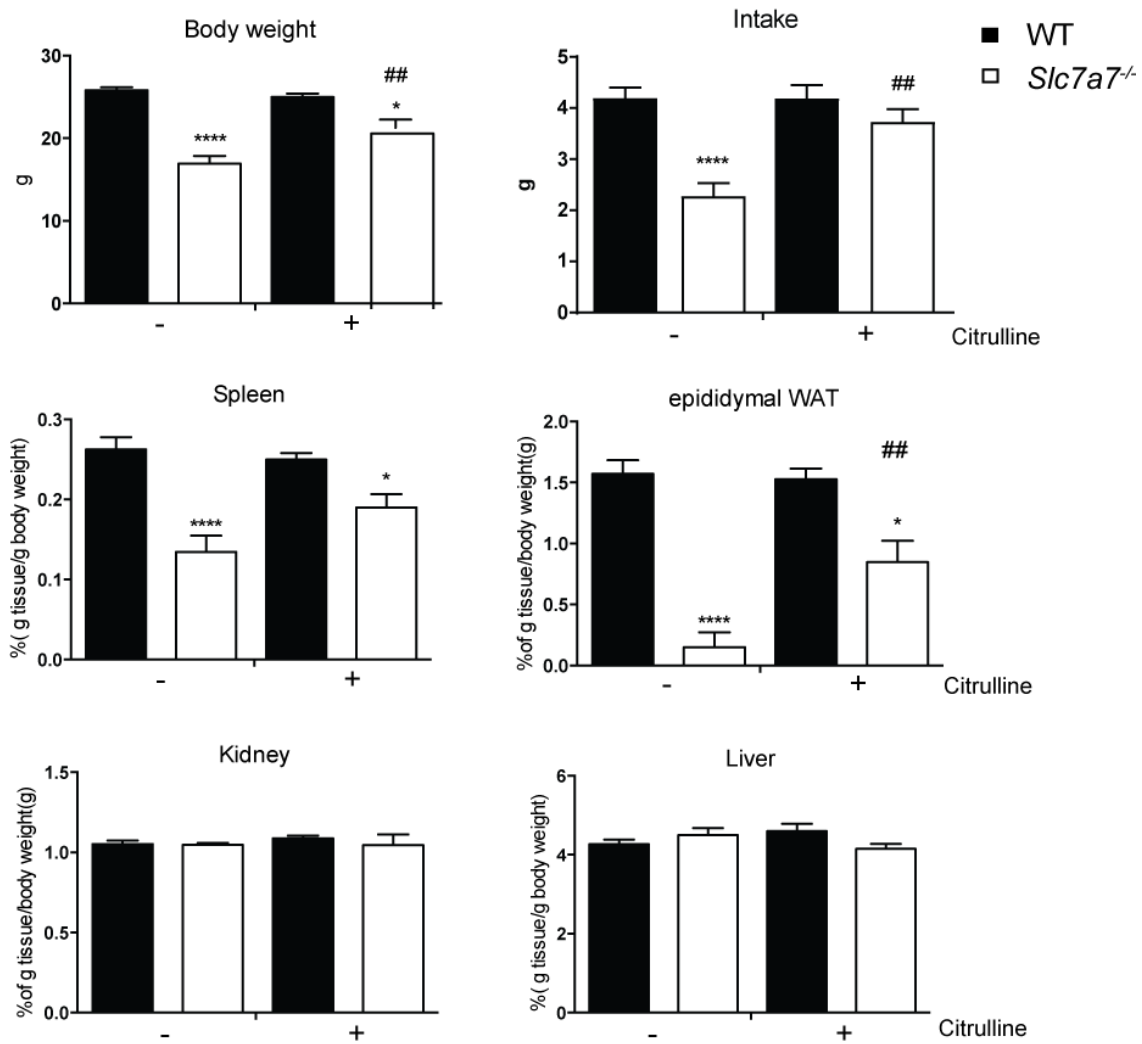


Figure 22. Body and tissue weight. Body weight, intake and weight of different tissues of control and *Slc7a7*^{-/-} animals. WAT, white adipose tissue. n=6 animals per group. Data±SEM. * *p*-value< 0.05, ** *p*-value<0.01, *** *p*-value<0.001, **** *p*-value<0.0001. * denotes differences between animals of distinct genotypes, # denotes differences between animals of same genotype.

Metabolic hallmarks of LPI are deficient renal reabsorption and intestinal malabsorption of cationic amino acids. Then, the next step to further validate *Slc7a7*^{-/-} mice as a proper animal model of human LPI was to check these processes. Hyperexcretion of arginine, ornithine and lysine was detected in urine of *Slc7a7*^{-/-} animals compared to wild type. Also the renal function, measured as renal clearance, was found to be impaired (Figure 23). The huge increase in renal excretion of cationic amino acids (mainly arginine) in the *Slc7a7*^{-/-} animals which received citrulline, is basically explained because the physiological conversion of citrulline into arginine in adult mammals predominantly occurs in the proximal tubules of kidney. Moreover, intestinal absorption of lysine was impaired while glucose absorption was normal in *Slc7a7*^{-/-} mice, indicating that malabsorption was specific for cationic amino acids (Figure 23).

RESULTS

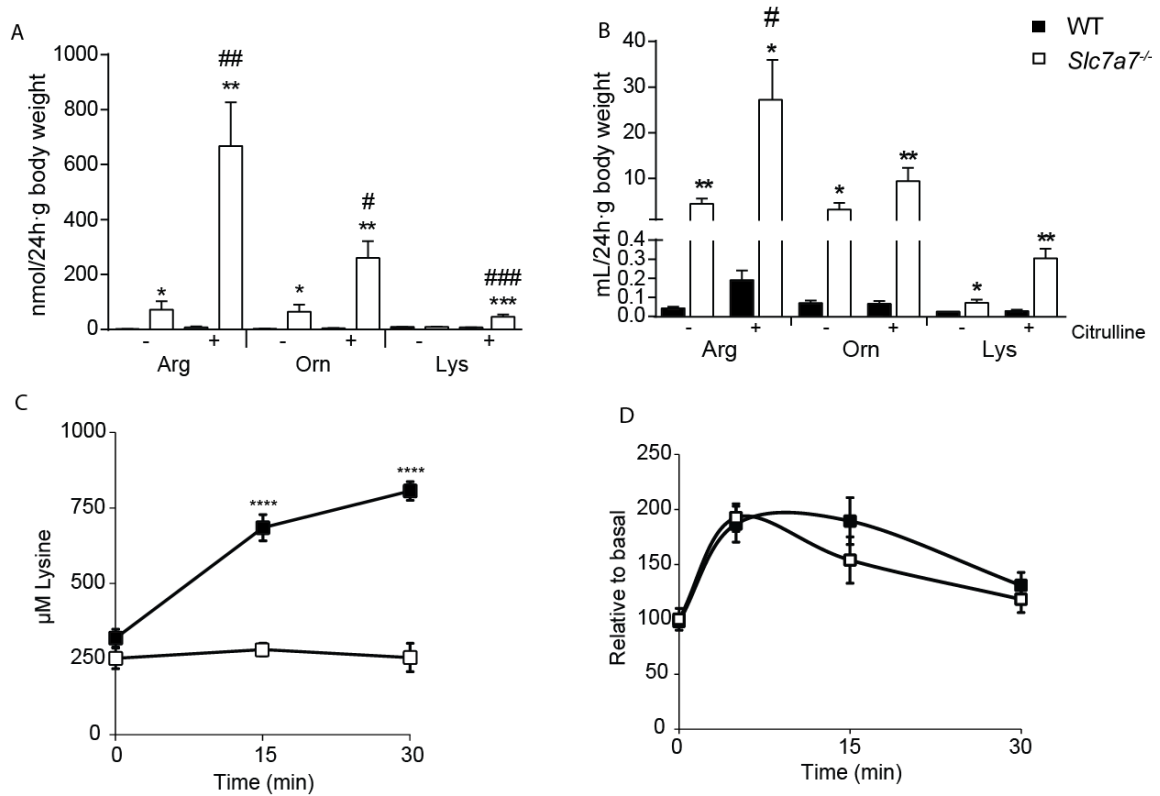


Figure 23. Metabolic hallmarks of LPI. **A.** Hyperexcretion of cationic amino acids. **B.** Renal clearance of cationic amino acids. **C.** Malabsorption of Lysine. **D.** Absorption of glucose. n=6 animals per group. Data±SEM. * p-value< 0.05, ** p-value<0.01, *** p-value<0.001. * denotes differences between animals of distinct genotypes, # denotes differences between animals of same genotype.

The deficient renal reabsorption together with the intestinal malabsorption of cationic amino acids, reduce the concentration of these amino acids in plasma (Figure 24). Since arginine and ornithine are intermediaries of the urea cycle, their reduction in plasma concentration drives a secondary defect of the urea cycle in human LPI, which is detected as hyperammonemia, increased glutamine levels in plasma and increased orotic aciduria. *Slc7a7*^{-/-} mice showed these characteristic traits of impaired urea cycle (Figure 24), confirming that the fall in the levels of cationic amino acids in plasma caused a defect in the urea cycle of *Slc7a7*^{-/-} animals, paralleling what happens in patients. Hyperammonemia also caused brain edema in *Slc7a7*^{-/-} animals, as indicated by the increase of water brain content (Figure 24).

As citrulline is converted into arginine, citrulline supplementation recovered the arginine plasma levels in *Slc7a7*^{-/-} animals and consequently the malfunction of urea cycle was less severe. It can be observed in the improvement of the levels of ammonia and glutamine in plasma, as well as in the recovery of the orotic aciduria and of the water brain content (Figure 24).

RESULTS

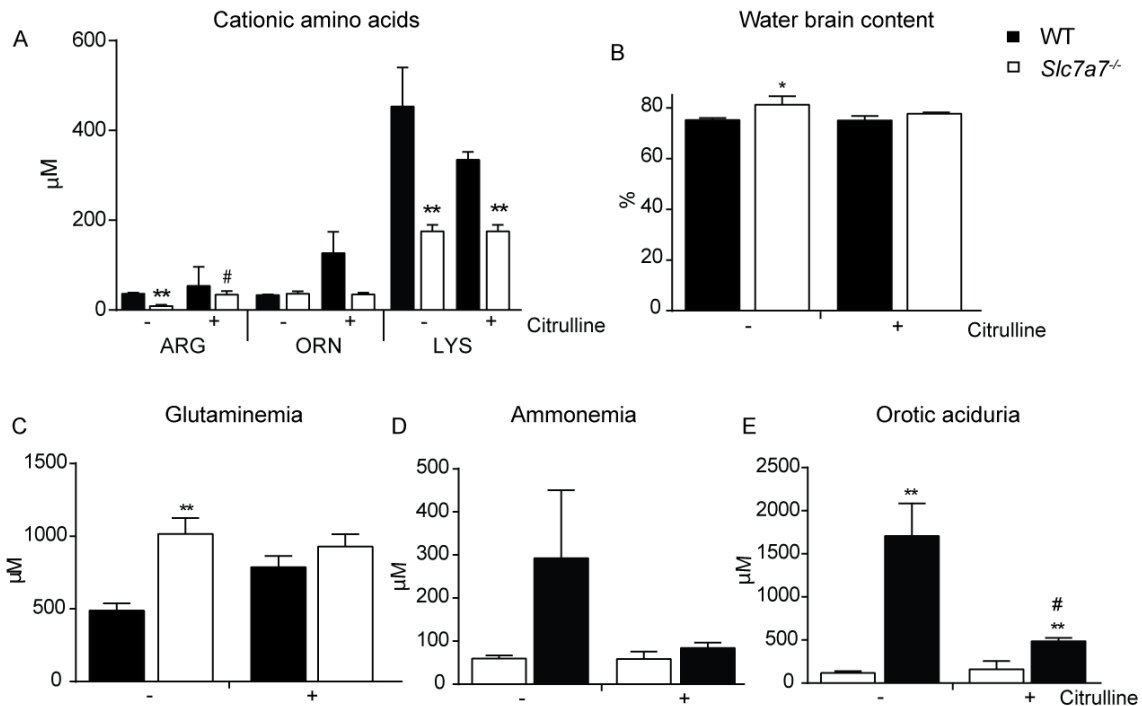


Figure 24. Secondary defect of the urea cycle. **A.** Cationic amino acids concentration in plasma. **B.** Water brain content. **C.** Glutaminemia. **D.** Hyperammonemia. **E.** Orotic aciduria. Data±SEM. * p -value < 0.05, ** p -value < 0.01, * denotes differences between animals of distinct genotypes, # denotes differences between animals of same genotype. $n=6$ animals per group.

Immune-related complications in LPI

Slc7a7^{-/-} mouse model develops Pulmonary Alveolar Proteinosis

Regarding the immune related complications in LPI, we first checked whether *Slc7a7*^{-/-} mice also develop the abnormalities reported in patients. Concurrently, to study the impact of the metabolic condition in the severity of LPI immune and hematological complications, we keep the experimental strategy and analyzed matched animals for sex, age and time after LPI induction treated with 8% protein diet and supplemented or not with citrulline (1g/L).

One of the most life threatening complications in LPI patients is Pulmonary alveolar proteinosis (PAP). We analyzed PAP development in *Slc7a7*^{-/-} mice by broncho-alveolar lavage fluid (BALF) cytology and lung histology. In addition we tried to diagnose PAP *in vivo* in *Slc7a7*^{-/-} animals by high-resolution computerized tomography (HRCT), but due to the severity of the disease, anesthesia was lethal in some cases, so we ruled out the possibility of *in vivo* diagnosis.

Histologically we found some animals with alveoli filled by a Periodic Acid Schiff (PAS) positive and diastase resistant material, which are characteristic features of lung surfactant. Regarding

RESULTS

the quantity of the accumulated material, we grouped the animals in three different degrees ranging from 0 to 2 (Figure 25). 0 means no surfactant accumulation, degree 1 represents infiltration of enlarged alveolar macrophages (AM) and degree 2 represents alveoli completely filled by surfactant. We analyzed a total of 20 *Slc7a7*^{-/-} mice and 15 wild type at different times after LPI induction and under different diet conditions (Figure 25). About one third (6 out of 20) of the total *Slc7a7*^{-/-} animals analyzed showed in some extent surfactant accumulation. The infiltration of enlarged AM in the alveoli was not observable before 25 days after LPI induction, and clear surfactant accumulation appeared after 35 days of LPI induction. In such situation, if the animals that were analyzed before the 25th day after LPI induction are not taken into account for statistics, the proportion of *Slc7a7*^{-/-} animals affected by PAP raises up until 40% (6 out of 15). Thus the percentage of *Slc7a7*^{-/-} animals and of LPI patients affected by PAP is highly similar (40% in analyzed mice versus 37.67% reported in patients) (Table 2).

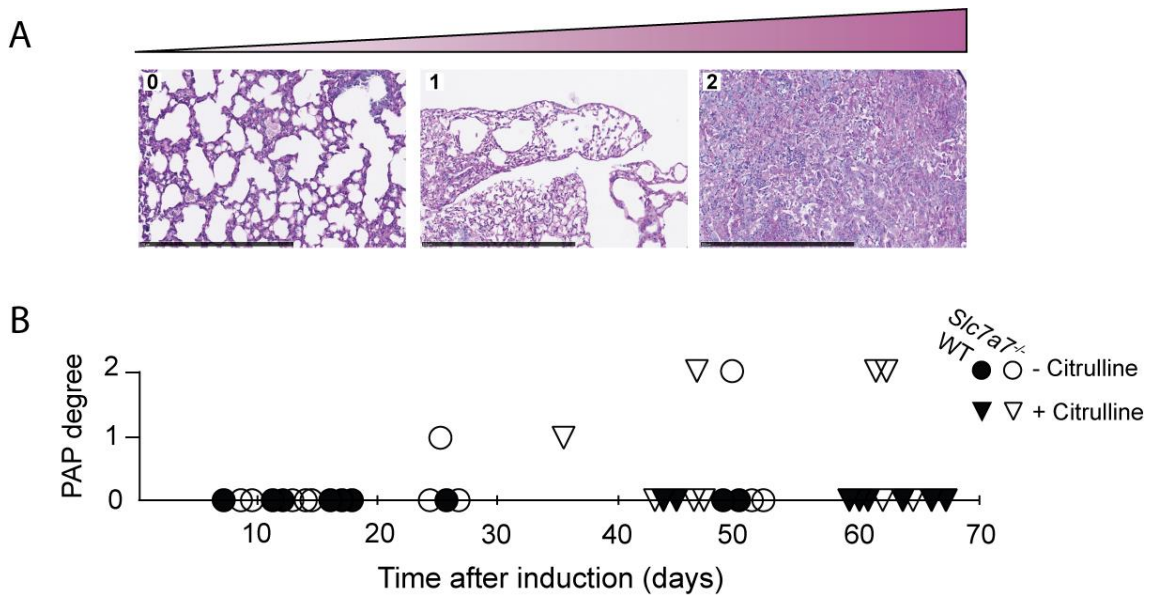


Figure 25. PAP development. **A.** representative images of the established PAP degrees. Sections from paraffin embedded lung were stained with PAS. Scale bars represent 500 μ m. **B.** distribution of animals analyzed for PAP. n=17 wild type and 20 *Slc7a7*^{-/-} animals. Individuals are plotted regarding the PAP degree assigned and the time point of sacrifice after the induction of the disease.

In other mouse models that develop PAP, it also took some time until differences in lung histology were observable. For instance, the lungs of GM-CSF knock out mice (Stanley *et al.*, 1994) were identical to wild type at birth, but striking differences were found by 3 weeks of age. In the case of *Bach2*^{-/-} mouse model (Nakamura *et al.*, 2013), infiltrations of enlarged AM in the alveoli were found by 8 weeks of age, and alveoli collapsed by surfactant accumulation were obviously evident by the age of 12 weeks. In the case of *Slc7a7*^{-/-} animals, the maximum

RESULTS

time point that animals were analyzed was 9 weeks after the induction of the disease. At this time, although alveoli collapsed by surfactant accumulations were evident, the lesions did not span all through over the lung. Only a restricted area was found to be affected by surfactant accumulation, probably indicating that PAP in *Slc7a7^{-/-}* animals is less severe than in other PAP mouse models. To further confirm that the accumulated material in alveoli was lung surfactant, we performed immunohistochemistry (IHC) in lung sections with anti-surfactant protein B (SP-B) antibody. The positive signal obtained in filled alveoli confirmed PAP development in *Slc7a7^{-/-}* mice (Figure 26). Another trait reported in PAP lesions and in LPI patients affected by lung disease, is fibrosis. By Masson's trichrome staining we also could observe fibrotic lesions in the lungs of *Slc7a7^{-/-}* mice affected by PAP (Figure 26).

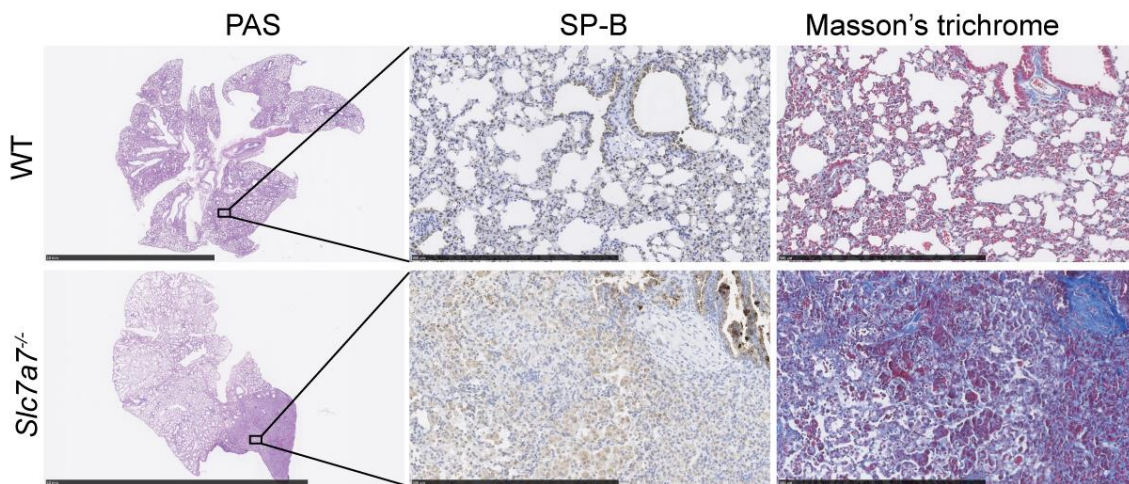


Figure 26. PAP histology. Representative lung images from wild type and *Slc7a7^{-/-}* animals stained with PAS, IHC for SP-B and Masson's trichrome. n=17 wild type and 20 *Slc7a7^{-/-}* animals. Scale bars represent 500 μ m.

Foamy and enlarged AM are also a characteristic finding in BALF cytology of patients and mice affected by PAP. To analyze the morphology of AM from *Slc7a7^{-/-}* mice, we performed bronchoalveolar lavages, cytospun the collected cells and stained them with Panoptic staining. We analyzed a total of 14 *Slc7a7^{-/-}* and 12 control animals ranging from 15 to 55 days after LPI induction and treated with low protein diet plus citrulline. We first calculated the percentage of foamy AM in each preparation. To avoid a biased calculation of this percentage, the number of counted cells was similar for wild type and *Slc7a7^{-/-}* preparations (1208.33 ± 99.7 and 1204.64 ± 76.3 in wild type and *Slc7a7^{-/-}* preparations respectively). The percentage of foamy AM found in *Slc7a7^{-/-}*, on average, was significantly increased compared to wild type (Figure 27). Nevertheless, only 5 out of 14 *Slc7a7^{-/-}* animals showed increased percentage of foamy

RESULTS

cells compared to the control animal with the highest percentage, which is in accordance with the PAP penetrance found by lung histology. As foamy classification is subjective, we measured the area of AM to thoroughly confirm this result. The average cells measured in control preparations was 716.92 ± 24.5 cells, while the average in *Slc7a7*^{-/-} preparations was 707.36 ± 49.35 cells. Based on these measurements, we established 5 categories and calculated the percentage of cells in each category. The most represented category in both genotypes was 150 to $249\mu\text{m}^2$. No statistical differences were found in this category between genotypes. However, *Slc7a7*^{-/-} population was down-represented compare to wild type in the lowest category and over-represented for the two highest categories. Thus, AM population from *Slc7a7*^{-/-} animals showed a clear shift to higher area ranges, proving that this cell population was enlarged in *Slc7a7*^{-/-} animals compared to wild type (Figure 27).

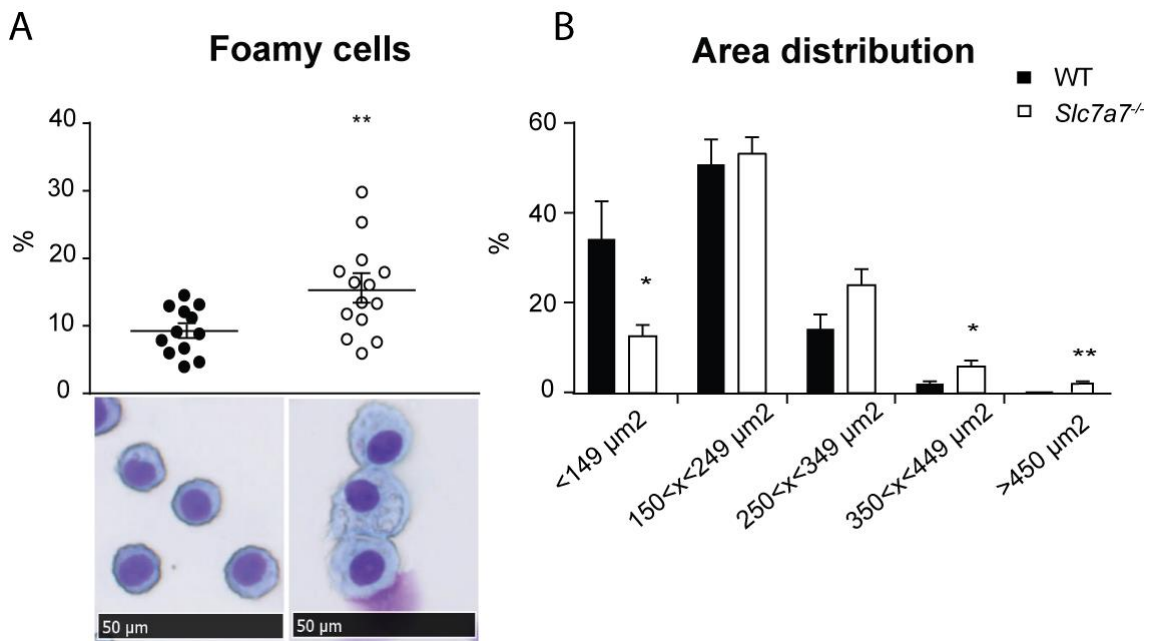


Figure 27. Cytological study of alveolar macrophages. **A.** Percentage of alveolar macrophages classified as foamy. Representative images of what was considered normal and foamy cells. Scale bars represent $50\mu\text{m}$. **B.** Area measurement of alveolar macrophages and distribution of the population among the area ranges defined. Data \pm SEM. $n = 12$ wild type and 14 *Slc7a7*^{-/-}. Animals were kept with low protein diet plus citrulline for 15-55 days. * p -value < 0.05 ; ** p -value < 0.01 .

Due to the low survival rate of *Slc7a7*^{-/-} animals not treated with citrulline at 25 days or longer time points, we could not assess the relationship of PAP development with the metabolic deficiency. Nevertheless we used the loss of body weight as a marker of severity of LPI. We compared this parameter between animals that showed histological findings of PAP (PAP degree 1-2) and those animals that were not affected by PAP. We did not find differences

RESULTS

between these two groups (Figure 28), suggesting that PAP development is not strictly dependent on the metabolic symptoms. Additionally, by the measurement of the area of AM, we also checked whether PAP development was strictly a matter of time after the induction of LPI. We did not observe any correlation between the time after de induction of the disease and an increased percentage of enlarged AM in *Slc7a7^{-/-}* animals (Figure 28). Then, we can mostly claim that the *Slc7a7^{-/-}* animals that did not presented PAP symptoms was not because they needed more time to develop the disease.

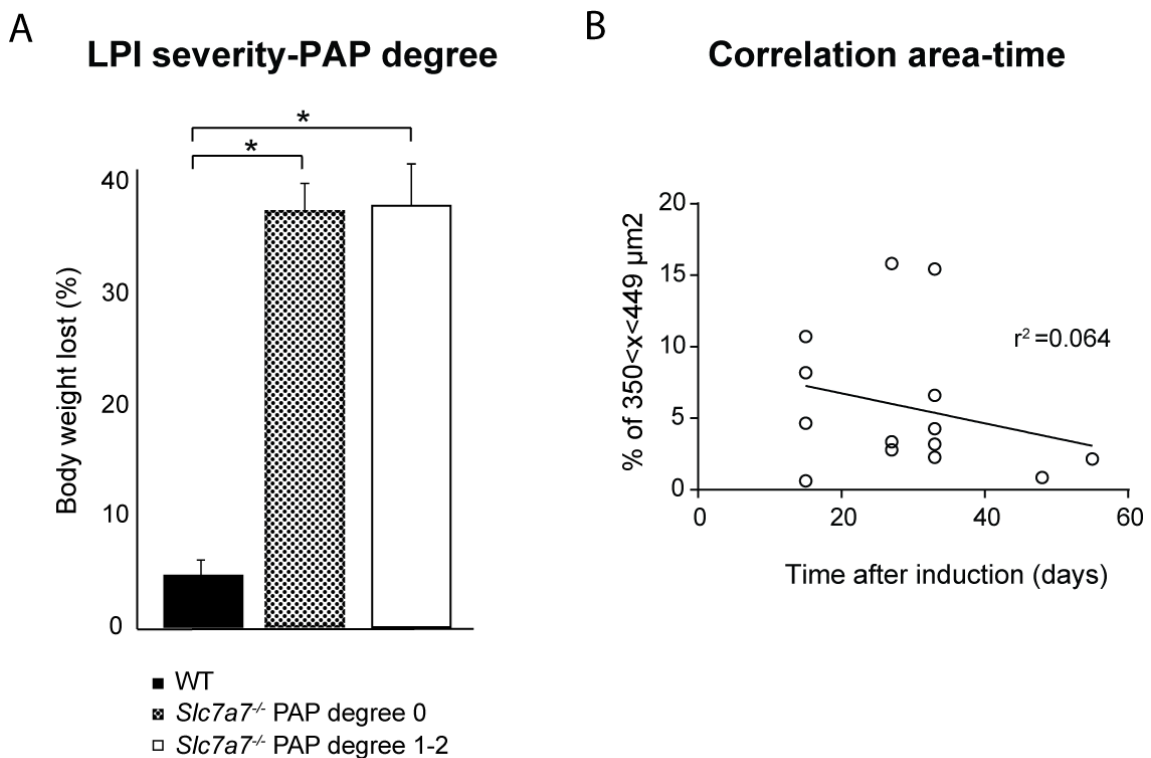


Figure 28. PAP development and LPI severity. **A.** Analysis of PAP development compared to severity of LPI. Percentage of loss of body weight at the day of sacrifice was used as the parameter to assess LPI severity. Comparison of percentage of body weight lost between animals affected and not affected by PAP. Data±SEM. n= 15 wild type and 20 *Slc7a7^{-/-}* animals. **B.** Pearson correlation between the percentage of cells in 350 to 449μm² category and time after LPI induction. n= 12 wild type and 14 *Slc7a7^{-/-}*. Animals were kept with low protein diet plus citrulline for 15-55 days. *p-value<0.05.

The best understood cause of PAP is a deficient response to GM-CSF by AM. Thus we wanted to investigate whether GM-CSF signaling pathway is altered in *Slc7a7^{-/-}* AM. To do this, we extracted RNA from freshly isolated AM of 9 *Slc7a7^{-/-}* and 4 wild type mice, which were treated during 40 days with citrulline supplementation. By qRT-PCR we checked the expression levels of different cationic amino acid transporters: γ^+ LAT1, γ^+ LAT2, CAT1, CAT2; genes involved in

RESULTS

GM-CSF signaling pathway: α and β chains of GM-CSF receptor, PU.1; and genes related to lipid metabolism *Pparg*, *Abcg1* and *Lpla2* (Figure 29).

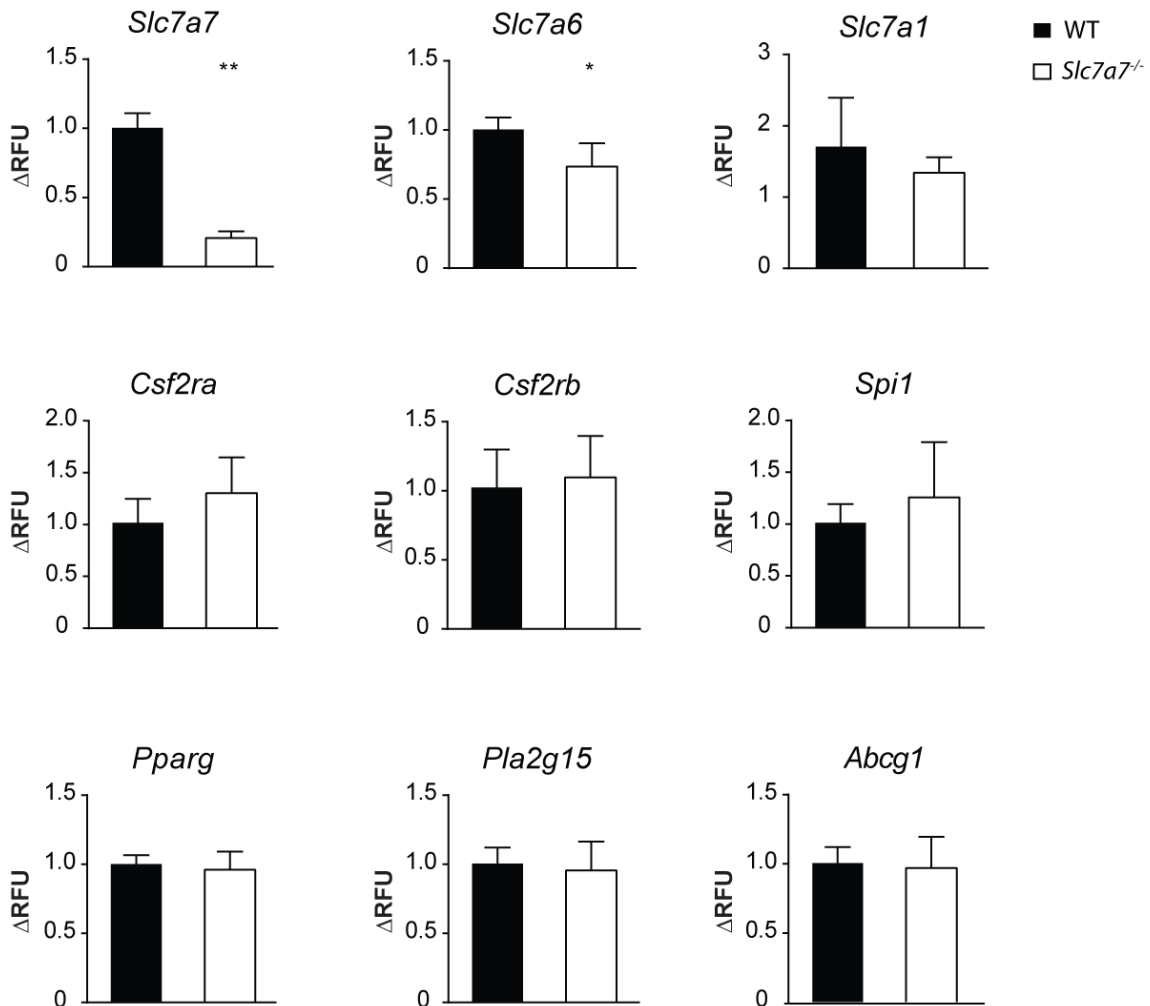


Figure 29. mRNA expression in alveolar macrophages. Results are expressed as the percentage of change compared to controls' expression and relative to *GAPDH* expression. Data \pm SEM. n= 4 wild type and 9 *Slc7a7*^{-/-}. *p-value<0.05; **p-value<0.01.

Regarding to arginine transporters, we confirmed the lack of expression of γ^+ LAT1 in *Slc7a7*^{-/-} mice. Surprisingly, instead of a compensation from his brother transporter, we found a significant decrease in γ^+ LAT2 (*Slc7a6*) expression. Also the expression of system γ^+ transporters was checked. The expression of CAT1 (*Slc7a1*) was very low (average Ct 29.8) and with no statistical differences between wild type and *Slc7a7*^{-/-}, while CAT2 (*Slc7a2*) expression was not detected (Ct >30). These results, but for γ^+ LAT2, agree with those published by Rotoli *et al.*, 2007 for human AM. Regarding GM-CSF signaling pathway we did not find differences between wild type and *Slc7a7*^{-/-} animals in any of both chains of the receptor (*Csf2ra* and

RESULTS

Csf2rb) neither in the master regulator PU.1 (*Spi1*). In addition, we did not observe differences in the expression of any of the analyzed genes involved in lipid homeostasis that are downstream of GM-CSF (*Pparg*, *Pla2g15* and *Abcg1*). These results agree with those reported by Barilli *et al.*, 2010 using monocyte derived macrophages and lead us to think that the cause of PAP in LPI is different to deficient response to GM-CSF. Because of the partial penetrance of PAP in LPI mice, it would be necessary to establish a relationship between gene expression and PAP development. However, after BAL performance PAP detection by lung histology may not be accurate. In addition, due to the low number of cells obtained by BAL, cytospin and RNA extraction from the same sample is not possible. These technical limitations together with difficulty of *in vivo* diagnosis by HCRT, did not allow us to establish a correlation between gene expression and PAP development in *Slc7a7^{-/-}* mice.

***Slc7a7^{-/-}* mouse model develops Hemophagocytic lymphohistiocytosis**

Hemophagocytic lymphohistiocytosis (HLH) is another concerning complication in LPI. The characteristic traits of HLH that most frequently present LPI patients are hepatosplenomegaly, persistent elevated ferritinemia and intermittent hemophagocytosis in spleen and bone marrow.

Hepatosplenomegaly was not present in *Slc7a7^{-/-}* mice. Liver's weight of *Slc7a7^{-/-}* animals was comparable to the wild type's (Figure 22). In addition, by gross examination no abnormalities were found in the liver of *Slc7a7^{-/-}* animals, and neither apparent histological abnormalities were found (Figure 30).

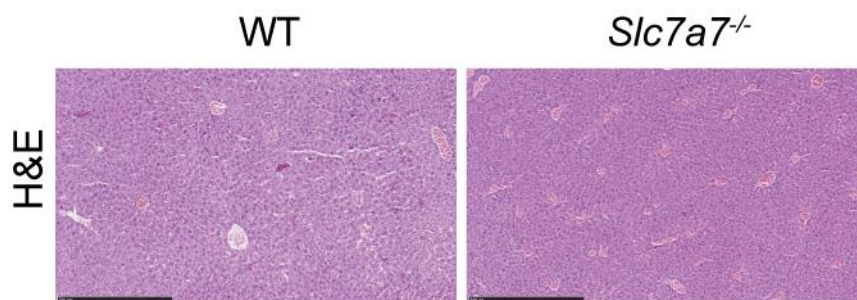


Figure 30. Liver examination. Representative images of liver sections from wild type and *Slc7a7^{-/-}* mice. Scale bars represent 500 μ m.

RESULTS

On the other hand, spleen weight was dramatically decreased in *Slc7a7*^{-/-} mice compared to wild type (Figure 22). In addition, H&E staining of spleens showed disorganization of the white and red pulp (Figure 31). IHC with Ki67 also revealed the loss of proliferation follicles in the white pulp (Figure 31). Specifically, B lymphocytes (CD45R⁺ IgM⁺) were reduced in the spleens of *Slc7a7*^{-/-} animals. Nevertheless, the group of animals treated with citrulline improved both the spleen weight (Figure 22) and the percentage of B cells was recovered (Figure 31).

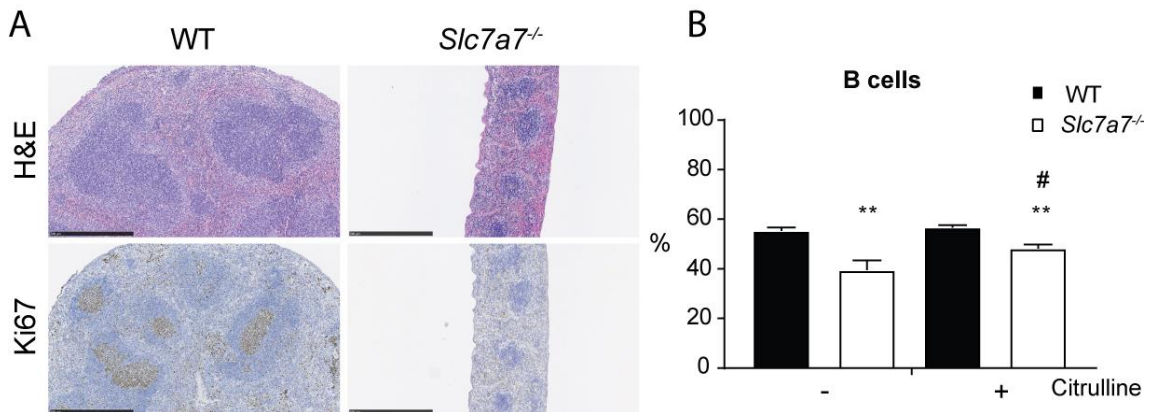


Figure 31. Spleen examination. A. Representative images of spleen sections from wild type and *Slc7a7*^{-/-} mice. Scale bars represent 500µm. B. Percentage of B lymphocytes (CD45R⁺ IgM⁺) analyzed by flow cytometry. Data±SEM. n= 6 wild type and *Slc7a7*^{-/-}. **p*-value<0.05; ***p*-value<0.01. * denotes differences between animals of distinct genotypes, # denotes differences between animals of same genotype.

Hyperferritinemia, another characteristic trait of HLH usually reported in LPI, is commonly associated to macrophage activation, however it can be found in LPI patients that apparently are not suffering any inflammatory process. Ferritin levels in plasma of *Slc7a7*^{-/-} and wild type animals were determined by ELISA. We found that, as well as in patients, *Slc7a7*^{-/-} mice also showed massive hyperferritinemia compared to wild type (Figure 32). Nevertheless, *Slc7a7*^{-/-} citrulline treated group showed a correction of ferritinemia levels, becoming similar to those in wild type animals.

RESULTS

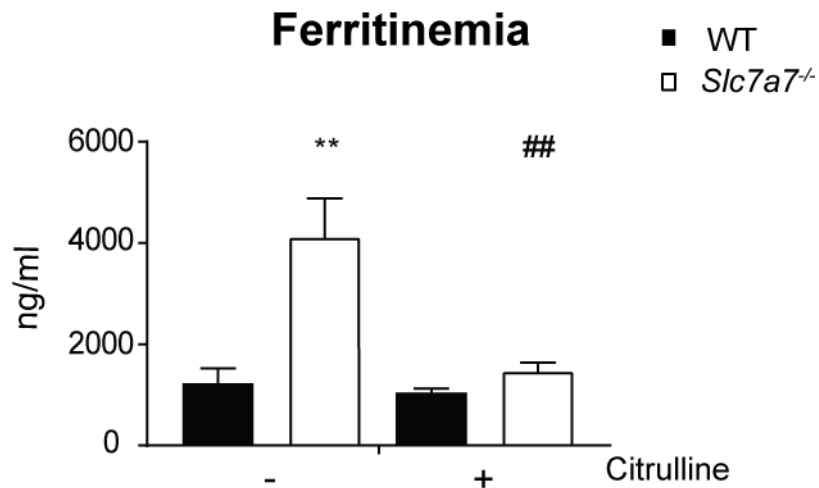


Figure 32. Ferritinemia. Ferritin levels in plasma measured by ELISA. n=11 animals per group in the not citrulline treated animals, and n=10 animals per group for the citrulline treated animals. **p*-value<0.05; ***p*-value<0.01. * denotes differences between different genotypes, # denotes differences between same genotype.

Another diagnostic trait of HLH is cytopenia in at least two different lineages. Although within the normal ranges, we found that *Slc7a7*^{-/-} mice have an unbalance in the percentages of lymphocytes and granulocytes compared to control animals. The percentage of granulocytes was increased in *Slc7a7*^{-/-} mice, while the percentage of lymphocytes was decreased compared to wild type animals. This unbalance was also corrected in the group of *Slc7a7*^{-/-} animals treated with citrulline (Figure 33).

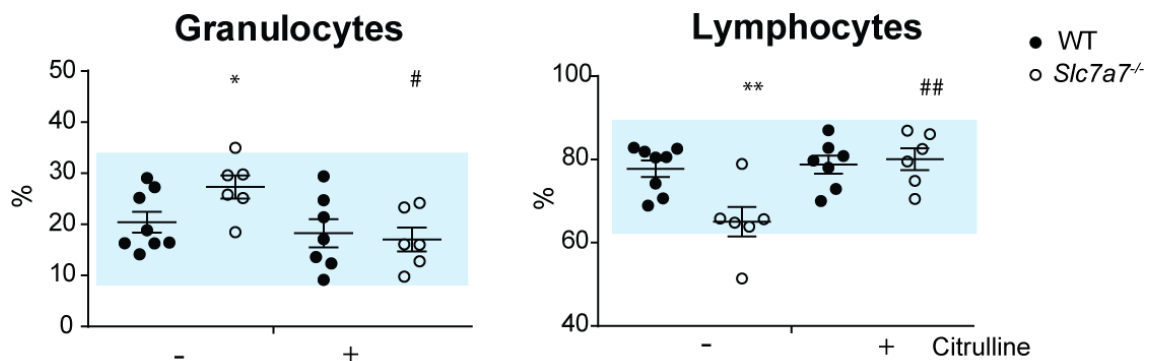


Figure 33. Hematologic analysis of white blood cells. n=8 wild type and 6 *Slc7a7*^{-/-} animals not treated with citrulline, and n=7 wild type and 6 *Slc7a7*^{-/-} treated animals. Data±SEM. Blue boxes represent the reference values for C57BL/6 males 8-10 weeks old (Charles River). **p*-value<0.05; ***p*-value<0.01. * denotes differences between different genotypes, # denotes differences between same genotype.

Because of mild forms of anemia have been frequently reported in LPI patients, hematologic analysis of red blood cells was performed. We found that hemoglobin concentration and hematocrit showed a tendency to be slightly decreased in *Slc7a7*^{-/-} respect to wild type

RESULTS

animals, and below the reference ranges. In addition, the number of red blood cells was not altered in *Slc7a7^{-/-}* animals, and showed a stronger decrease of the mean corpuscular volume (MCV) and the mean corpuscular hemoglobin (MCH) respect to wild type. Both parameters also improved in the group of animals that received citrulline (Figure 34). Different types of anemia have been reported in LPI patients, however, specifically microcytic hypochromic anemia has been reported in the first Korean case of LPI published (Ko *et al.*, 2012). Regarding the platelets, *Slc7a7^{-/-}* mice also showed a decreased in the volume of platelets. Interestingly, citrulline treatment recovered all the altered parameters (Figure 34).

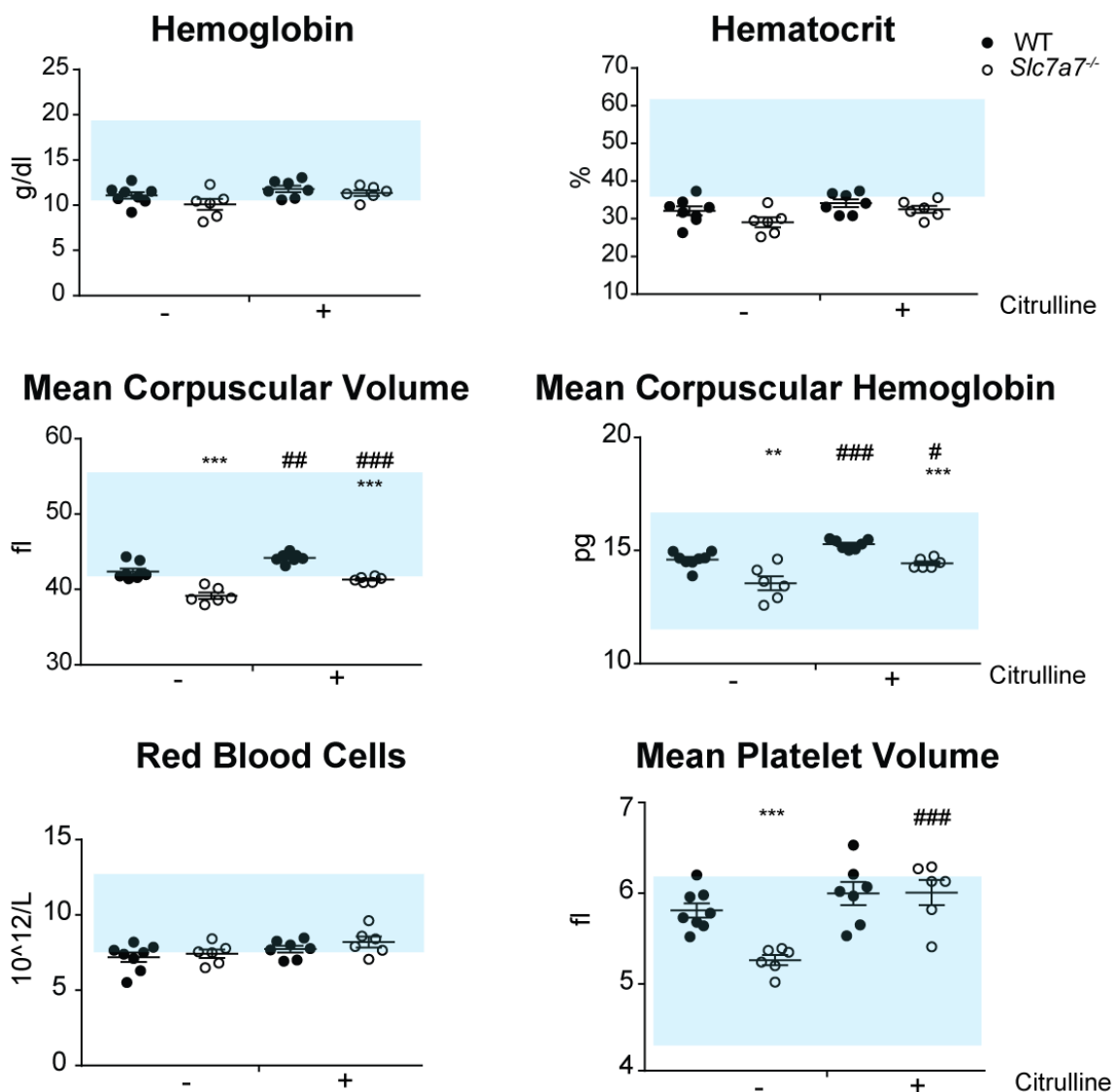


Figure 34. Hematologic analysis of red blood cells and platelets. n=8 wild type and 6 *Slc7a7^{-/-}* animals not treated with citrulline, and n=7 wild type and 6 *Slc7a7^{-/-}* treated animals. Data±SEM. Blue boxes represent the reference values for C57BL/6 males 8-10 weeks old (Charles River). **p*-value<0.05; ***p*-value<0.01. * denotes differences between different genotypes, # denotes differences between same genotype.

***Slc7a7*^{-/-} mouse model suffers defective erythropoiesis**

The half-life of erythrocytes in C57BL/6 mice is about 22 days. Nevertheless all the alterations in hematologic parameters were observed within the first two weeks after the induction of LPI, which let us to hypothesize that erythropoiesis should be impaired in *Slc7a7*^{-/-} mice. It has been described that the erythroid precursors during the successive developmental stages show differences in the expression of the major transmembrane and skeletal proteins as well as in their size (Chen *et al.*, 2009). A *bona fide* marker to distinguish among the different stages of differentiation is CD44, the receptor for hyaluronic acid. Using CD44 and erythroid-specific glycophorin A (TER-119) antibodies together with forward scatter parameter (FSC), different erythroblast populations can be distinguished. Selecting first all the TER-119 positive cells, and then the expression levels of CD44 as a function of FSC, four different clusters can be solved. Cells in region I have the morphological characteristic of proerythroblasts, the cells found in region II are basophilic erythroblasts, those in region III are polychromatic erythroblasts, region IV is a mixed population of orthochromatic erythroblasts (IV-A) and non-nucleated reticulocytes (IV-B) and finally, the cells in region V are mature erythrocytes (Chen *et al.*, 2009). Curiously, *Slc7a7*^{-/-} showed a clear unbalance among the different population rates compared to wild type animals. In *Slc7a7*^{-/-} mice the earlier stages of erythroblasts were clearly diminished, while enucleated reticulocytes and mature erythrocytes were highly increased (Figure 35). Interestingly, this striking unbalance was absent in the group of *Slc7a7*^{-/-} mice that received citrulline. Thus citrulline supplementation mitigates defective erythropoiesis in *Slc7a7*^{-/-} animals.

RESULTS

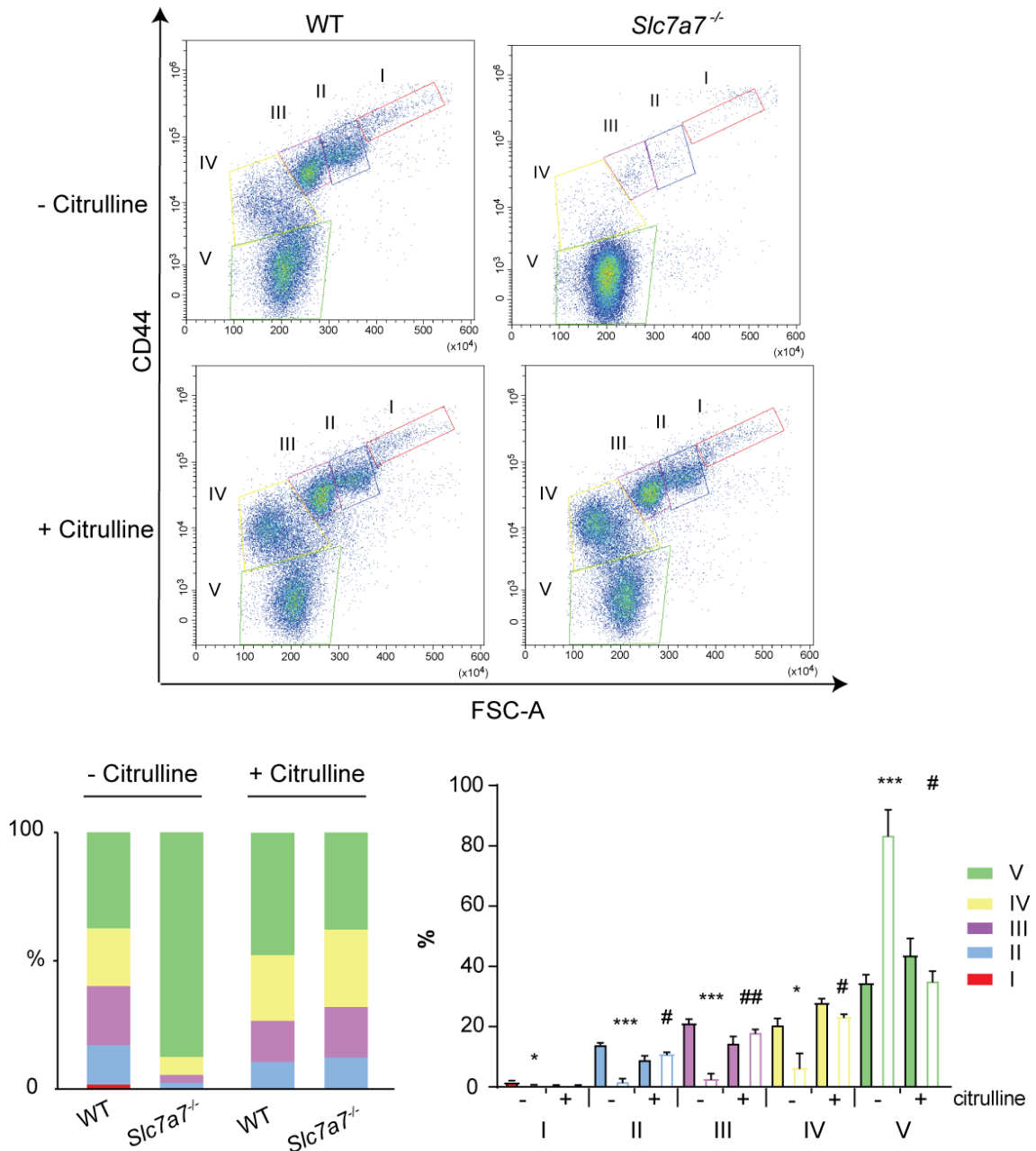


Figure 35. Erythropoietic analysis. Erythroid progenitor populations in the bone marrow were analyzed as described by Chen *et al.*, 2009. Upper panels show a pseudo-color dot plot with the 5 defined regions. Lower panels show the quantification of the populations and the statistic differences between groups. Wild type samples are represented as filled bars and *Slc7a7*^{-/-} samples are represented as empty bars. Cells were firstly gated in TER119⁺. n=5 wild type and 3 *Slc7a7*^{-/-} in both treated and not treated groups. **p*-value<0.05; ***p*-value<0.01. * denotes differences between different genotypes, # denotes differences between same genotype.

Macrophages accumulate abnormally iron in LPI

Moreover, we identified a new trait of LPI in *Slc7a7*^{-/-} mice; abnormal iron accumulations in different tissues. Sections from spleen, bone marrow, lung and liver were stained with Perls' Prussian blue (Perls') and showed increased iron (blue color) accumulations compared to wild

RESULTS

type (Figure 36). In the case of liver, these iron accumulations were not distinguishable by histology, but it was further confirmed by total non-heme iron determination. In the case of lung, only alveolar macrophages (AM) with iron accumulations were found in those lungs of *Slc7a7*^{-/-} mice affected by PAP. In addition, by total non-heme iron determination it was shown that citrulline treatment improved iron accumulation in spleen and liver (Figure 36).

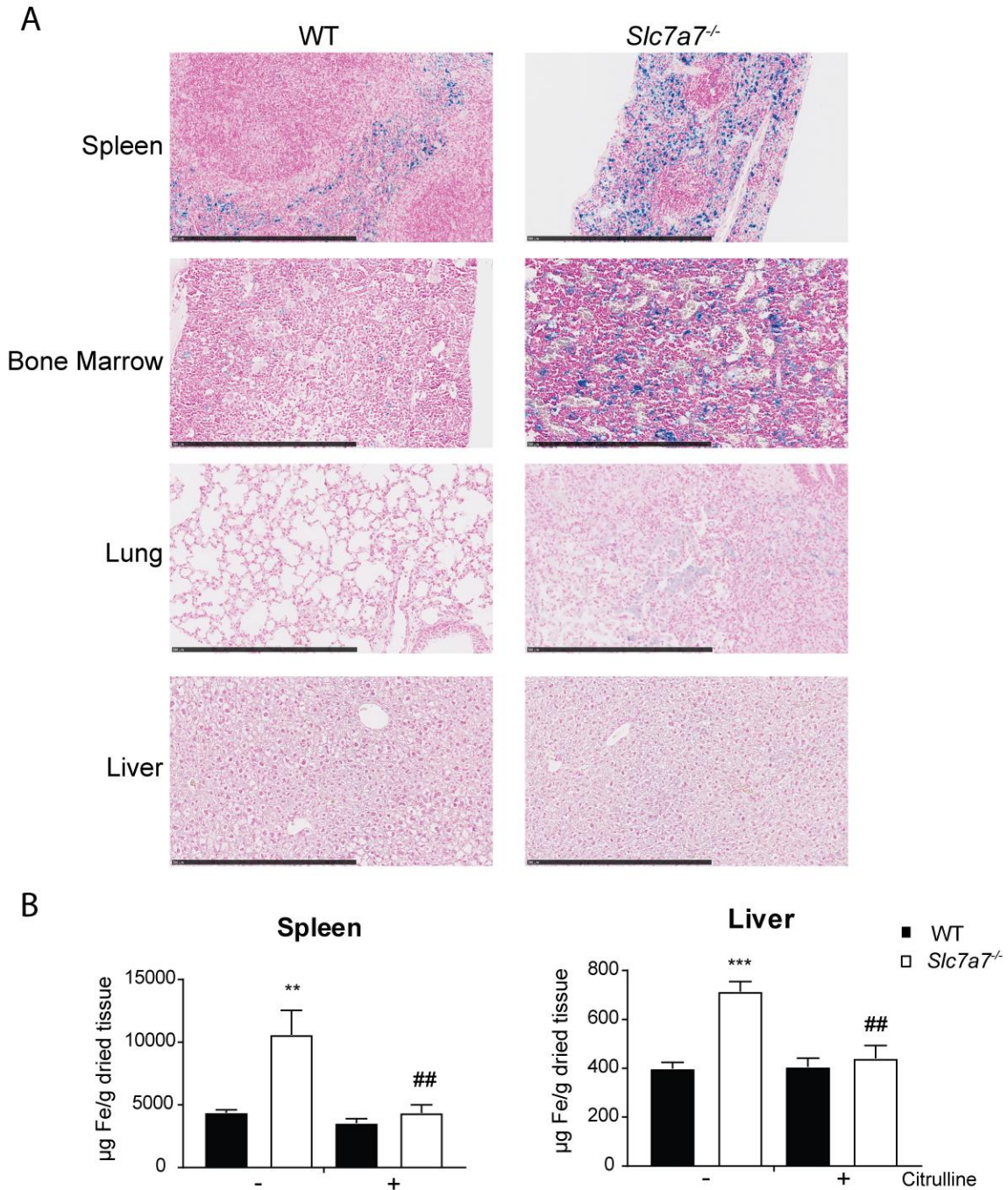


Figure 36. Iron accumulation in tissues. **A.** Sections from spleen, bone marrow (after decalcification), lung and liver embedded in paraffin were stained with Perls' Prussian Blue. Scale bars represent 500µm. **B.** Total non-heme iron quantification. Data±SEM. Spleen n=11 wild type and 10 *Slc7a7*^{-/-}; Liver n=9 wild type and 8 *Slc7a7*^{-/-}. **p*-value<0.05; ** *p*-value<0.01. * denotes differences between different genotypes, # denotes differences between same genotype.

RESULTS

Co-staining of Perls' with the specific macrophage marker F4/80, identified macrophages as the cells that accumulated iron in the spleen. Moreover, this co-staining allowed us to notice that in *Slc7a7*^{-/-} sections, some iron deposits were not surrounded by membrane, probably coming from dead macrophages. Among the cells accumulating iron, there can be found cells with modest iron quantities and cells almost collapsed by iron deposits (Figure 37).

As explained in the introduction, iron retention by macrophages may occur in situations of chronic inflammation. Under these circumstances, persistent elevated IL-6 plasma levels induce hepatocytes to secrete hepcidin. Then hepcidin induces iron retention by macrophages by promoting ferroportin degradation. Thus we examined this regulatory axis as the putative mechanism that drives iron accumulation by macrophages in *Slc7a7*^{-/-} animals. First, we isolated mRNA from total liver to check hepcidin (*Hamp1*) expression. mRNA levels of hepcidin were found to be slightly increased in *Slc7a7*^{-/-} compared to wild type. However, in contrast with iron tissue quantification, this increase was not corrected in the animals treated with citrulline (Figure 37). Moreover, IL-6 levels in plasma of *Slc7a7*^{-/-} mice were not different to those in the wild type littermates (Figure 37). As IL-6 was not different in the animals not treated with citrulline, it was not checked in the group of treated animals. Therefore, a state of chronic inflammation do not seem to be the cause of the iron accumulation found in *Slc7a7*^{-/-} animals.

RESULTS

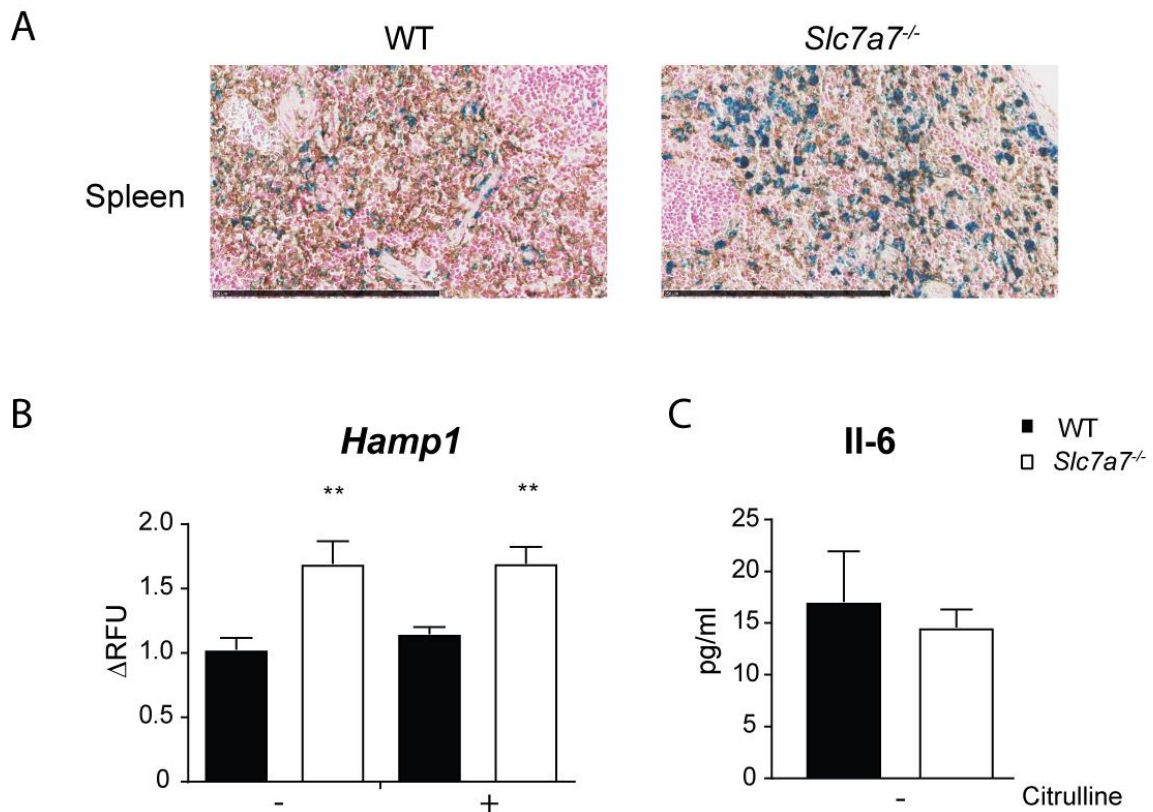


Figure 37. Iron accumulation in macrophages. **A.** Spleen sections were co-stained with Perls' Prussian Blue and IHC for F4/80. Scale bars represent 250 μ m. **B.** Hepcidin (*Hamp1*) mRNA expression in total liver. Results are expressed as the percentage of change compared to controls' expression and relative to actin (*Actb*) expression. Data \pm SEM. n=6 or more per group and condition. **C.** II-6 plasma levels. Data \pm SEM. n=6 mice per group. **p*-value<0.05; ***p*-value<0.01.

Slc7a7^{LysM}^{-/-} mouse model

The results obtained so far, showed that citrulline treatment recovered erythropoiesis, the hematologic parameters, hyperferritinemia and the iron accumulation in macrophages from some different tissues of *Slc7a7*^{-/-} animals. Thus to get a further idea about the necessity of the metabolic condition for the development of the immune and hematologic complications in *Slc7a7*^{-/-} mice, we generated a mouse model targeting specifically myeloid cells. To do this, we crossed *Slc7a7* floxed animals with *Lyz2* (LysM)_Cre animals (*Slc7a7*^{LysM}^{-/-}). By this strategy we restricted the ablation of *Slc7a7* to myeloid cells, avoiding then the metabolic consequences of losing *Slc7a7* in kidney and intestine. To rule out any possible side effect of tamoxifen, these animals were fed for a week with tamoxifen diet as well as the *Slc7a7*^{-/-} ones. qRT-PCR of *Slc7a7* in alveolar macrophages (AM), bone marrow derived macrophages (BMDM) and red pulp macrophages (RPM) confirmed the decay of *Slc7a7* expression in macrophages (Figure 38).

RESULTS

In addition western blot of γ^+ LAT1 in kidney confirmed the intact expression of the protein in this tissue (Figure 38).

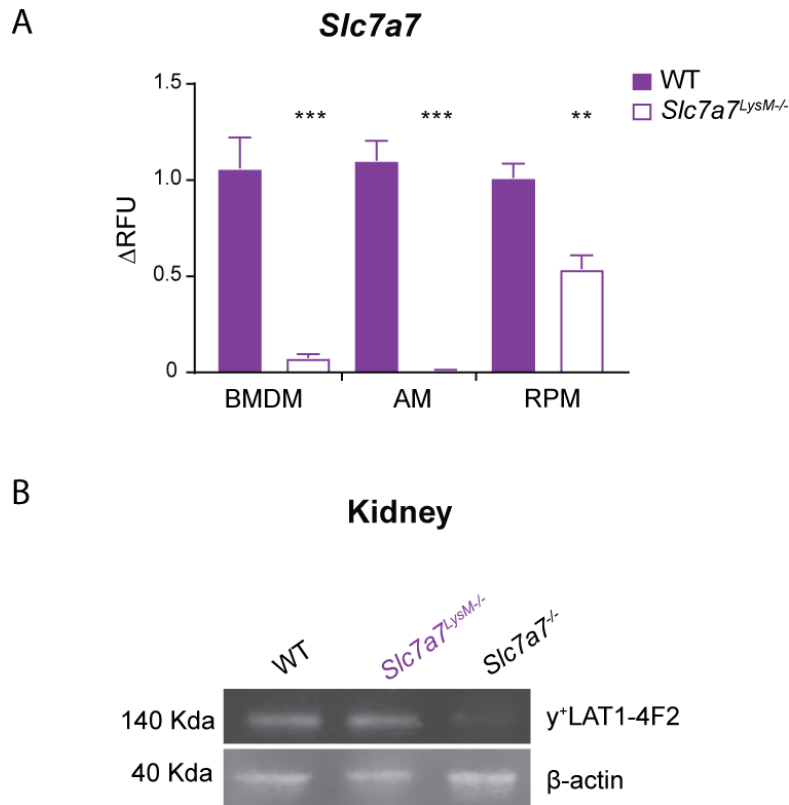


Figure 38. Validation of *Slc7a7*^{LysM}^{-/-} mouse model. **A.** *Slc7a7* mRNA expression in different macrophage populations. Results are expressed as the percentage of change compared to controls' expression and relative to actin (*Actb*) expression. Data \pm SEM. n=6 animals per group. **B.** Western Blot of γ^+ LAT1 in total kidney. * p -value<0.05; ** p -value<0.01; *** p -value<0.001

Slc7a7^{LysM}^{-/-} were viable, did not suffer loss of body weight, and the weight of affected tissues in *Slc7a7*^{-/-} mice such as spleen or WAT was normal (Figure 39). As expected, *Slc7a7*^{LysM}^{-/-} animals did not show hypoargininemia neither hyperammonemia, as revealed the orotic acid levels in urine (Figure 39).

RESULTS

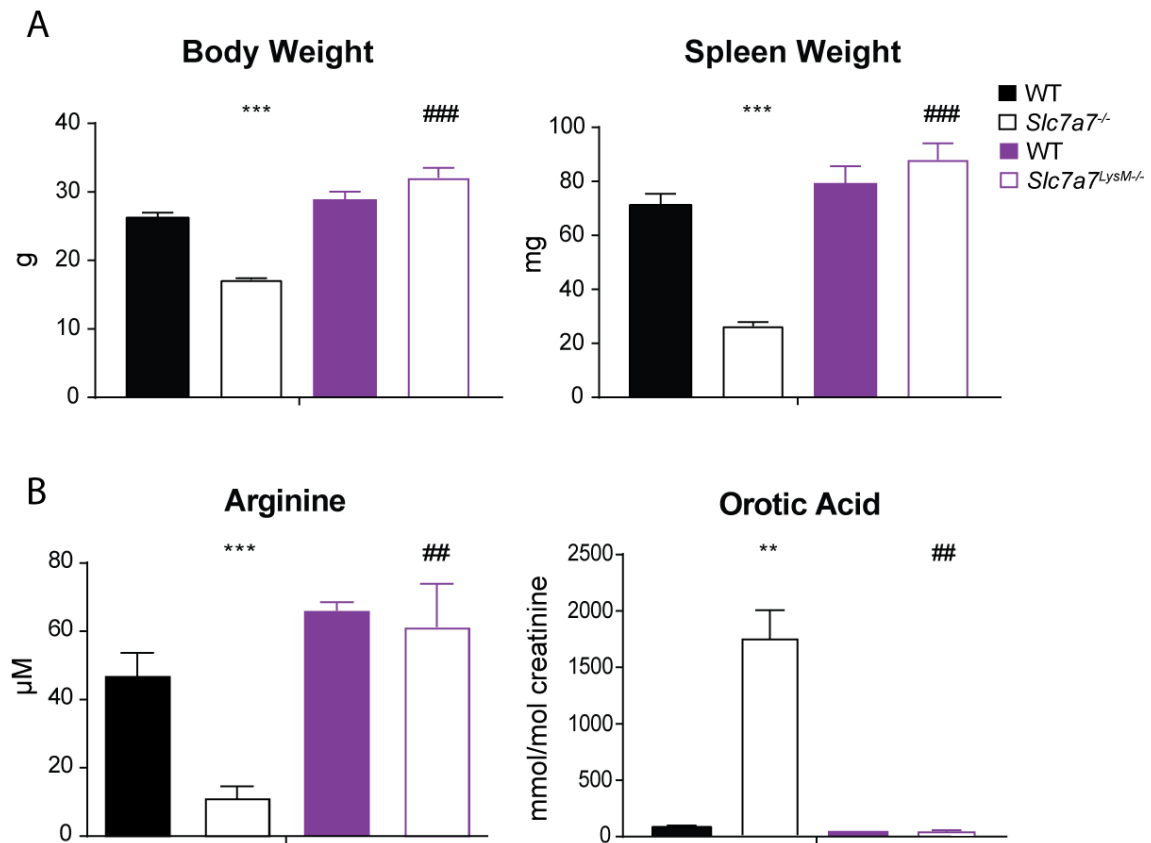


Figure 39. Analysis of metabolic status in *Slc7a7*^{LysM}^{-/-} mouse model. A. Body and spleen weight of wild type and *Slc7a7*^{LysM}^{-/-} and compared to *Slc7a7*^{-/-}. n=6 animals per group. **B.** Quantification of argininemia and orotic aciduria in wild type and *Slc7a7*^{LysM}^{-/-} and compared to *Slc7a7*^{-/-}. n=6 animals per group. Data±SEM. **p*-value<0.05; ***p*-value<0.01; ****p*-value<0.001. * denotes differences between different genotypes, # denotes differences between knock out animals.

Slc7a7^{LysM}^{-/-} mice did not present signs of HLH. They did not present abnormalities in spleen or liver by gross examination. Moreover the percentage of lymphocytes and granulocytes was balanced and ferritinemia was absolutely similar to wild type animals (Figure 40).

RESULTS

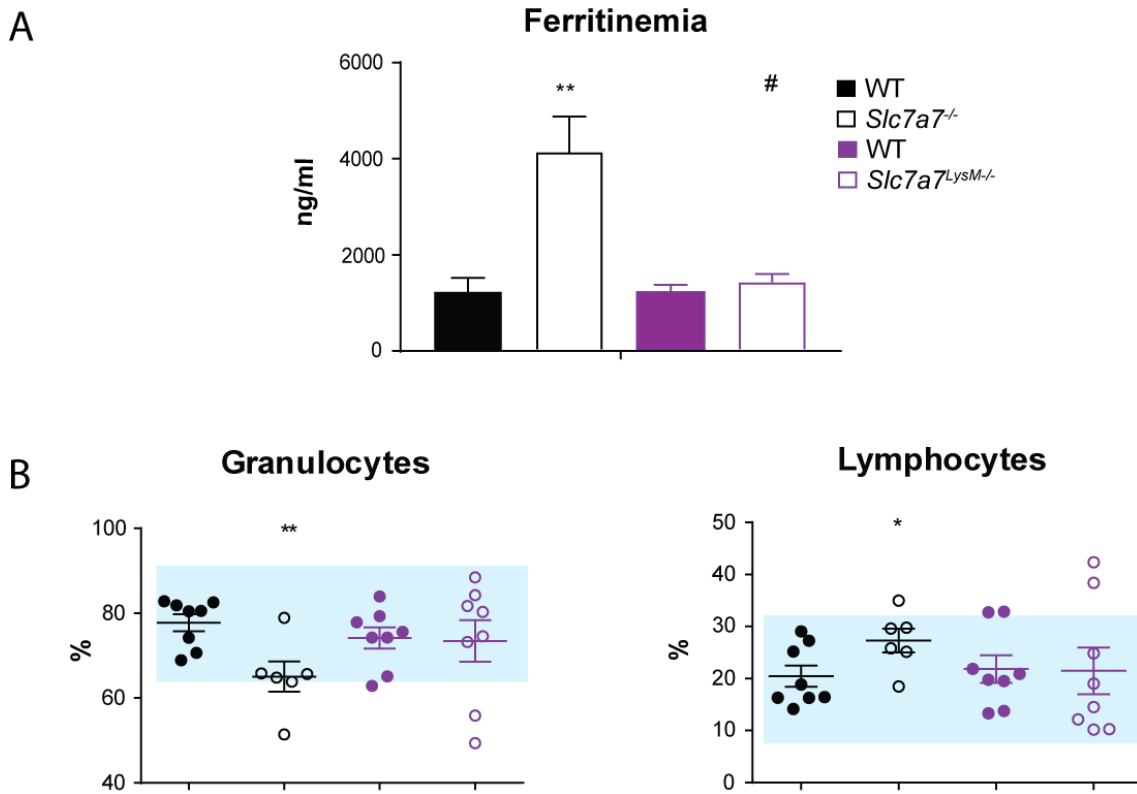


Figure 40. HLH symptoms in *Slc7a7*^{LysM-/-} mouse model. A. Ferritin plasma levels of wild type and *Slc7a7*^{LysM-/-} and compared to *Slc7a7*^{-/-}. Data±SEM. n=6 animals wild type and *Slc7a7*^{LysM-/-}. **B.** Hematologic analysis of white blood cells. Data±SEM. n=8 animals for both wild type and *Slc7a7*^{LysM-/-} groups and n=6 for *Slc7a7*^{-/-} group. Blue boxes represent the reference values for C57BL/6 males 8-10 weeks old (Charles River). **p*-value<0.05; ** *p*-value<0.01. * denotes differences between different genotypes, # denotes differences between knock out animals.

In addition, hematologic analysis was also done in *Slc7a7*^{LysM-/-} mice, showing that these animals did not present anemia, and that the MCV, MCH and the mean platelet volume were comparable to wild type mice (Figure 41).

RESULTS

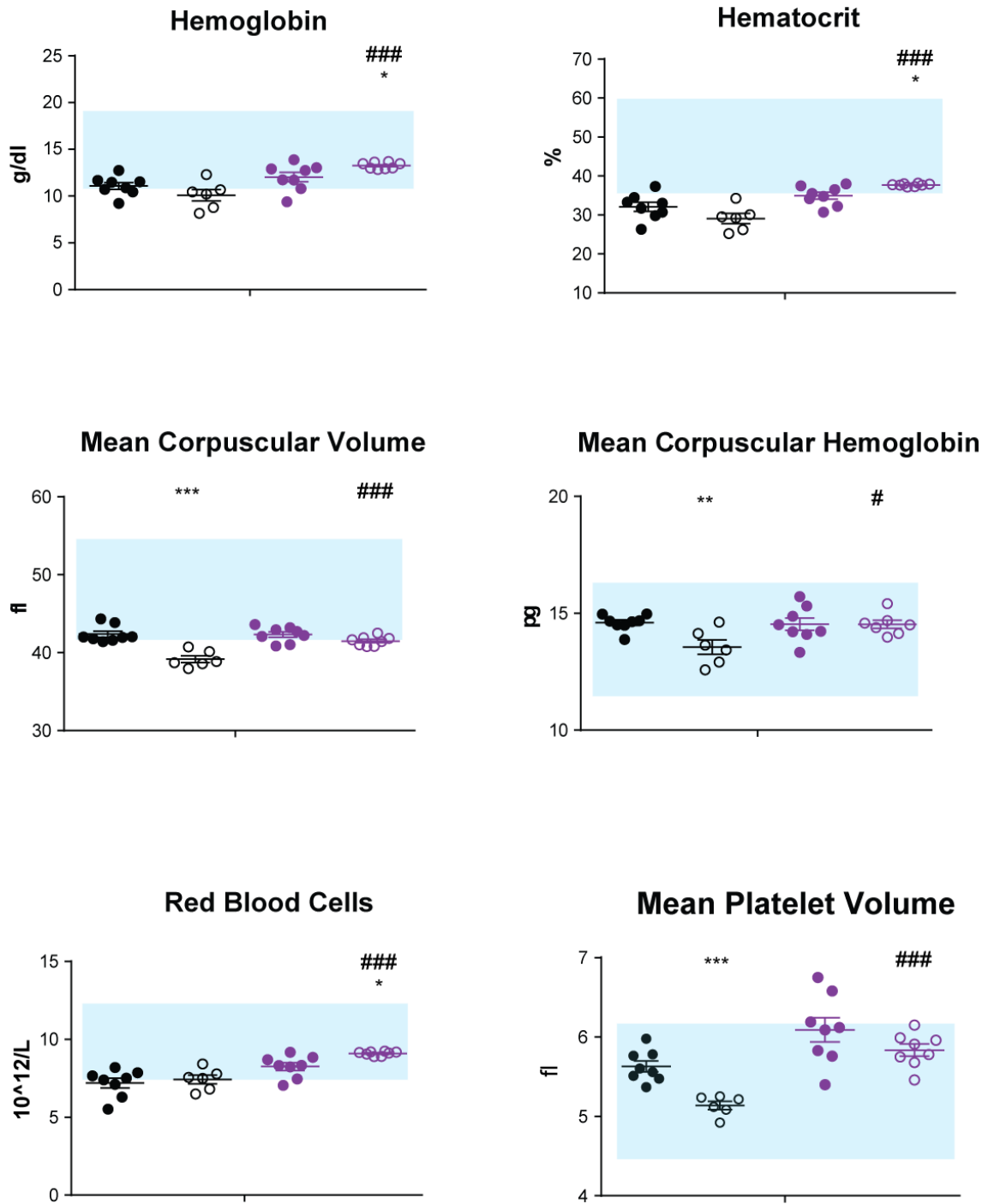


Figure 41. Hematologic analysis of red blood cells and platelets in *Slc7a7^{LysM}^{-/-}* mouse model. n=8 animals for both wild type and *Slc7a7^{LysM}^{-/-}* groups and n=6 animals for *Slc7a7^{-/-}* group. Data±SEM. Blue boxes represent the reference values for C57BL/6 males 8-10 weeks old (Charles River). **p*-value<0.05; ***p*-value<0.01; ****p*-value<0.001. * denotes differences between different genotypes, # denotes differences between knock out animals.

RESULTS

Moreover, *Slc7a7^{LysM^{-/-}}* mice did not present alterations in the populations of erythroid precursors compared to wild type littermates (Figure 42).

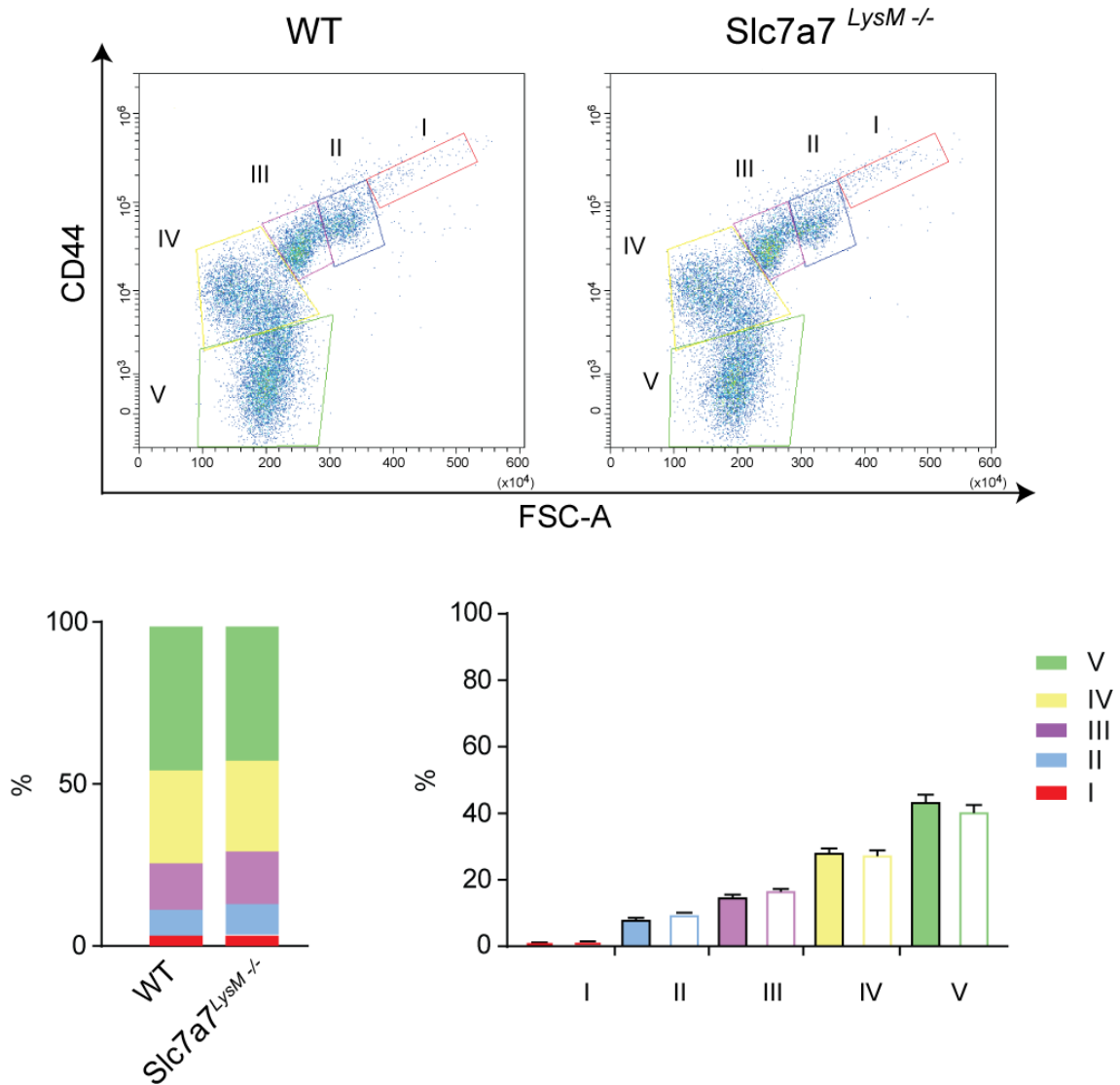


Figure 42. Erythropoietic analysis. Erythroid progenitor populations in the bone marrow were analyzed as described by Chen *et al.*, 2009. Upper panels show a pseudo-color dot plot with the 5 defined regions. Lower panels show the quantification. Cells were gated in TER119⁺. n=3 wild type and 3 *Slc7a7^{LysM^{-/-}}*.

In addition, Perls' staining of spleen and bone marrow did not reveal increased iron accumulation in these tissues of *Slc7a7^{LysM^{-/-}}* mice (Figure 43), and PAS staining did neither revealed abnormalities in the lungs of these animals (Figure 43).

RESULTS

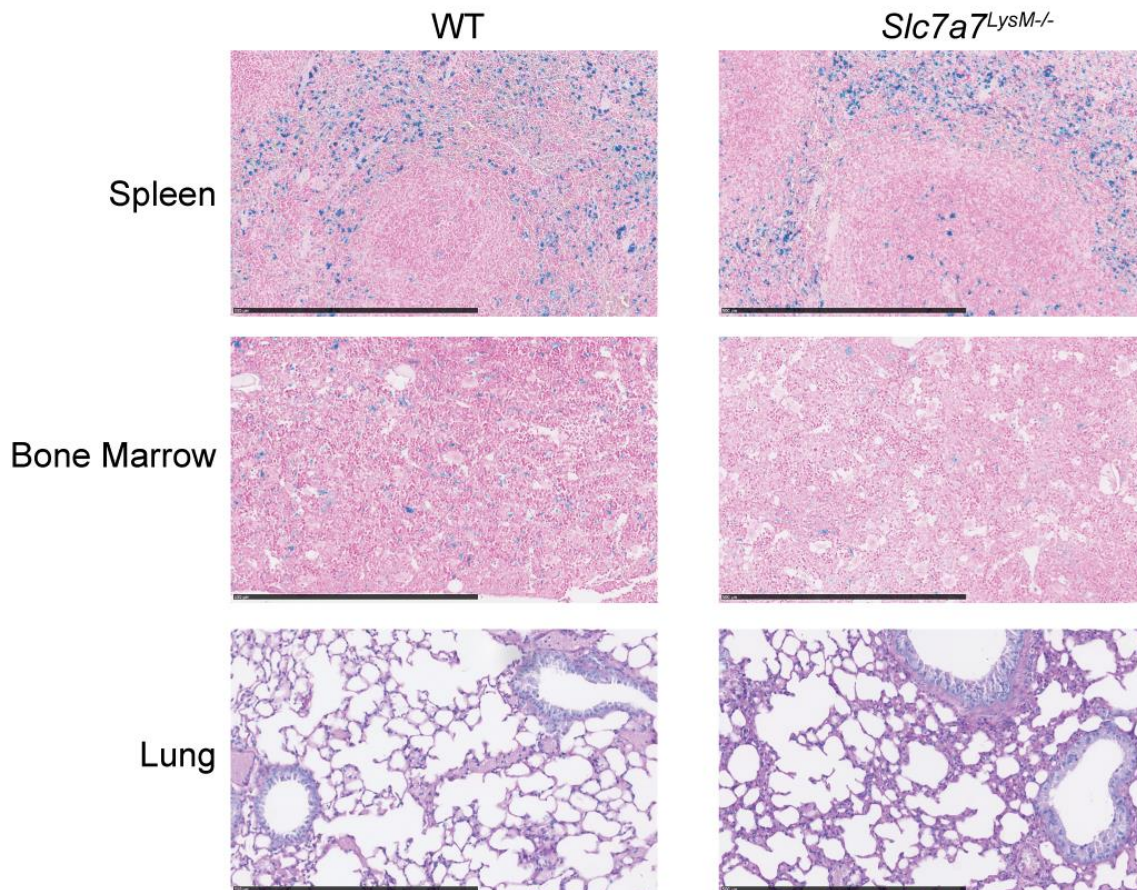


Figure 43 Histologic analysis of *Slc7a7*^{LysM^{-/-}} mouse model. Representative sections of spleen and bone marrow, of wild type and *Slc7a7*^{LysM^{-/-}} animals stained with Perls' Prussian Blue. Lung sections were stained with PAS. Scale bars represent 500µm.

Molecular characterization of *Slc7a7*^{-/-} red pulp macrophages

To gain a better understand of the molecular processes altered in RPM of *Slc7a7*^{-/-} mice, we sorted this cell population and performed transcriptomic analysis. RPM have been defined to highly express F4/80 and Vcam1 and to be low/negative for Cd11b expression (Kohyama *et al.*, 2008). In addition we hypothesized that iron deposits may be altering their cellular complexity, producing detectable changes in the side scatter parameter (SSC) depending on the quantity of accumulated iron. Consequently, the strategy used to isolate the RPM population was to sort splenocytes strongly positive for F4/80 and Vcam1 and low/negative for Cd11b. Afterwards, within this population we distinguished two subpopulations regarding their complexity: SSC^{hi} and SSC^{lo}. The isolated populations were cytopspun and stained in order to validate the sorting strategy (Figure 44).

RESULTS

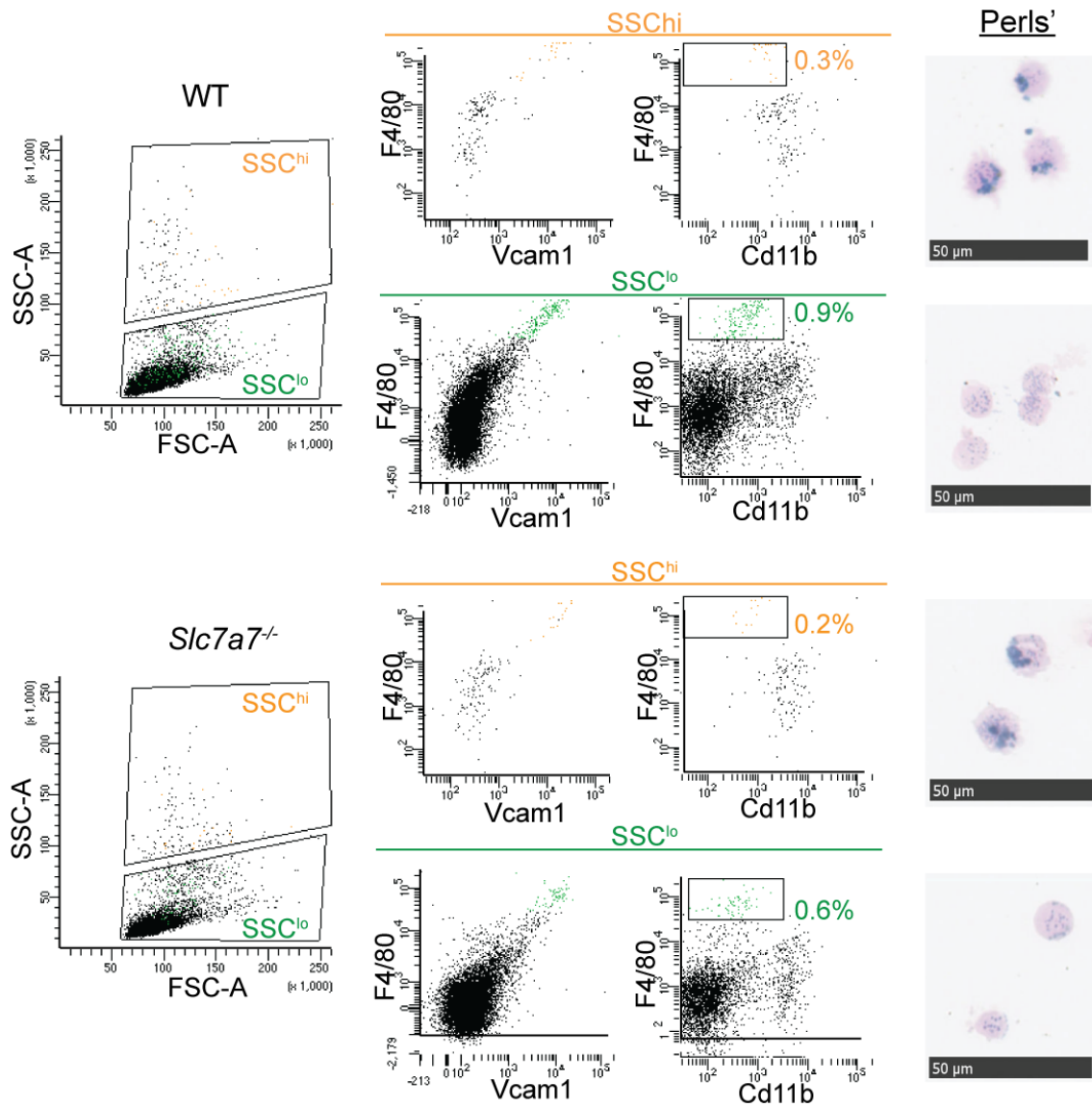


Figure 44. Sorting strategy of RPM. Average percentage of sorted populations over the living cells are shown. Legend: highest complexity RPM subpopulation (SSC^{hi}) is colored in orange, lowest complexity RPM subpopulation (SSC^{lo}) is colored in green. Representative images of Perls' staining of isolated cells. Scale bars represent 50 μm.

By Panoptic staining we first corroborated that the sorted cells looked like macrophages. Then, Perls' staining also confirmed that sorted cells presented iron deposits and that the SSC^{hi} subpopulation contained bigger iron deposits than the SSC^{lo} (Figure 44). *Slc7a7*^{-/-} RPM showed a slight weaker signal for F4/80 than the wild type ones. In accordance with previous reports, the whole RPM population accounted for ~1.2% of total splenocytes in wild type animals (Kohyama *et al.*, 2008) and this percentage was significantly reduced in *Slc7a7*^{-/-} mice (Figure 45). Within the RPM population, the SSC^{lo} subpopulation was the most representative one, accounting for ~75% of the total RPM in wild type and *Slc7a7*^{-/-} animals. In both subpopulations

RESULTS

of *Slc7a7*^{-/-} mice, *Slc7a7* expression was effectively reduced, falling down between a 65 and 75% respectively compared to wild type (Figure 45).

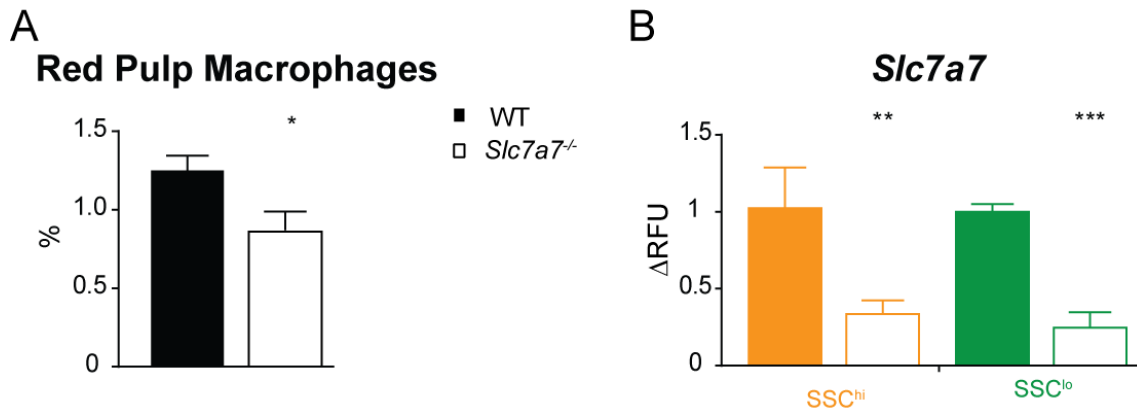


Figure 45. Red Pulp Macrophages. **A.** Percentage of total red pulp macrophages. Data±SEM. n= 10 mice per group. **B.** y⁺LAT1 (*Slc7a7*) mRNA expression in sorted populations. Results are expressed as the percentage of change compared to controls' expression and relative to actin (*Actb*) expression. n= 4 mice per group. Highest complexity RPM subpopulation (SSC^{hi}) is colored in orange, lowest complexity RPM subpopulation (SSC^{lo}) is colored in green. Data±SEM. **p*-value<0.05; ***p*-value<0.01; ****p*-value<0.001.

For the transcriptomic study, 4 animals per group (wild type and *Slc7a7*^{-/-}) were used. Then, following the mentioned sorting strategy, 16 samples of 7000 cells were collected. mRNA was purified and hybridized for a microarray experiment. Thus, the experimental design included four groups (wild type SSC^{hi}/SSC^{lo} and *Slc7a7*^{-/-} SSC^{hi}/SSC^{lo}) and each of those groups comprised four samples. This strategy allowed us to make comparisons between samples regarding their genotype (wild type versus *Slc7a7*^{-/-}) and their cellular complexity (SSC^{hi} versus SSC^{lo}).

Principal components analysis (PCA) revealed that samples gathered by genotype rather than by complexity (Figure 46). Indeed, establishing a threshold of false discovery rate (FDR) <0.25 and for an absolute fold change (FC)>1.5, no genes came out as differentially expressed for the comparison between wild type SSC^{hi} and wild type SSC^{lo}. Using the same threshold for the comparison between *Slc7a7*^{-/-} SSC^{hi} and *Slc7a7*^{-/-} SSC^{lo} only 8 genes came out as differentially expressed (Table 9). These results together proved that the differences in cellular complexity found by flow cytometry in RPM, did not translate in big transcriptomic changes.

Gene set enrichment analysis (GSEA) is a computational method that determines whether an *a priori* defined set of genes shows statistically significant concordant differences between two biological states (*e.g.* phenotypes). With the results obtained from GSEA, we performed pathway mapping with the [KEGG pathway database](#). This allows to draw pathway maps for biological interpretation of higher-level systemic functions such as metabolism, human diseases or cellular processes among others. To do this analysis, we first calculated the

RESULTS

differences between wild type and *Slc7a7*^{-/-} in SSC^{hi} subpopulation. Then, the same was calculated for wild type and *Slc7a7*^{-/-} in SSC^{lo}. Finally, differences of these differences were calculated and used for the analysis. This allowed to perform a GSEA analysis focusing on the genotypes, but without losing the information obtained for the different subpopulations of RPM.

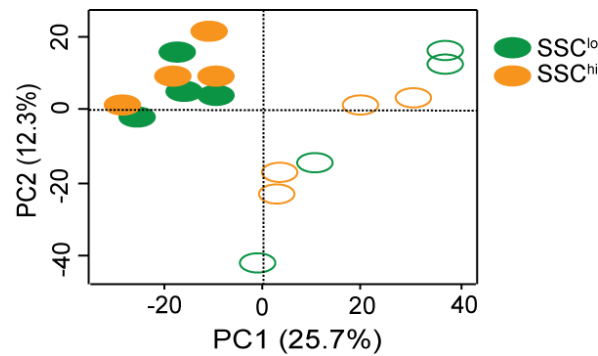


Figure 46. Principal components analysis. Filled ellipses represent wild type samples; empty ellipses represent *Slc7a7*^{-/-} samples.

Gene symbol	Gene title	SSC ^{hi} -SSC ^{lo} FC	SSC ^{hi} -SSC ^{lo} FDR	SSC ^{hi} -SSC ^{lo} P-val
Cd3d	CD3 antigen, delta polypeptide	-1.66	0.07	3.31E-06
Fkbp9	FK506 binding protein 9	-1.57	0.12	1.06E-05
Gfm1	G elongation factor, mitochondrial 1	-1.5	0.19	5.29E-05
Ppp3r1 /// Wdr92	protein phosphatase 3, regulatory subunit B, alpha isoform (calcineurin B, type I) /// WD repeat domain 92	-1.58	0.21	9.01E-05
Mrpl41	mitochondrial ribosomal protein L41	-1.62	0.22	0.0001
1700017B05Rik	RIKEN cDNA 1700017B05 gene	-1.52	0.23	0.0002
Nsg2	neuron specific gene family member2	-2.1	0.24	0.0003
Rcan3	regulator of calcineurin 3	-1.53	0.24	0.0003

Table 9. Genes differentially expressed. Summary of genes differentially expressed for *Slc7a7*^{-/-} SSC^{hi} versus *Slc7a7*^{-/-} SSC^{lo} with FDR<0.25 and FC>1.5.

RESULTS

We established a threshold of $FDR < 0.25$ and nominal $p\text{-value} < 0.05$, for pathway selection. Following these criteria, 35 pathways came out as differentially expressed between *Slc7a7*^{-/-} and wild type samples. Curiously, all the 35 pathways identified were down-regulated, while no pathways up-regulated fulfilled this criteria. Among the pathways that came out as differentially expressed, clearly predominated those that represent immune system, immune diseases or processes/diseases that typically result in inflammation (16 out of 35). Also those pathways related to cell cycle and proliferation represented an important percentage (7 out of 35) of the differentially expressed pathways (Figure 47).

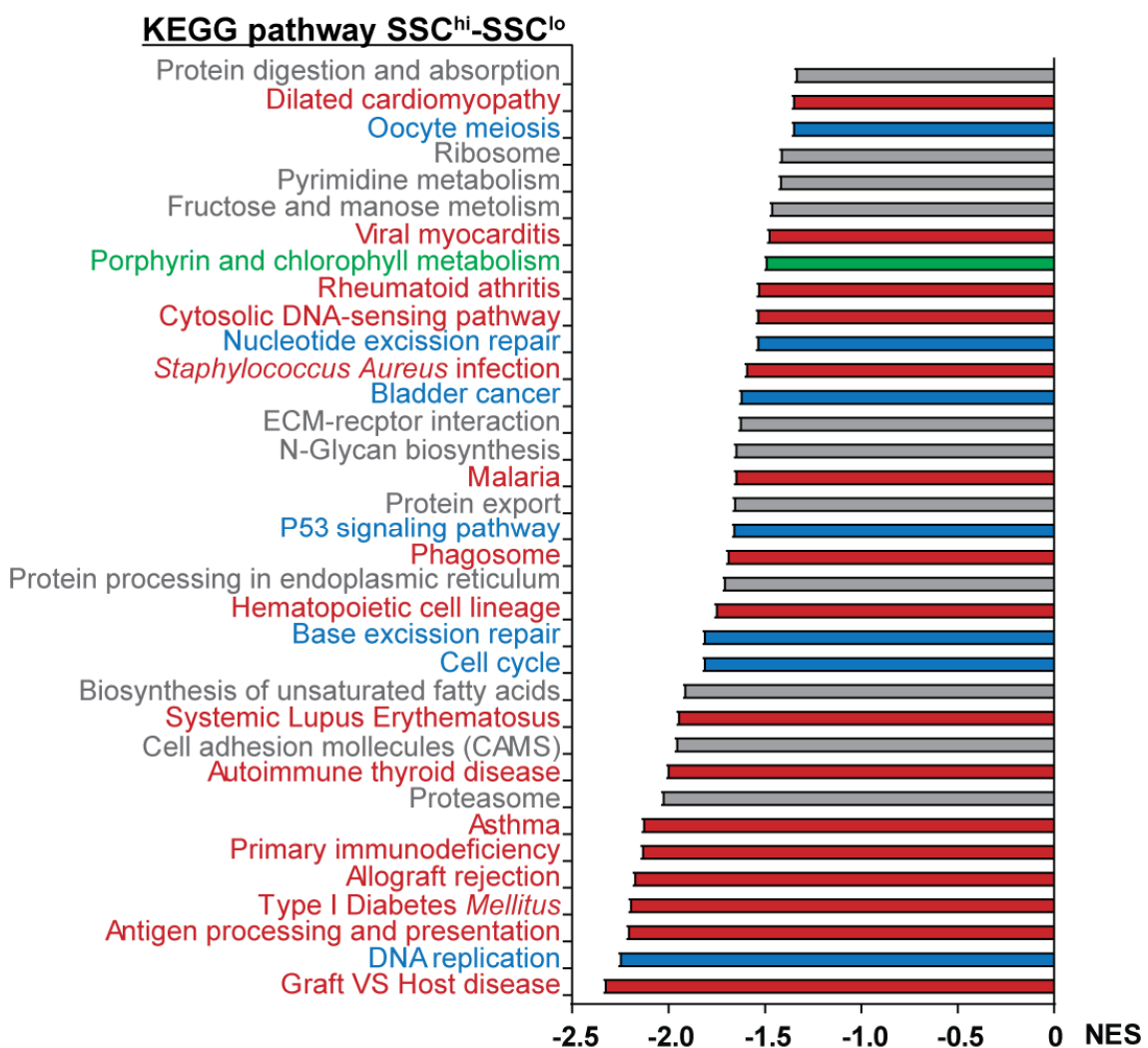


Figure 47. Gene set enrichment analysis with KEGG pathway database. The differences of the differences for SSC^{hi} and SSC^{lo} between wild type and *Slc7a7*^{-/-} samples were used. X axis is the normalized enrichment score. $FDR < 0.25$ and $p\text{-value} < 0.05$. In red, pathways related to immune and/or inflammatory processes. In blue, pathways related to cell cycle and proliferation. In green, pathways related to iron metabolism. In grey, others.

RESULTS

Interestingly and according with the phenotype of iron accumulation found by spleen histology, porphyrin and chlorophyll metabolism pathway came out as down-regulated in *Slc7a7*^{-/-} samples compared to wild type.

To get a more specific idea about the expression of genes involved in heme metabolism in macrophages, we took advantage of the results published by Haldar *et al.*, 2014. The system used in that work was bone marrow derived macrophages (BMDM) *in vitro* differentiated for one week with GM-CSF and treated with hemin (heme from now on) or vehicle. Firstly, we selected those genes that heme induced a FC>3 compared to vehicle in wild type cells. This collection of genes was plotted as a heat map to have a general view of the expression pattern of this pathway in *Slc7a7*^{-/-} RPM compared to wild type (Figure 48). It can be observed that heme metabolism is increased in *Slc7a7*^{-/-} samples, with an increased expression of characteristic markers such as SpiC (*SpiC*) and heme oxygenase 1 (*Hmox1*). However other genes that should be also increased, did not showed this trend. A gene that clearly exemplifies this situation is ferroportin (*Slc40a1*), the only iron exporter identified in mammalian cells so far. We should expect a notably increment of its expression in *Slc7a7*^{-/-} samples, however it did not changed compared to wild type (Figure 48).

RESULTS

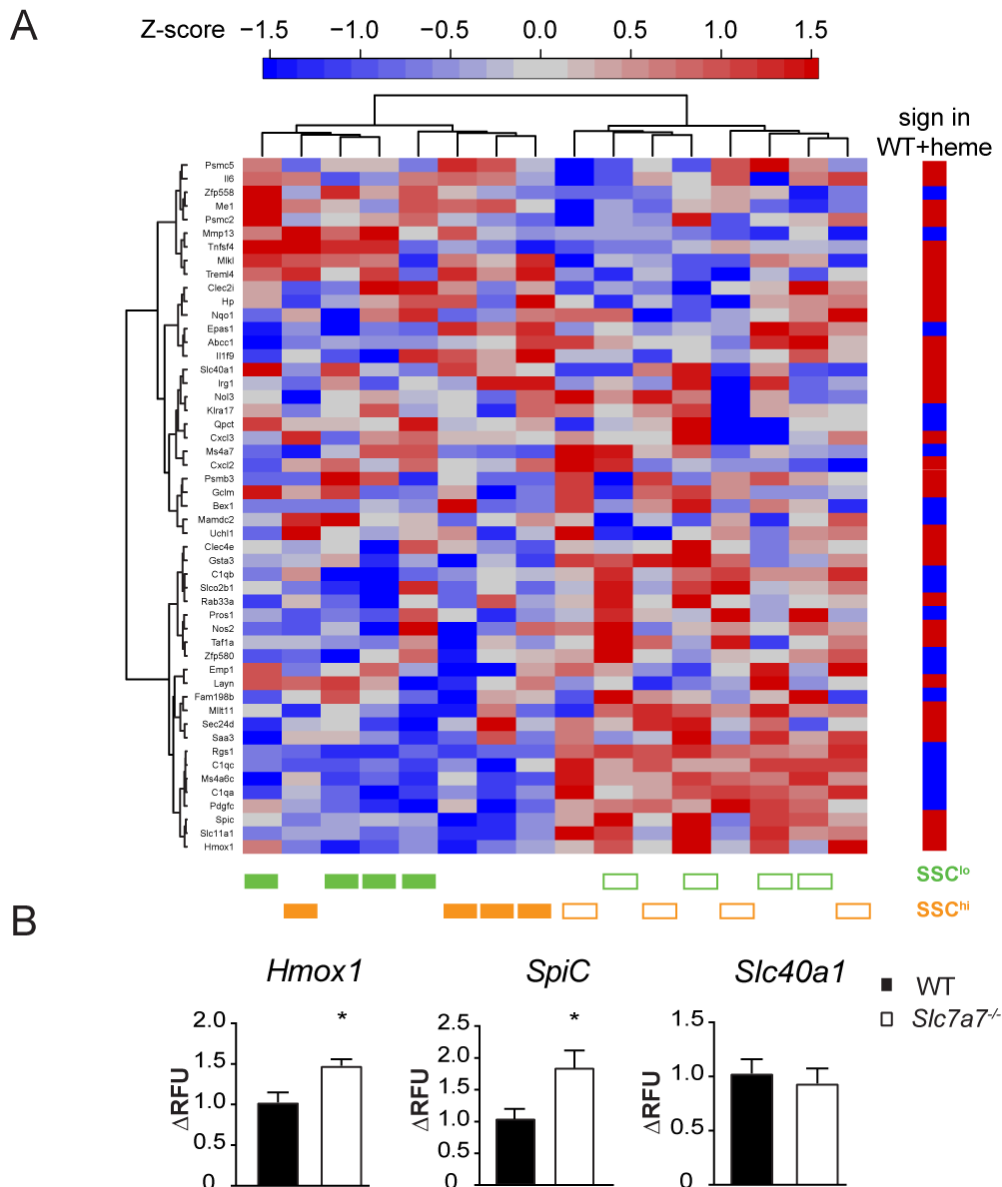


Figure 48. Heatmap for heme metabolism markers. **A.** Heatmap representation. Right bar shows the expected sign in case of active heme metabolism. Lower boxes show *Slc7a7*^{-/-} (empty) and wild type (filled) samples clusterization. **B.** qRT-PCR of selected genes. Results are expressed as the percentage of change compared to controls' expression and relative to actin (*Actb*) expression. Data±SEM. n=5 for wild type and *Slc7a7*^{-/-}.

Haldar *et al.*, 2014 showed that genes downstream of the regulatory axis Bach1-SpiC are essential for heme metabolism in macrophages. In that article, authors claim that heme releases SpiC transcription factor from its repression by Bach1, going then into the nucleus and activating a whole program that allows macrophages to get into mature differentiation state and to metabolize heme properly. So again we took advantage of their published results, and defined the Bach1-dependent genes as those genes which the difference in FC between wild type and *Bach1*^{-/-} heme versus vehicle >3 (Figure 49). The genes that fulfilled this criteria were plotted in a heat map with the differential expression between *Slc7a7*^{-/-} and wild type RPM

RESULTS

(Figure 49). We did not identified a clear correlation of differential expression of Bach1 dependent genes in *Slc7a7^{-/-}* RPM compared to wild type.

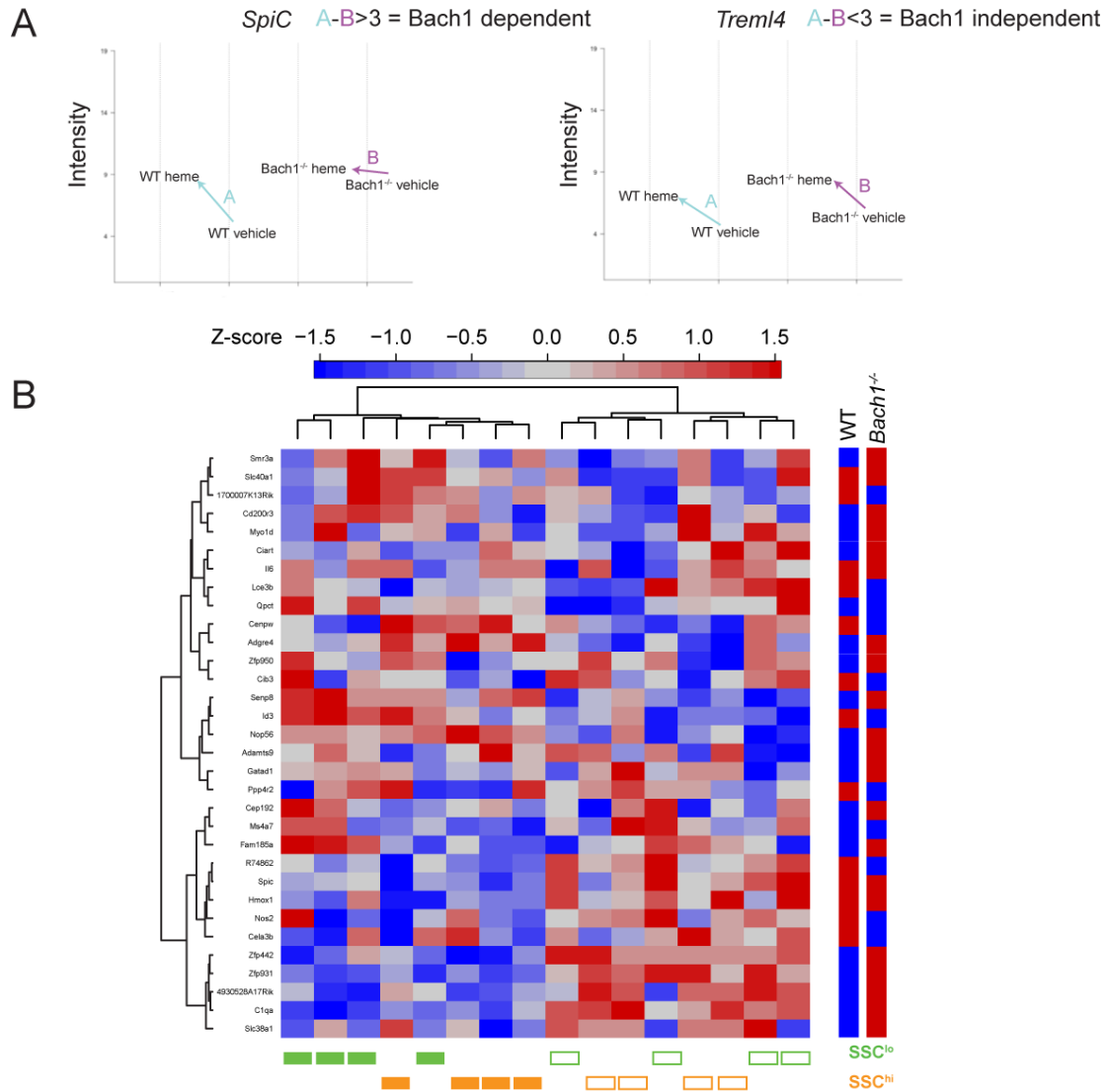


Figure 49. Heatmap for Bach1-dependent genes. **A.** Exemplificative image of Bach1 dependent genes definition. A represents the fold change between the expression of a given gene in vehicle versus heme treated wild type cells. B represents the same parameter in *Bach1^{-/-}* cells. Left plot shows *SpiC* as example of a Bach1-dependent gene, while right plot represents *Trem14* as example of a Bach1-independent gene **B.** Heatmap for Bach1 dependent genes. Right bar shows the sign in wild type and *Bach1^{-/-}* heme treated samples. Lower boxes show *Slc7a7^{-/-}* (empty) and wild type (filled) samples clusterization.

Increased erythrophagocytosis in bone marrow and spleen is a characteristic trait of HLH, and it has been reported as a common trait in LPI patients diagnosed for HLH. Regarding the iron accumulation observed in *Slc7a7^{-/-}* macrophages, heme from aged or damaged red blood cells (RBC) is the main source of iron uptake by RPM. Thus, increased erythrophagocytosis can be another potential factor contributing to the increased iron phenotype. We then analyzed the

RESULTS

expression levels of a collection of genes selected from different studies (reviewed in the introduction sections: hemophagocytic lymphohistiocytosis and iron and macrophages), which have been reported to be involved in erythrophagocytosis in macrophages. The expression pattern found clearly fitted with increased erythrophagocytosis in *Slc7a7*^{-/-} samples compared to wild type (Figure 50). The gene expression of some of the selected markers was further analyzed by qRT-PCR, confirming the results obtained by transcriptomic analysis (Figure 50). This confirmation was only done for SSC^{lo} samples, since it is the predominant subpopulation within RPM.

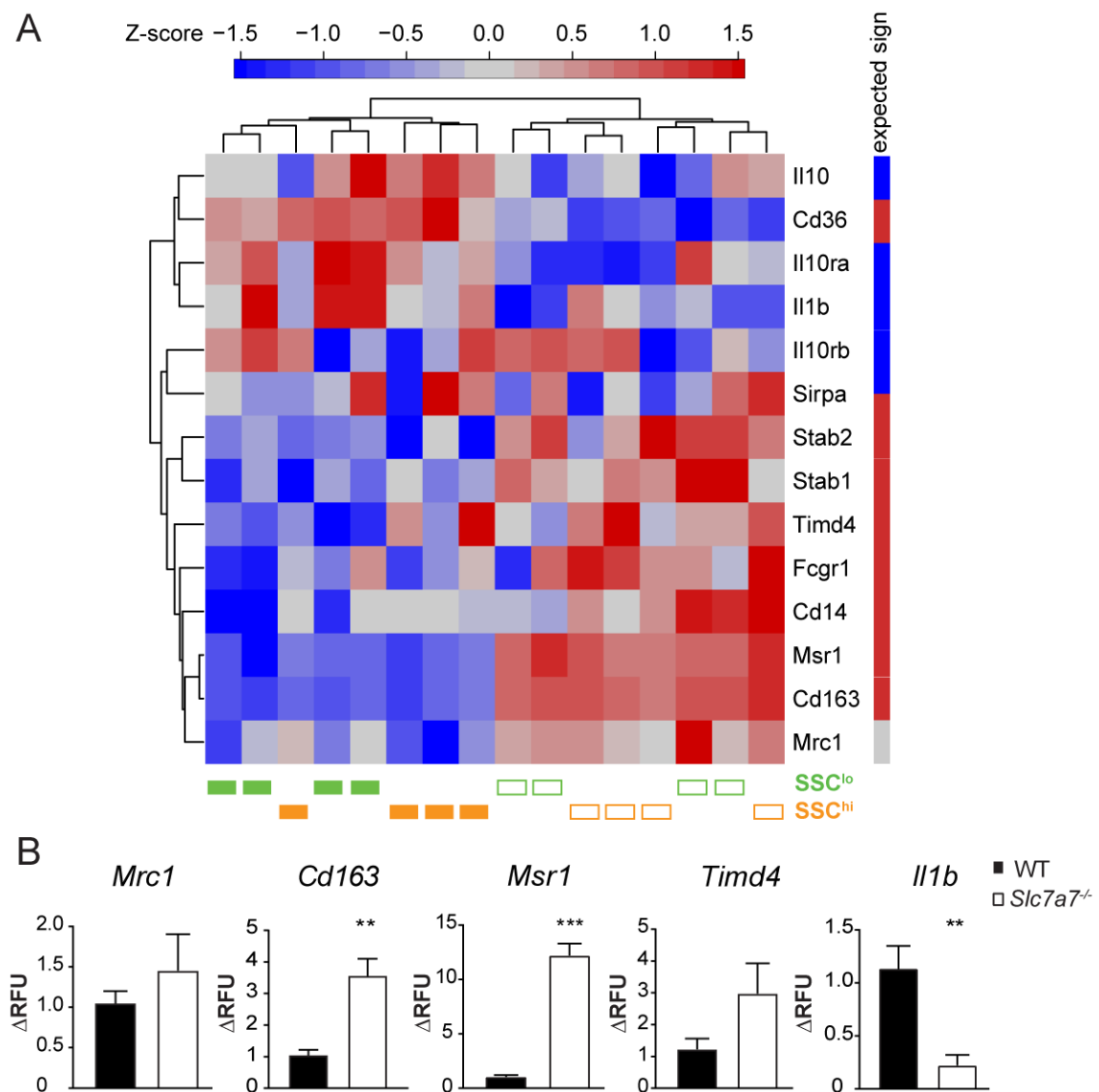


Figure 50. Erythrophagocytosis. **A.** Heatmap representation of erythrophagocytosis markers. Right bar shows the expected sign in case of active erythrophagocytosis. Lower boxes show *Slc7a7*^{-/-} (empty) and wild type (filled) samples clusterization. **B.** qRT-PCR of selected genes. Results are expressed as the percentage of change compared to controls' expression and relative to actin (*Actb*) expression. Data±SEM. n=5 for wild type and *Slc7a7*^{-/-}.

RESULTS

We then analyzed RPM population in *Slc7a7^{LysM^{-/-}}* mice. In this mouse model we did not distinguish between SSC^{hi} and SSC^{lo} subpopulations. The percentage of RPM was similar in wild type and *Slc7a7^{LysM^{-/-}}* animals, and for both groups it was ~1.2% of total splenocytes (Figure 51).

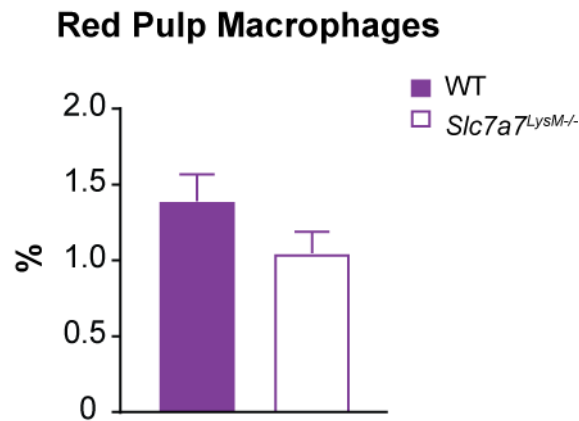


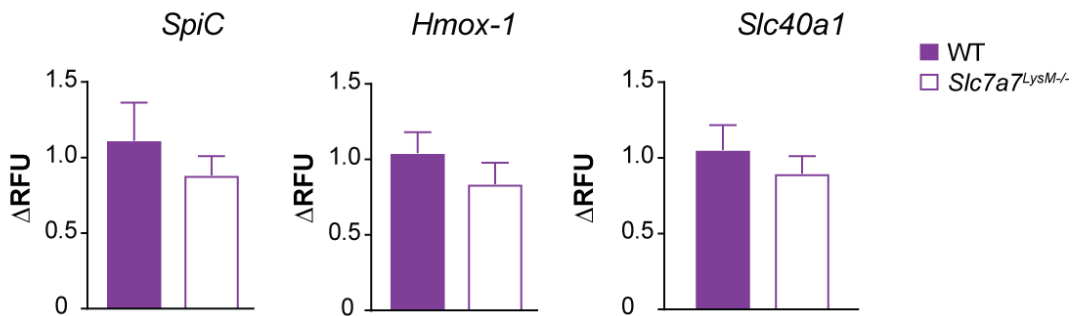
Figure 51. Percentage of RPM in LysM mouse model. n=5 for wild type and *Slc7a7^{LysM^{-/-}}*. Data±SEM.

We then analyzed the expression levels of the selected markers that were altered in *Slc7a7^{-/-}* RPM. No markers of increased heme metabolism came out, finding the expression levels of *SpiC*, *Hmox-1* and ferroportin similar in *Slc7a7^{LysM^{-/-}}* and wild type (Figure 52). We neither observed a gene expression pattern of increased erythrophagocytosis. *Il1b*, *Msr1* and *Timd4* expression levels were also similar between *Slc7a7^{LysM^{-/-}}* and wild type animals. Curiously, *Cd163* expression was found to be reduced in *Slc7a7^{LysM^{-/-}}* RPM (Figure 52).

RESULTS

A

Heme metabolism



B

Erythrophagocytosis

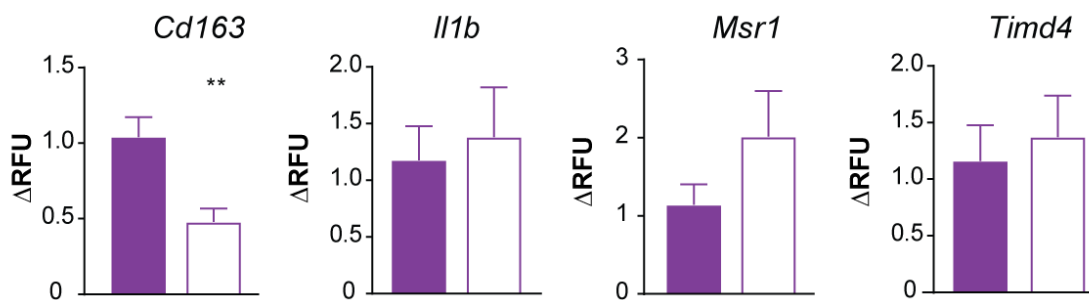


Figure 52 . qRT-PCR of selected markers. A. Heme metabolism related markers. **B.** Erythrophagocytosis related markers. Results are expressed as the percentage of change compared to controls' expression and relative to actin (*Actb*) expression. Data±SEM. n=6 for wild type and *Slc7a7^{LysM}-/-*.

In the *Slc7a7^{LysM}-/-* mouse model, erythropoietic abnormalities, anemia markers, unbalance between lymphocytes and granulocytes and hyperferritinemia were absent. Moreover expression levels of markers of iron metabolism were similar in red pulp macrophages of *Slc7a7^{LysM}-/-* and wild type animals, and we neither observed a gene expression pattern of increased erythrophagocytosis in this cell population. All together these results showed no LPI immune-related alterations in *Slc7a7^{LysM}-/-* animals, and defined the need of the metabolic dysfunction to develop them.

***In vitro* experiments: effect of LPI metabolic environment in iron export and erythrophagocytosis**

To better understand the molecular mechanism behind iron retention by macrophages in LPI, we decided to perform *in vitro* experiments using bone marrow derived macrophages (BMDM)

RESULTS

as cellular model. Firstly, we corroborated that BMDM from *Slc7a7^{-/-}* animals efficiently lost γ^+ LAT1 expression (Figure 53). Keeping in mind the results obtained so far, we designed an approach to evaluate the impact of the metabolic environment generated in LPI (LPI environment from now on) due to the loss of function of γ^+ LAT1 in kidney and intestine. We mimicked physiological blood conditions of arginine and ammonia *in vitro* and stimulated BMDM to study their response. Thus, three different experimental conditions were established regarding the arginine and ammonia concentration expected in animals:

- Control (wild type): 50 μ M arginine, no ammonia
- Pathologic (LPI): 20 μ M arginine, 1mM ammonia
- Recovery (LPI + Citrulline): 20 μ M arginine, 1mM ammonia, 250 μ M citrulline

As arginine is the sole substrate of iNOS for NO production, we hypothesized that LPI environment can be reducing NO production by macrophages. Moreover, as explained in the introduction, it has been described a regulatory feedback between NO and iron-related proteins. Following this idea, BMDM were firstly stimulated with LPS and IFN γ , and NO production was evaluated as soluble nitrates. After 48h of stimulation, a significant reduction of NO was detected in BMDM under LPI conditions. Moreover, the addition of citrulline recovered the NO production to control levels. This effect was independent BMDM's genotype but specific for the culture conditions (Figure 53).

We then assessed whether the different media conditions also affect iron export via ferroportin expression. Consequently, BMDM were stimulated with iron chloride (FeCl₃) for 48h and ferroportin expression was checked by western blot. Similar results were obtained compared to NO production. In this case ferroportin expression was slightly higher in *Slc7a7^{-/-}* than wild type BMDM in wild type condition. LPI culture media produced a reduction in ferroportin expression of wild type and *Slc7a7^{-/-}* BMDM although it was statistically significant only in *Slc7a7^{-/-}* cells. Finally, addition of citrulline again recovered ferroportin expression levels (Figure 54).

RESULTS

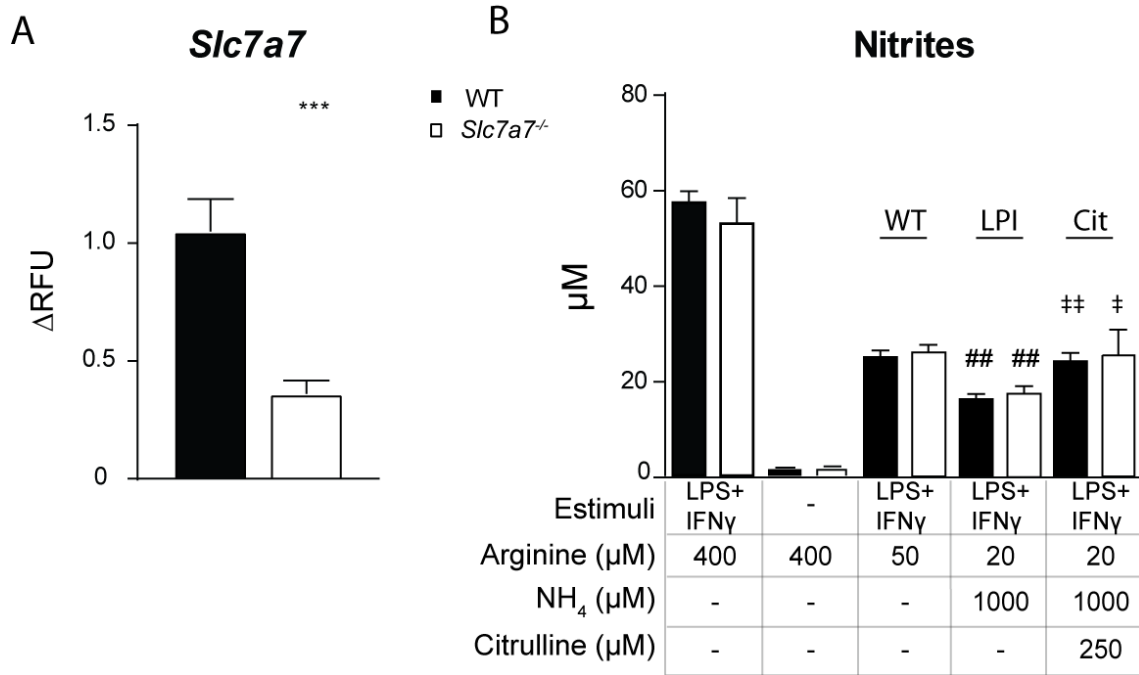


Figure 53. BMDM and NO production. **A.** qRT-PCR of *Slc7a7*. Results are expressed as the percentage of change compared to controls' expression and relative to actin (*Actb*) expression. n=6 for WT and *Slc7a7*^{LysM-/-}. **B.** Nitric oxide production. Bone marrow derived macrophages were stimulated with LPS plus IFN γ under the indicated culture conditions and nitrates in the medium were quantified. Data \pm SEM. n=6 for wild type and *Slc7a7*^{-/-}. *p-value<0.05; ** p-value<0.01; ***p-value<0.001. * denotes differences between different genotypes, # and ‡ denotes differences between same genotype and different culture condition.

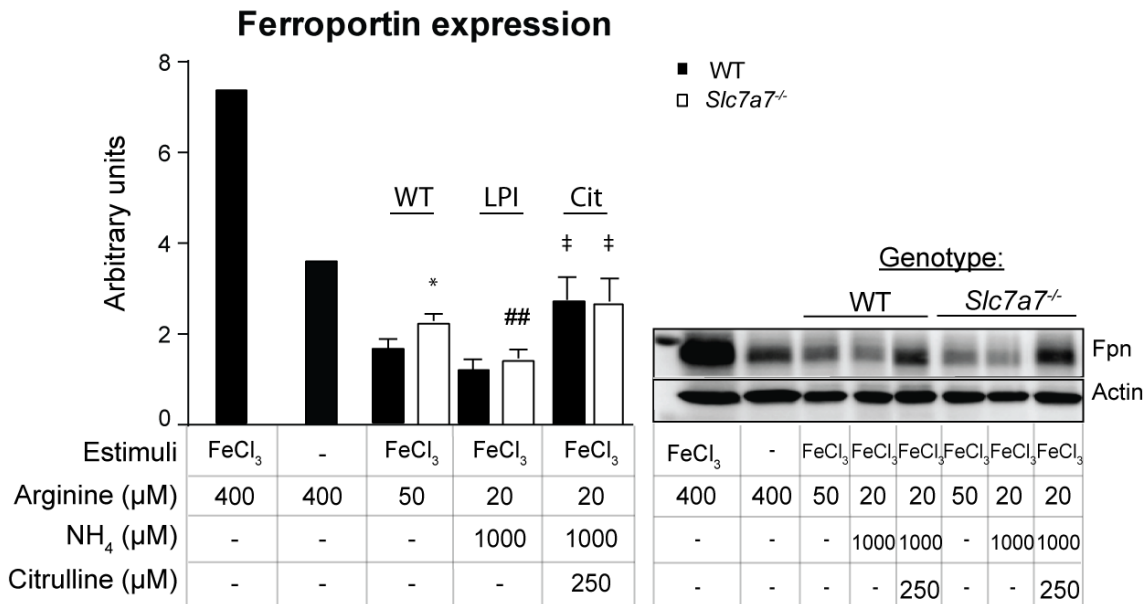


Figure 54. Ferroportin expression. Bone marrow derived macrophages were stimulated with FeCl $_3$ under the indicated culture conditions and ferroportin expression was measured by western blot. Right plot is the quantification of the different blots. Left blot is representative for the rest of results obtained. Data \pm SEM. n=6 for wild type and *Slc7a7*^{-/-}. *p-value<0.05; **p-value<0.01. * denotes differences between different genotypes, # and ‡ denotes differences between same genotype and different culture condition.

RESULTS

Taking into account that erythropoiesis is altered in *Slc7a7*^{-/-} mice, and regarding the markers of active erythrophagocytosis found in *Slc7a7*^{-/-} RPM, we wondered whether the cause of the rise in this process is due to a malfunctioning of the macrophages or because of erythrocytes are defective and need to be replaced. To address this question, we performed an erythrophagocytosis *in vitro* assay, where BMDM are co-incubated for two hours with previously labeled erythrocytes. Finally, those macrophages that have engulfed erythrocytes can be distinguished by flow cytometry.

First, we assessed the number of BMDM from wild type and *Slc7a7*^{-/-} animals that engulfed *Slc7a7*^{-/-} or wild type erythrocytes. The result obtained shows that irrespectively of the macrophages' genotype, there is a clear trend of higher phagocytosis of *Slc7a7*^{-/-} erythrocytes (Figure 55). The number of experiments needs to be increased in order to confirm this trend statistically. Then we performed a sort of competitive assay, where BMDM were co-incubated with a mix of *Slc7a7*^{-/-} and wild type erythrocytes. By this strategy, it can be defined whether *Slc7a7*^{-/-} erythrocytes are more prone to be engulfed than the wild type ones under the same circumstances. The result obtained showed that indeed this was the case, and *Slc7a7*^{-/-} erythrocytes, somehow, are more "appetizing" for macrophages than the wild type ones (Figure 55). This is indicating that *Slc7a7*^{-/-} erythrocytes probably suffer some kind of abnormality and display more "eat-me" signals on their membrane.

RESULTS

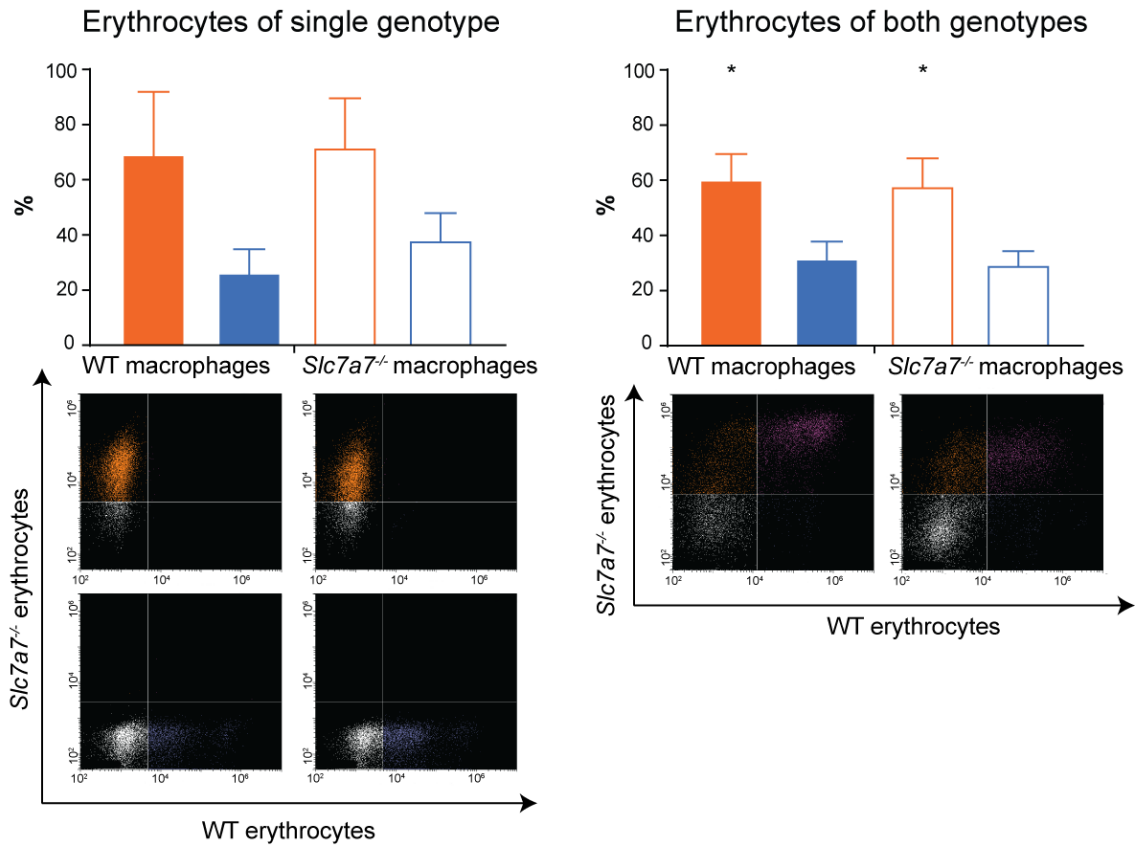


Figure 55. *In vitro* erythrophagocytosis assay. Bone marrow derived macrophages were co-cultured with previously labeled erythrocytes. Wild type erythrocytes were labeled with CellVue Claret and are represented in blue, while *Slc7a7*^{-/-} erythrocytes were labeled with PKH26 and are represented in orange. Wild type macrophages are represented as filled bars and *Slc7a7*^{-/-} macrophages are represented as empty bars. Data±SEM. n=3 for WT and *Slc7a7*^{-/-} in the single genotype experiment and n=6 for WT and *Slc7a7*^{-/-} in the mixed genotypes experiment. **p*-value<0.05.

DISCUSSION

Historically LPI has been conceived as a dichotomic disease: on one hand the metabolic hallmarks; on the other hand the immune and hematologic complications (Sebastio, Sperandeo and Andria, 2011). However, in this study we describe that the metabolic condition is essential for the development of, at least, some of the immune and hematologic complications of LPI.

Since the initial description of LPI in Finland by Perheetupa and Visakorpi in 1965, cases of LPI have been reported worldwide. Clinical symptoms of LPI appear after weaning, a fact that can be explained by the endogenous arginine biosynthesis in mammals. Adult mammals synthesize arginine from citrulline mainly in the proximal tubules of the kidney. The endogenous biosynthesis of arginine covers the daily requirement under steady state condition, but a complement of arginine from diet may become necessary when demand increases (Wouter J. de Jonge *et al.*, 2002). In addition, it seems that during the weaning period of mammals, the supply of arginine from milk is not enough to meet the body requirements and a high degree of endogenous synthesis is needed (Davis, Fiorotto and Reeds, 1993). Endogenous arginine biosynthesis during this period occurs in intestine rather than in kidney. It has been shown that in suckling rats, enterocytes in small intestine express Argininosuccinate synthase (*Ass1*) and Argininosuccinate lyase (*Asl*), the enzymes required for arginine biosynthesis. After weaning, the enterocytes lose the expression of these enzymes and start to express *Arg1*, changing then their capacity of arginine synthesis for the capacity of arginine consumption (de Jonge *et al.*, 1998). This physiological process is likely shared with humans, since destruction of enterocytes in necrotizing colitis in preterm neonatal also results in a selective decrease of circulating arginine (Richir *et al.*, 2007). Then, one could hypothesize that this metabolic switch in arginine biosynthesis after weaning may be a plausible explanation for the appearance of the clinical symptoms in LPI. This assumption could be true if somehow kidney is less effective than intestine in the production of arginine. A very naïve reasoning could be that the number of enterocytes in small intestine is huge compared to the number of epithelial cells in the proximal tubules.

The lack of γ^+ LAT1 in kidney and intestine drives a secondary defect of the urea cycle, and all together define the metabolic hallmarks of LPI: malabsorption and deficient renal reabsorption of cationic amino acids followed by hyperammonemia and orotic aciduria. Similarly to patients, *Slc7a7^{-/-}* mice also developed these metabolic hallmarks after de induction of the disease, and also same as in patients, all these symptoms improved when citrulline was supplemented to diet. The low survival as well as the quick loss of body weight is likely due to a multiorgan failure caused by the defect of the urea cycle, since other animal models of urea cycle

disorders such as the one for argininosuccinic aciduria (Argininosuccinate lyase (Asl) knock out mouse model) performs a very similar phenotype. Moreover, when those animals were treated to restore the urea cycle, showed an improvement similar to *Slc7a7*^{-/-} mice treated with citrulline (Erez *et al.*, 2011). Indeed, this phenotype can be specifically assigned to hyperammonemia, because mice lacking *Arg1* develop hyperammonemia and hyperargininemia, and also suffered a similar loss of body weight and low survival (Sin *et al.*, 2013).

Although all LPI patients share the metabolic hallmarks of LPI, a great deal of clinical heterogeneity has been reported regarding the immune and hematologic complications. The huge heterogeneity found among patients (Ogier de Baulny, Schiff and Dionisi-Vici, 2012a), the fact of an absent relationship between the genotype and the phenotype (Sebastio, Sperandeo and Andria, 2011) and the lack of a proper animal model (Sperandeo *et al.*, 2007) have complicated research in LPI complications. This study presents *Slc7a7*^{-/-} as the first viable mouse model to study the immune and hematologic complications of human LPI. Despite of possible differences between the physiology of human and mice, we have shown that *Slc7a7*^{-/-} animals develop at least some of the complications reported in patients: anemia, PAP, hyperferritinemia and increased erythrophagocytosis. Nevertheless, other complications such as glomerulonephritis were not observed in the *Slc7a7*^{-/-} mice analyzed so far. Maybe different strategies should be followed to check whether *Slc7a7*^{-/-} mice are free of these complications or whether we could not detect them due to technical reasons. For instance, kidney disease have been reported to appear in older patients of LPI (Mauhin *et al.*, 2017), then maybe a long-term follow up is needed to detect some of these complications in mice. In addition, a striking difference between the symptoms reported in patients and the mouse model was observed: hepatosplenomegaly. It has been widely described in human LPI, while the liver of *Slc7a7*^{-/-} animals was unaffected and the spleen size was even reduced rather than enlarged. A reduction of the spleen size was also reported in a mouse model which by the overexpression of *Arg1* in the intestine becomes hypoargininemic but no hyperammonemic during the first three weeks of age (De Jonge *et al.*, 2002). In that article, authors discuss that this decrease in the splenic weight is due to a defective development of the immune system. Moreover, it was further demonstrated that the reduction in arginine availability specifically affects B, but not T, lymphocytes development in the bone marrow. This generates a reduction in the number of B cells leaving the bone marrow, which consequently results in a diminution of the number of B cells in periphery tissues such as spleen, thymus and Peyer's patches (Wouter J de Jonge *et al.*, 2002). In addition, *Asl* knock out mice were also reported to suffer a diminished germinal

center formation and relative lymphocyte depletion in the spleen (Erez *et al.*, 2011). In the case of *Slc7a7*^{-/-} mouse model, we have also corroborated that the proliferation follicles in the spleen are depleted and that the percentage of B cells (IgM⁺ CD45R⁺) in this tissue was also reduced compared to wild type littermates.

Regarding PAP development, we could not study whether citrulline supplementation also exerts beneficial effects. Nevertheless, since no *Slc7a7*^{LysM^{-/-}} animals developed PAP, it seems clear that the metabolic derangement should also impact somehow in the appearance of this phenotype. As well as in patients only a percentage of *Slc7a7*^{-/-} animals developed PAP. Thus, there should be some modulatory factors influencing PAP development in LPI. It seems that hyperammonemia is not one of these factors, since loss of body weight is dependent on hyperammonemia while PAP is not. Surfactant is mainly composed by lipids, and defective GM-CSF signaling pathway impairs key genes involved in lipid metabolism such as PPAR γ . LPI patients suffer severe dyslipidemia, it can be then a potential modulatory factor of PAP in LPI. Dysfunction of alveolar macrophages (AM) has been postulated to be responsible of PAP development in LPI. A possible hypothesis is that dyslipidemia could be affecting the lipid composition of surfactant, impairing then its recognition by AM via scavenger receptors. Nevertheless, the molecular mechanism that drives PAP development in LPI remains unknown. The use of recombinant GM-CSF has shown controversial outcomes. The results obtained from *Slc7a7*^{-/-} mouse model do not allow valuing the convenience of its use and/or its delivery pattern. Whole lung-heart transplantation was demonstrated to be inefficient in an LPI patient (Santamaria *et al.*, 2004). Although not implemented for human beings, new experimental approaches where only AM are replaced have been reported in a mouse model of inherited PAP due to knock out of GM-CSF (Suzuki *et al.*, 2014), and efforts for its translation into human treatment are being conducted nowadays (Hetzl *et al.*, 2017). However, if the metabolic environment of LPI is leading the appearance of PAP, these approaches would likely fail too. In conclusion, more thorough studies are needed to establish the mechanisms of pathology of PAP in LPI and define a better treatment.

A clear limitation of the LPI mouse model is the low survival of the mice when not treated with citrulline. However, all the described immune abnormalities but PAP, were perfectly detectable within the first two weeks after the induction of the disease. This allowed us to set up an experimental approach to assess the potential impact of the metabolic derangement over the immune complications. After corroborate that citrulline supplementation in diet ameliorates the metabolic symptoms in *Slc7a7*^{-/-} animals, we established two experimental groups based on the treatment that animals received (low protein diet +/- citrulline).

Concerning HLH, we have shown that *Slc7a7*^{-/-} mice developed the common traits reported for LPI patients, with the exception of the already discussed splenomegaly: hyperferritinemia, anemia and increased hemophagocytosis. Interestingly, anemia and hyperferritinemia undergone a clear amelioration in the group of animals which received citrulline in comparison with those animals who did not. This gave us a first clue about the metabolic impact on the immune complications. We then further corroborated this fact by the generation of the *Slc7a7*^{LysM^{-/-}} mouse model. As these animals have restricted the expression of Cre recombinase to some myeloid populations (macrophages mainly), they are completely free of the metabolic part of the disease. And excitingly, all the altered parameters that were recovered with citrulline supplementation, were basically absent in *Slc7a7*^{LysM^{-/-}} mouse model. This model demonstrated that just by knocking out γ^+ LAT1 in macrophages is not enough to develop HLH related complications.

Additionally, we have characterized what seems to be a new feature of macrophages in LPI: aberrant iron accumulation. Although it is not described as a characteristic feature of LPI, some clues allow us to believe that it can be also occurring in patients as well: 1) increased iron accumulation was observed in the alveolar macrophages of three LPI patients who developed PAP (K Parto *et al.*, 1994), 2) ferritinemia has been shown to likely reflect iron status of macrophages (Cohen *et al.*, 2010), thus the hyperferritinemia reported in LPI patients could be indicating an increase of iron load in macrophages. As a matter of fact, iron accumulation in the different tissues analyzed, together with hyperferritinemia, improved in the group of animals that received citrulline, supporting the idea of a possible relationship between them. In addition, increased iron was not present in the spleen and bone marrow of *Slc7a7*^{LysM^{-/-}} mice, confirming also the necessity of the LPI's metabolic environment for the development of this phenotype.

At the molecular level, transcriptomic analysis of red pulp macrophages (RPM) supported this phenotype. RPM of *Slc7a7*^{-/-} mice showed a down-regulated pathway of porphyrin and chlorophyll metabolism, even though they show increased iron deposits. This is clearly suggesting that these cells are struggling to metabolize iron properly. To analyze more precisely the genes involved in heme metabolism in macrophages, we took advantage of the published transcriptomic analysis reported by Haldar *et al.*, 2014 . In this study, bone marrow derived macrophages (BMDM) differentiated for one week with GM-CSF, were stimulated with heme and transcriptomically analyzed. Despite of this cellular model and freshly isolated RPM are obviously different populations, this is the closest system we have found to compare with our results. By this approach we could corroborate that heme metabolism of *Slc7a7*^{-/-} RPM is

more active than in wild type, finding increased the expression of characteristic markers for this process such as heme oxygenase 1 and SpiC transcription factor. Nevertheless, a clear defect of this pathway is also observed, since other paradigmatic genes such as ferroportin, the main iron exporter of mammalian cells, are not up-regulated as well. We then compared the expression of genes downstream of Bach1-SpiC regulatory axis between *Slc7a7*^{-/-} and wild type RPM, but unfortunately we did not observe a clear pattern that could indicate a general repression of this chord.

The impact of the metabolic environment in this phenotype was further demonstrated by *in vitro* experiments, where *Slc7a7*^{-/-} and wild type BMDM were stimulated with iron under controlled conditions of arginine and ammonia. These experiments showed that LPI metabolic environment impairs the expression of ferroportin, and consequently it is expected a reduction in the export of iron. Since ferroportin expression is recovered when citrulline is supplemented, it is easy to think that the reduction of extracellular arginine is the main contributor to this effect. Concerning the regulation that governs this process, we have also demonstrated *in vitro* that LPI metabolic environment makes BMDM to produce a lesser amount of nitric oxide (NO), and that the addition of citrulline also recovers the NO production. As it has been reported that some iron-related proteins such as ferroportin are regulated through NO via Nrf2 transcription factor (Weiss *et al.*, 1993; Nairz *et al.*, 2013), we checked the expression levels of some of the Nrf2 target genes in the transcriptomic results of *Slc7a7*^{-/-} RPM. Although some of the Nrf2 target genes are tissue specific and we could not obtain a list of the target genes specifically regulated by Nrf2 in murine red pulp macrophages, we checked the expression levels of some genes reported to be regulated by Nrf2 in a cell line of human lymphoblastoid cells (Chorley *et al.*, 2012). Interestingly, a good number of genes that would be expected to be upregulated in a situation of active heme metabolism because of Nrf2 activation, were not so in *Slc7a7*^{-/-} RPM, suggesting that may be an outage in this signaling pathway ([Appendix I](#)).

The microarray study also revealed that *Slc7a7*^{-/-} RPM have a general decrease in pathways related to inflammation. This is interesting, because LPI patients suffer difficulties to respond to infections of common bacteria (Ogier de Baulny, Schiff and Dionisi-Vici, 2012b). It opens a window of opportunity to investigate why these macrophages show this fall in inflammatory pathways; is it a self-autonomous response? Is the LPI's metabolic environment driving this shrinkage? Which specific pathways are down-regulated? And, does it make LPI patients more susceptible to any specific type of bacteria? Further studies will be needed to answer these questions.

Moreover, by analyzing erythroid precursor populations in bone marrow of *Slc7a7*^{-/-} mice, we identified an obvious alteration in the erythropoiesis of these animals. This trait has not been neither specifically described in LPI, however increased number of reticulocytes in blood have been reported in patients (Kurko, 2016; Ouederni *et al.*, 2017), allowing to hypothesize that probably some kind of hematopoietic alterations can also be present in human LPI. Defective erythropoiesis is likely behind anemia of *Slc7a7*^{-/-} mice, but in addition, it is also probably contributing to iron retention by macrophages. The main iron source for RPM comes from the aged or damaged erythrocytes that need to be replaced. When erythrocytes are aged or damaged, show a specific molecular pattern on their membrane that is recognized by macrophages as an “eat me” signal. If defective erythrocytes are being generated in the bone marrow, they are probably also being quickly recognized by the RPM at their pass through the spleen. Indeed, the transcriptomic analysis of RPM revealed an expression pattern of highly active erythrophagocytosis in *Slc7a7*^{-/-} compared to wild type mice. Notably, erythropoiesis improved in the group of *Slc7a7*^{-/-} mice that received citrulline, and *Slc7a7*^{LysM}^{-/-} RPM did not show altered erythropoiesis neither increased expression of erythrophagocytosis markers, pointing again to the metabolic environment of LPI as a critical factor for the development of the hematologic alterations.

In this regard, hypoargininemia is probably playing a key role. When the arginine transporter CAT1 was ablated *in vivo*, those animals developed anemia and died on the day of birth (Perkins *et al.*, 1997). Those animals showed a reduction in the average of circulating RBC, in the total hemoglobin and in the mean corpuscular volume of these cells. In addition, they showed a large increase in the circulating nucleated RBC and a reduced cellularity in the bone marrow, mainly due to the loss of erythroid precursors. Then, the ablation of an arginine importer revealed dramatic consequences for erythropoiesis. Moreover, while CAT2 and CAT3 expression was negligible in different cord blood cell populations, CAT1 was shown to be expressed in all those populations, and to be the main y⁺ transporter in the glycophorin A positive (erythroid precursors) cells (Shima *et al.*, 2006). Thus, CAT1 ablation was basically preventing the entrance of arginine in these cells. Erythroleukemic K652 cells are a cell line committed to erythroid differentiation in presence of appropriate concentration of sodium butyrate. However when these cells were cultured with the appropriate concentration of sodium butyrate but in an arginine-free medium, they hardly differentiated. This effect is specific for arginine, since histidine and lysine (the other substrates of CAT1) resulted in similar differentiation rates than complete medium (Shima *et al.*, 2006). This supports the hypothesis of hypoargininemia as a hard contributor to the hematologic alterations in LPI. Nevertheless,

we could not distinguish *in vivo* between the specific effect of hypoargininemia and the contribution of the rest of metabolic symptoms of LPI such as dyslipidemia, decreased food intake or hyperammonemia. Indeed, patients that only suffer hypoargininemia do not develop the wide variety of complications reported in LPI, then a combination of some different factors is probably driving this specific phenotype. In this regard it will be interesting to treat *Slc7a7*^{-/-} animals with sodium benzoate, an ammonia scavenger which presumably will recover hyperammonemia and its consequent decrease in food intake, but hypoargininemia would remain. Then we could isolate the effect of hypoargininemia from the contribution of hyperammonemia.

Altogether these results are very interesting, because during decades the focus of research in LPI complications have been macrophages. However, by *in vitro* erythrophagocytosis experiments we have demonstrated that irrespectively of the genotype of macrophages, red blood cells from *Slc7a7*^{-/-} mice were more actively engulfed. In addition, as mentioned above, anemia and increased erythrophagocytosis are very likely a direct outcome of a defect in erythropoiesis, which eventually is influenced by hypoargininemia. Even more, hyperferritinemia is likely reflecting the iron status of macrophages, and assuming that iron retention by macrophages is a direct consequence of increased hemophagocytosis plus defective heme metabolism, hypoargininemia is found again as an important contributor to hyperferritinemia. Fascinatingly, all these alterations were recovered in the animals that received citrulline and were basically absent in *Slc7a7*^{LysM}^{-/-} mice. Then, it is already known that the loss of function of γ^+ LAT1 in kidney and intestine causes hypoargininemia, which in turn drives a secondary defect in the urea cycle; however it is also contributing to the hematopoietic abnormalities of LPI.

So far we have demonstrated that the metabolic environment plays a key role in the development of the LPI's complications, and that the ablation of γ^+ LAT1 in macrophages is not enough for the appearance of the reported abnormalities. Then, there is still one open question: is LPI's metabolic environment enough by itself to develop all these alterations? Or is necessary the combination of the metabolic environment together with the loss of function of γ^+ LAT1 in macrophages and hematopoietic stem cells (HSC)? To tackle this question, a bone marrow transplantation experiment is currently ongoing in our laboratory. By this approach, on one hand wild type animals should receive HSC from *Slc7a7*^{-/-} mice, and on the other hand *Slc7a7*^{-/-} animals should receive HSC from wild type mice. Then, first combination would result in a scenario similar to *Slc7a7*^{LysM}^{-/-} mouse model, while the second combination would answer to the mentioned question. So far, results from a preliminary experiment showed that two

Slc7a7^{-/-} animals hosting wild type HSC, lost spleen weight, presented microcytic RBC and it was not clear whether they had increased iron in their spleens. In the next weeks, we will have more precise data from a larger number of animals.

Hopefully, the lessons learned from *Slc7a7*^{-/-} mouse model can be translated to LPI patients. The current opinion in LPI is that although citrulline is necessary for the treatment of the metabolic disease, it may be deleterious for the immune complications. The rationale for this opinion relies on the idea that LPI complications are caused by an aberrant over-activation of macrophages. By losing γ ⁺LAT1 function, macrophages would be accumulating abnormally arginine and generating excessive amounts of nitric oxide. Then citrulline supplementation would be harmful because it would be essentially priming this reaction, exacerbating the over-activation of macrophages. However the results obtained with *Slc7a7*^{-/-} mouse model define a totally opposite situation, where the scarce of extracellular arginine is probably the main responsible of the development of immune and hematologic complications. In this regard, two recent studies with LPI patients seem to support this new concept. The first one is a 9 month old Tunisian LPI case who was referred to hospital with a suspicion of familial HLH (Ouederni *et al.*, 2017). After differential diagnosis and further investigations, the boy was finally diagnosed for LPI and received a specific treatment consisting in protein intake restriction and citrulline supplementation. This particular case allows comparing the progress of HLH in LPI after the implementation of the specific treatment for the metabolic hallmarks. Interestingly, some months after the treatment started, the patient experienced an increase in hemoglobin concentration and in the mean corpuscular volume at the same time than a reduction in reticulocytes count and in ferritinemia (Ouederni *et al.*, 2017). Thus HLH symptoms and metabolic condition improved together, suggesting a relationship between them similar to the one observed in *Slc7a7*^{-/-} mouse model.

The second study is a retrospective analysis of a cohort of LPI patients, from birth to adulthood (Mauhin *et al.*, 2017). Authors calculated the average of plasma arginine among the patients, and those patients with lower argininemia than the average, died earlier. Then, hypoargininemia can be considered as a poor prognosis factor in LPI, and even though LPI patients receive citrulline supplementation, hypoargininemia is still present in most of them. Nowadays, dosage of citrulline supplementation is restricted due to its controversial effect in immune complications, however authors in this article hypothesize that low plasma arginine may be related to cardiovascular complications, argue against potential side effects over the immune complications, and finally, recommend to reassess the dosage.

For the time being, the results presented in this thesis validate *Slc7a7*^{-/-} mouse model as a proper animal model to study human LPI. Regarding the immune and hematopoietic complications, the results obtained are graphically summarized in Figure 56. We have characterized that the metabolic environment plays an essential role in the development of these complications, and after reviewing the literature, we speculate that hypoargininemia may be crucial in this process. In addition, we hypothesize that defective erythropoiesis in *Slc7a7*^{-/-} mice, is likely behind anemia, increased erythrophagocytosis, iron retention and hyperferritinemia in LPI. Altogether, the scenario we propose changes the current paradigm in the LPI's immune and hematologic complications, setting the focus on the metabolic derangement instead than in macrophage dysfunction. Thus, the results presented in this thesis can be considered as a proof of concept and may have a great impact in the future understanding and treatment of LPI.

KIDNEY and INTESTINE

LIVER

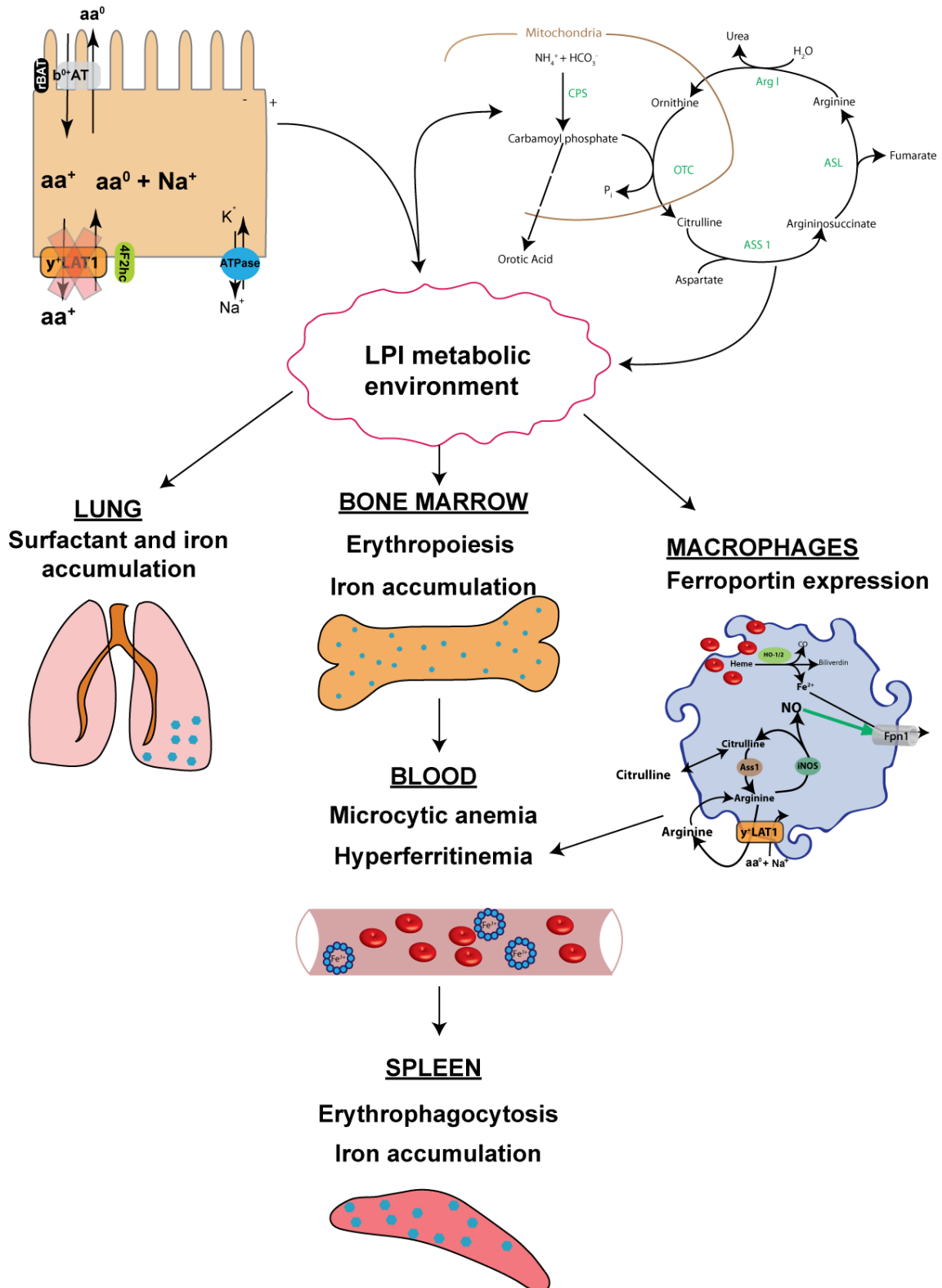


Figure 56. Graphical summary. The loss of function of y^+LAT1 in kidney and intestine, produces a metabolic environment that triggers the immune and hematopoietic complications of LPI.

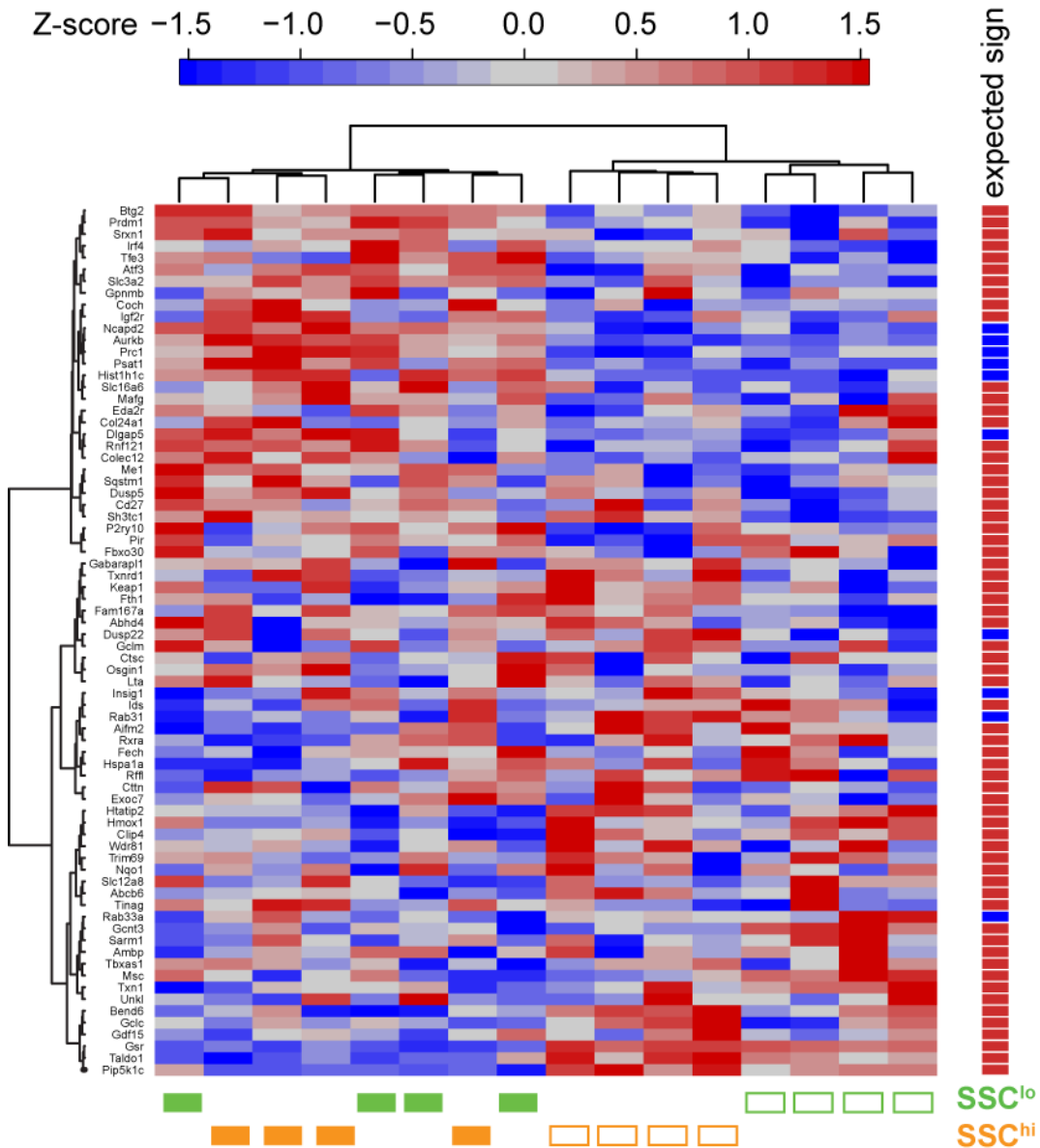
CONCLUSIONS

CONCLUSIONS

1. Despite possible differences between mouse and human, *Slc7a7*^{-/-} animals recapitulate metabolic hallmarks, PAP development, hyperferritinemia, microcytic and hypochromic anemia and increased erythrophagocytosis of human LPI, which makes *Slc7a7*^{-/-} mice the first viable animal model to study this disease.
2. The metabolic environment generated due to the loss of function of γ^+ LAT1 in kidney and intestine, is absolutely essential for the development of immune and hematopoietic complications in LPI. In this regard, hypoargininemia is likely playing a relevant role, although the contribution of the rest of metabolic abnormalities has not been ruled out. Recovery of these LPI complications by citrulline supplementation and the absence of these symptoms in mice with *Slc7a7* ablation restricted to myeloid lineage support this hypothesis.
3. In addition, two new characteristic traits of LPI have been observed in mice: defective erythropoiesis and iron retention by macrophages. Aberrant iron accumulation in alveolar macrophages and increased reticulocytosis have been reported in some LPI cases, which allow to think that these traits can be operating also in human beings. Defective erythropoiesis is likely behind anemia and increased erythrophagocytosis, and consequently contributing to iron retention by macrophages and hyperferritinemia in LPI.

APPENDIX I

APPENDIX I. Heatmap of Nrf2 target genes.



Right bar shows the expected sign in case of Nrf2 activation. Lower boxes shows *Slc7a7*^{-/-} (empty) and wild type (bold) samples clusterization. SSC^{hi} (orange) and SSC^{lo} (green). The list of Nrf2 target genes was taken from Chorley *et al.*, 2012, and are Nrf2 target genes in a cell line of human lymphoblastoid cells.

BIBLIOGRAPHY

- A-Gonzalez, N., Quintana, J. A., García-Silva, S., Mazariegos, M., González de la Aleja, A., Nicolás-Ávila, J. A., Walter, W., Adrover, J. M., Crainiciuc, G., Kuchroo, V. K., Rothlin, C. V., Peinado, H., Castrillo, A., Ricote, M. and Hidalgo, A. (2017) 'Phagocytosis imprints heterogeneity in tissue-resident macrophages.', *The Journal of experimental medicine*, pp. 1–16. doi: 10.1084/jem.20161375.
- Agassandian, M. and Mallampalli, R. K. (2013) 'Surfactant phospholipid metabolism', *Biochimica et Biophysica Acta - Molecular and Cell Biology of Lipids*. Elsevier B.V., 1831(3), pp. 612–625. doi: 10.1016/j.bbalip.2012.09.010.
- Aoki, M., Fukao, T., Fujita, Y., Watanabe, M., Teramoto, T., Kato, Y., Suzuki, Y. and Kondo, N. (2001) 'Lysinuric protein intolerance in siblings : complication of systemic lupus erythematosus in the elder sister A novel mutation causing pyruvate kinase deficiency responsible for a severe neonatal respiratory distress syndrome and jaundice', *European journal of pediatrics*, pp. 522–523.
- Ashburner, M., Ball, C. A., Blake, J. A., Botstein, D., Butler, H., Cherry, J. M., Davis, A. P., Dolinski, K., Dwight, S. S., Eppig, J. T., Harris, M. A., Hill, D. P., Issel-Tarver, L., Kasarskis, A., Lewis, S., Matese, J. C., Richardson, J. E., Ringwald, M., Rubin, G. M. and Sherlock, G. (2000) 'Gene ontology: tool for the unification of biology. The Gene Ontology Consortium.', *Nature genetics*. United States, 25(1), pp. 25–29. doi: 10.1038/75556.
- Barilli, A., Rotoli, B. M., Visigalli, R., Bussolati, O., Gazzola, G. C., Gatti, R., Dionisi-Vici, C., Martinelli, D., Goffredo, B. M., Font-Llitjós, M., Mariani, F., Luisetti, M. and Dall'Asta, V. (2012) 'Impaired phagocytosis in macrophages from patients affected by lysinuric protein intolerance.', *Molecular genetics and metabolism*. Elsevier Inc., 105(4), pp. 585–9. doi: 10.1016/j.ymgme.2012.01.008.
- Barilli, A., Rotoli, B. M., Visigalli, R., Bussolati, O., Gazzola, G. C., Kadija, Z., Rodi, G., Mariani, F., Ruzza, M. L., Luisetti, M. and Dall'Asta, V. (2010) 'In Lysinuric Protein Intolerance system γ +L activity is defective in monocytes and in GM-CSF-differentiated macrophages.', *Orphanet journal of rare diseases*. BioMed Central Ltd, 5(1), p. 32. doi: 10.1186/1750-1172-5-32.
- Becher, B., Schlitzer, A., Chen, J., Mair, F., Sumatoh, H. R., Teng, K. W. W., Low, D., Ruedl, C., Riccardi-Castagnoli, P., Poidinger, M., Greter, M., Ginhoux, F. and Newell, E. W. (2014) 'High-dimensional analysis of the murine myeloid cell system', *Nature Immunology*, 15(12), pp. 1181–1189. doi: 10.1038/ni.3006.
- Behrens, E. M., Canna, S. W., Slade, K., Rao, S., Kreiger, P. A., Paessler, M., Kambayashi, T. and Koretzky, G. A. (2011) 'Repeated TLR9 stimulation results in macrophage activation syndrome-like disease in mice', *Journal of Clinical Investigation*, 9(11). doi: 10.1172/JCI43157DS1.
- Benjamini, Y. and Hochberg, Y. (1995) 'Controlling the False Discovery Rate: A Practical and Powerful Approach to Multiple Testing', *Journal of the Royal Statistical Society*, 57(1), pp. 289–300.
- Boas, F. E., Forman, L. and Beutler, E. (1998) 'Phosphatidylserine exposure and red cell viability in red cell aging and in hemolytic anemia.', *Proceedings of the National Academy of Sciences of the United States of America*, 95(March), pp. 3077–3081. doi: <http://dx.doi.org/10.1073/pnas.95.6.3077>.
- Bogdan, C. (2001) 'Nitric oxide and the immune response.', *Nature immunology*, 2(10), pp. 907–16. doi: 10.1038/ni1001-907.
- Bogdan, C. (2015) 'Nitric oxide synthase in innate and adaptive immunity: An update', *Trends in Immunology*. Elsevier Ltd, 36(3), pp. 161–178. doi: 10.1016/j.it.2015.01.003.

Bolstad, B. M., Collin, F., Brettschneider, J., Simpson, K., Cope, L., Irizarry, R. A. and Speed, T. P. (2005) 'Quality Assessment of Affymetrix GeneChip Data', in Gentleman, R., Carey, V. J., Huber, W., Irizarry, R. A., and Dudoit, S. (eds) *Bioinformatics and Computational Biology Solutions Using R and Bioconductor*. New York, NY: Springer New York, pp. 33–47. doi: 10.1007/0-387-29362-0_3.

Bröer, A., Wagner, C. A., Lang, F. and Bröer, S. (2000) 'The heterodimeric amino acid transporter 4F2hc/y+LAT2 mediates arginine efflux in exchange with glutamine.', *The Biochemical journal*, 349 Pt 3, pp. 787–95. Available at: <http://www.pubmedcentral.nih.gov/articlerender.fcgi?artid=1221206&tool=pmcentrez&rendertype=abstract>.

Broer and Stefan (2008) 'Amino Acid Transport Across Mammalian Intestinal and Renal Epithelia', *Physiological reviews*, 88, pp. 249–286. doi: 10.1152/physrev.00018.2006.

Bronte, V. and Zanovello, P. (2005) 'Regulation of immune responses by L-arginine metabolism.', *Nature reviews. Immunology*, 5(8), pp. 641–54. doi: 10.1038/nri1668.

Burger, P., Hilarius-stokman, P., Korte, D. De, Berg, T. K. Van Den, Bruggen, R. Van and De, W. (2012) 'CD47 functions as a molecular switch for erythrocyte phagocytosis CD47 functions as a molecular switch for erythrocyte phagocytosis', 119(23), pp. 5512–5521. doi: 10.1182/blood-2011-10-386805.

Canna, S. W., Costa-Reis, P., Bernal, W. E., Chu, N., Sullivan, K. E., Paessler, M. E. and Behrens, E. M. (2014) 'Alternative activation of laser-captured murine hemophagocytes', *Arthritis and Rheumatology*, 66(6), pp. 1666–1671. doi: 10.1002/art.38379.

Chen, K., Liu, J., Heck, S., Chasis, J. A., An, X. and Mohandas, N. (2009) 'Resolving the distinct stages in erythroid differentiation based on dynamic changes in membrane protein expression during erythropoiesis', *Proceedings of the National Academy of Sciences*, 106(41), pp. 17413–17418. doi: 10.1073/pnas.0909296106.

Chillarón, J., Estévez, R., Mora, C., Wagner, C. a, Suessbrich, H., Lang, F., Gelpí, J. L., Busch, A. E., Zorzano, A., Palacín, M., Testar, X. and Palaci, M. (1996) 'Membranes and Bioenergetics : Obligatory Amino Acid Exchange via Systems b₀, + -like and y + L-like : a tertiary active transport mechanism for renal reabsorption of cystine and dibasic amino acids', *The Journal of biological chemistry*, 271(30), pp. 17761–17770. doi: 10.1074/jbc.271.30.17761.

Chorley, B. N., Campbell, M. R., Wang, X., Karaca, M., Sambandan, D., Bangura, F., Xue, P., Pi, J., Kleeberger, S. R. and Bell, D. A. (2012) 'Identification of novel NRF2-regulated genes by ChiP-Seq: Influence on retinoid X receptor alpha', *Nucleic Acids Research*, 40(15), pp. 7416–7429. doi: 10.1093/nar/gks409.

Cibrian, D., Saiz, M. L., de la Fuente, H., Sánchez-Díaz, R., Moreno-Gonzalo, O., Jorge, I., Ferrarini, A., Vázquez, J., Punzón, C., Fresno, M., Vicente-Manzanares, M., Daudén, E., Fernández-Salguero, P. M., Martín, P. and Sánchez-Madrid, F. (2016) 'CD69 controls the uptake of L-tryptophan through LAT1-CD98 and AhR-dependent secretion of IL-22 in psoriasis', *Nature Immunology*, 17(8), pp. 985–996. doi: 10.1038/ni.3504.

Clausen, B. E., Burkhardt, C., Reith, W., Renkawitz, R. and Forster, I. (1999) 'Conditional gene targeting in macrophages and granulocytes using LysMcre mice.', *Transgenic research*. Netherlands, 8(4), pp. 265–277.

Closs, E. I., Boissel, J. P., Habermeier, A. and Rotmann, A. (2006) 'Structure and function of cationic amino acid transporters (CATs)', *Journal of Membrane Biology*, 213(2), pp. 67–77. doi: 10.1007/s00232-006-0875-7.

- Cohen, L. A., Gutierrez, L., Weiss, A., Leichtmann-Bardoogo, Y., Zhang, D. L., Crooks, D. R., Sougrat, R., Morgenstern, A., Galy, B., Hentze, M. W., Lazaro, F. J., Rouault, T. A. and Meyron-Holtz, E. G. (2010) 'Serum ferritin is derived primarily from macrophages through a nonclassical secretory pathway', *Blood*, 116(9), pp. 1574–1584. doi: 10.1182/blood-2009-11-253815.
- Davis, T. A., Fiorotto, M. L. and Reeds, P. J. (1993) 'Amino Acid Compositions of Body and Milk Protein Change during the Suckling Period in Rats', *The Journal of Nutrition*, 123(5), pp. 947–956. Available at: <http://jn.nutrition.org/content/123/5/947.short>.
- Deves, R. and Angelo, S. (1996) 'Changes in membrane and surface potential explain the opposite effects of low ionic strength on the two lysine transporters of human erythrocytes', *J Biol Chem*, 271(50), pp. 32034–32039.
- Devés, R., Chavez, P. and Boyd, C. (1992) 'Identification of a new transport system (γ +L) in human erythrocytes that recognizes lysine and leucine with high affinity', *journal of physiology*, 454, pp. 491–501.
- Dirocco, M., Garibotto, G., Rossi, G. A., Caruso, U., Taccone, A., Picco, P., Borrone, C., Pediatría, D., Pneumologia, D., Pediatrica, C., Radiologia, S., Gaslini, I. G. and Gaslini, L. G. (1993) 'Role for haematological pulmonary and renal complications in the long-term prognosis of patients with lysinuric protein intolerance', *European journal of pediatrics*, 152, pp. 437–438.
- Donovan, A., Brownlie, A., Zhou, Y., Shepard, J., Pratt, S. J., Moynihan, J., Paw, B. H., Drejer, A., Barut, B., Zapata, A., Law, T. C., Brugnara, C., Lux, S. E., Pinkus, G. S., Pinkus, J. L., Kingsley, P. D., Palis, J., Fleming, M. D., Andrews, N. C. and Zon, L. I. (2000) 'Positional cloning of zebrafish ferroportin1 identifies a conserved vertebrate iron exporter.', *Nature*, 403(6771), pp. 776–781. doi: 10.1038/35001596.
- Douda, D. N., Farmakovski, N., Dell, S., Grasemann, H. and Palaniyar, N. (2009) 'SP-D counteracts GM-CSF-mediated increase of granuloma formation by alveolar macrophages in lysinuric protein intolerance', 15, pp. 1–15. doi: 10.1186/1750-1172-4-29.
- Dunja, F. A., Hentze, M. W. and Galy, B. (2009) 'Cell-autonomous and systemic context-dependent functions of iron regulatory protein 2 in mammalian iron metabolism', *Blood*, 113(3), pp. 679–687. doi: 10.1182/blood-2008-05-155093.
- Duval, M., Fenneteau, O., Faye, A., Emilie, D., Yotnda, P., Drapier, J., Schlegel, N., Sterkers, G. and Vilmer, E. (1999) 'Intermittent Hemophagocytic Lymphohistiocytosis is a regular feature of lysinuric protein intolerance', *Journal of Pediatrics*, 134(2), pp. 8–11.
- Dzierzak, E. and Philipsen, S. (2013) 'Erythropoiesis : Development and Differentiation', pp. 1–16.
- El-Gayar, S., Thüning-Nahler, H., Pfeilschifter, J., Rölinghoff, M. and Bogdan, C. (2003) 'Translational control of inducible nitric oxide synthase by IL-13 and arginine availability in inflammatory macrophages.', *Journal of immunology (Baltimore, Md. : 1950)*, 171(9), pp. 4561–8. doi: 10.4049/jimmunol.171.9.4561.
- Erez, A., Nagamani, S. C. S., Shchelochkov, O. A., Premkumar, M. H., Campeau, P. M., Chen, Y., Garg, H. K., Li, L., Mian, A., Bertin, T. K., Black, J. O., Zeng, H., Tang, Y., Reddy, A. K., Summar, M., O'Brien, W. E., Harrison, D. G., Mitch, W. E., Marini, J. C., Aschner, J. L., Bryan, N. S. and Lee, B. (2011) 'Requirement of argininosuccinate lyase for systemic nitric oxide production', *Nature Medicine*, 17(12), pp. 1619–1626. doi: 10.1038/nm.2544.
- Espino, M., Font-Llitjós, M., Vilches, C., Salido, E., Prat, E., De Heredia, M. L., Palacín, M., Nunes, V. and Hérault, Y. (2015) 'Digenic inheritance in cystinuria mouse model', *PLoS ONE*,

10(9), pp. 1–12. doi: 10.1371/journal.pone.0137277.

Fan, S., Zhao, Y., Li, X., Du, Y., Wang, J., Song, X., Zhou, F., Chen, H., Chen, G., Mao, Y. and Lan, Q. (2013) 'Genetic variants in SLC7A7 are associated with risk of glioma in a Chinese population', *Exp Biol Med (Maywood)*, 238(9), pp. 1075–1081. doi: 10.1177/1535370213498977.

Franchini, M. (2006) 'Hereditary iron overload: Update on pathophysiology, diagnosis, and treatment', *American Journal of Hematology*, 81(3), pp. 202–209. doi: 10.1002/ajh.20493.

Gautier, L., Cope, L., Bolstad, B. M. and Irizarry, R. A. (2004) 'affy--analysis of Affymetrix GeneChip data at the probe level.', *Bioinformatics (Oxford, England)*. England, 20(3), pp. 307–315. doi: 10.1093/bioinformatics/btg405.

Geissmann, F., Jung, S. and Littman, D. R. (2003) 'Blood monocytes consist of two principal subsets with distinct migratory properties', *Immunity*, 19(1), pp. 71–82. doi: 10.1016/S1074-7613(03)00174-2.

Gentleman, R., Huber, W., Carey, V., Irizarry, R. & Dudoit, S. (2005) *Bioinformatics and Computational Biology Solutions Using R and Bioconductor*. Edited by S. S. Media.

Gentleman, R. C., Carey, V. J., Bates, D. M., Bolstad, B., Dettling, M., Dudoit, S., Ellis, B., Gautier, L., Ge, Y., Gentry, J., Hornik, K., Hothorn, T., Huber, W., Iacus, S., Irizarry, R., Leisch, F., Li, C., Maechler, M., Rossini, A. J., Sawitzki, G., Smith, C., Smyth, G., Tierney, L., Yang, J. Y. H. and Zhang, J. (2004) 'Bioconductor: open software development for computational biology and bioinformatics.', *Genome biology*. England, 5(10), p. R80. doi: 10.1186/gb-2004-5-10-r80.

Gomez Perdiguero, E., Klapproth, K., Schulz, C., Busch, K., Azzoni, E., Crozet, L., Garner, H., Trouillet, C., de Bruijn, M. F., Geissmann, F. and Rodewald, H.-R. (2014) 'Tissue-resident macrophages originate from yolk-sac-derived erythro-myeloid progenitors', *Nature*. Nature Publishing Group, 518(7540), pp. 547–551. doi: 10.1038/nature13989.

Gonzalez-Roca, E., Garcia-Albéniz, X., Rodriguez-Mulero, S., Gomis, R. R., Kornacker, K. and Auer, H. (2010) 'Accurate expression profiling of very small cell populations', *PLoS ONE*, 5(12). doi: 10.1371/journal.pone.0014418.

Gordon, W. C., Gibson, B., Leach, M. T. J. and Robinson, P. (2007) 'Haemophagocytosis by myeloid precursors in lysinuric protein intolerance.', *British journal of haematology*, 138(1), p. 1. doi: 10.1111/j.1365-2141.2007.06594.x.

Goss, V., Hunt, A. N. and Postle, A. D. (2013) 'Regulation of lung surfactant phospholipid synthesis and metabolism', *Biochimica et Biophysica Acta - Molecular and Cell Biology of Lipids*. Elsevier B.V., 1831(2), pp. 448–458. doi: 10.1016/j.bbali.2012.11.009.

Gregory, C. D. (2000) 'CD14-dependent clearance of apoptotic cells: relevance to the immune system.', *Current opinion in immunology*, 12(1), pp. 27–34. Available at: <http://www.ncbi.nlm.nih.gov/pubmed/10679400>.

Grohmann, U. and Bronte, V. (2010) 'Control of immune response by amino acid metabolism', *Immunological reviews*, 236, pp. 243–264. doi: 10.1111/j.1600-065X.2010.00915.x; 10.1111/j.1600-065X.2010.00915.x.

Grom, A. A. and Mellins, E. D. (2010) 'Macrophage activation syndrome: advances towards understanding pathogenesis.', *Current opinion in rheumatology*, 22(5), pp. 561–6. doi: 10.1097/01.bor.0000381996.69261.71.

Guilliams, M., De Kleer, I., Henri, S., Post, S., Vanhoutte, L., De Prijck, S., Deswarte, K., Malissen,

- B., Hammad, H. and Lambrecht, B. N. (2013) 'Alveolar macrophages develop from fetal monocytes that differentiate into long-lived cells in the first week of life via GM-CSF.', *The Journal of experimental medicine*, 210(10), pp. 1977–92. doi: 10.1084/jem.20131199.
- Güzel-Ozantürk, A., Özgül, R. K., Unal, O., Hişmi, B., Aydın, H. İ., Sivri, S., Tokatlı, A., Coşkun, T., Aksöz, E. and Dursun, A. (2013) 'Molecular and clinical evaluation of Turkish patients with lysinuric protein intolerance.', *Gene*, 521(2), pp. 293–5. doi: 10.1016/j.gene.2013.03.033.
- Haldar, M., Kohyama, M., So, A. Y. L., Kc, W., Wu, X., Briseño, C. G., Satpathy, A. T., Kretzer, N. M., Arase, H., Rajasekaran, N. S., Wang, L., Egawa, T., Igarashi, K., Baltimore, D., Murphy, T. L. and Murphy, K. M. (2014) 'Heme-mediated SPI-C induction promotes monocyte differentiation into iron-recycling macrophages', *Cell*, 156(6), pp. 1323–1334. doi: 10.1016/j.cell.2014.01.069.
- Hashimoto, D., Chow, A., Noizat, C., Teo, P., Beasley, M. B., Leboeuf, M., Becker, C. D., See, P., Price, J., Lucas, D., Greter, M., Mortha, A., Boyer, S. W., Forsberg, E. C., Tanaka, M., van Rooijen, N., García-Sastre, A., Stanley, E. R., Ginhoux, F., Frenette, P. S. and Merad, M. (2013) 'Tissue-resident macrophages self-maintain locally throughout adult life with minimal contribution from circulating monocytes', *Immunity*, 38(4), pp. 792–804. doi: 10.1016/j.immuni.2013.04.004.
- Hetzel, M., Suzuki, T., Hashtchin, A. R., Arumugam, P., Carey, B., Schwabbauer, M., Kuhn, A., Meyer, J., Schambach, A., Van Der Loo, J., Moritz, T., Trapnell, B. C. and Lachmann, N. (2017) 'Function and Safety of Lentivirus-Mediated Gene Transfer for *CSF2RA* -Deficiency', *Human Gene Therapy Methods*, X(X), p. hgtb.2017.092. doi: 10.1089/hgtb.2017.092.
- Homer, R., Zheng, T. and Chupp, G. (2002) 'Pulmonary type II cell hypertrophy and pulmonary lipoproteinosis are features of chronic IL-13 exposure', *American journal of physiology. Lung cellular and molecular physiology*, 8023, pp. 52–59. Available at: <http://ajplung.physiology.org/content/283/1/L52.short> (Accessed: 29 October 2014).
- Hume, D. A. (2011) 'Applications of myeloid-specific promoters in transgenic mice support in vivo imaging and functional genomics but do not support the concept of distinct macrophage and dendritic cell lineages or roles in immunity', *Journal of Leukocyte Biology*, 89(4), pp. 525–538. doi: 10.1189/jlb.0810472.
- Hvidberg, V., Maniecki, M. B., Jacobsen, C., Højrup, P., Møller, H. J. and Moestrup, S. K. (2005) 'Identification of the receptor scavenging hemopexin-heme complexes', *Blood*, 106(7), pp. 2572–2579. doi: 10.1182/blood-2005-03-1185.
- Ikegami, M., Whitsett, J. A., Chroneos, Z. C., Ross, G. F., Reed, J. A., Bachurski, C. J., Jobe, A. H., Chro-, Z. C. and Bachur-, C. J. (2000) 'IL-4 increases surfactant and regulates metabolism in vivo', (14), pp. 75–80.
- Iriguchi, S., Kikuchi, N., Kaneko, S., Noguchi, E., Morishima, Y., Matsuyama, M., Yoh, K., Takahashi, S., Nakauchi, H. and Ishii, Y. (2015) 'T-cell - Restricted T-bet overexpression induces aberrant hematopoiesis of myeloid cells and impairs function of macrophages in the lung', *Blood*, 125(2), pp. 370–382. doi: 10.1182/blood-2014-05-575225.
- Irizarry, R. A., Hobbs, B., Collin, F., Beazer-Barclay, Y. D., Antonellis, K. J., Scherf, U. and Speed, T. P. (2003) 'Exploration, normalization, and summaries of high density oligonucleotide array probe level data.', *Biostatistics (Oxford, England)*. England, 4(2), pp. 249–264. doi: 10.1093/biostatistics/4.2.249.
- Janeway, C. A. J., Travers, P., Walport, M. and Schlomchik, M. J. (2001) *Immunobiology: The Immune System in Health and Disease*. 5th editio. New York: Garland Science. doi: NBK27090.

- Jessen, B., Kögl, T., Sepulveda, F. E., de Saint Basile, G., Aichele, P. and Ehl, S. (2013) 'Graded defects in cytotoxicity determine severity of hemophagocytic lymphohistiocytosis in humans and mice.', *Frontiers in immunology*, 4(December), p. 448. doi: 10.3389/fimmu.2013.00448.
- de Jonge, W. J., Dingemans, M. A., de Boer, P. A. J., Lamers, W. H. and Moorman, A. F. M. (1998) 'Arginine-Metabolizing Enzymes in the Developing Rat Small Intestine', *Pediatric Research*. International Pediatrics Research Foundation, Inc., 43, p. 442. Available at: <http://dx.doi.org/10.1203/00006450-199804000-00002>.
- de Jonge, W. J., Hallemeesch, M. M., Kwikkers, K. L., Ruijter, J. M., De Vries, C. G. De, Van Roon, M. A., Meijer, A. J., Marescau, B., De Deyn, P. P., Deutz, N. E. P. and Lamers, W. H. (2002) 'Overexpression of arginase I in enterocytes of transgenic mice elicits a selective arginine deficiency and affects skin, muscle, and lymphoid development', *American Journal of Clinical Nutrition*, 76(1), pp. 128–140.
- de Jonge, W. J., Kwikkers, K. L., te Velde, A. A., van Deventer, S. J. H., Nolte, M. A., Mebius, R. E., Ruijter, J. M., Lamers, M. C. and Lamers, W. H. (2002) 'Arginine deficiency affects early B cell maturation and lymphoid organ development in transgenic mice', *The Journal of Clinical Investigation*, pp. 1539–1548. doi: 10.1172/JCI16143.
- Kamada, Y., Nagaretani, H., Tamura, S., Ohama, T., Maruyama, T., Hiraoka, H., Yamashita, S., Yamada, A., Kiso, S., Inui, Y., Ito, N., Kayanoki, Y., Kawata, S. and Matsuzawa, Y. (2001) 'Vascular endothelial dysfunction resulting from L-arginine deficiency in a patient with lysinuric protein intolerance', 108(5), pp. 663–664. doi: 10.1172/JCI200111260. Introduction.
- Kamoda, T., Nagai, Y., Shigeta, M., Kobayashi, C., Sekijima, T., Shibasaki, M. and Nakamura, N. (1998) 'Lysinuric protein intolerance and systemic lupus erythematosus.', *European journal of pediatrics*, 157(2), pp. 130–1. Available at: <http://www.ncbi.nlm.nih.gov/pubmed/9504787>.
- Kanehisa, M. and Goto, S. (2000) 'KEGG: kyoto encyclopedia of genes and genomes.', *Nucleic acids research*. England, 28(1), pp. 27–30.
- El Kasmi, K. C., Qualls, J. E., Pesce, J. T., Smith, A. M., Thompson, R. W., Henao-Tamayo, M., Basaraba, R. J., König, T., Schleicher, U., Koo, M.-S., Kaplan, G., Fitzgerald, K. A., Tuomanen, E. I., Orme, I. M., Kanneganti, T.-D., Bogdan, C., Wynn, T. A. and Murray, P. J. (2008) 'Toll-like receptor-induced arginase 1 in macrophages thwarts effective immunity against intracellular pathogens.', *Nature immunology*, 9(12), pp. 1399–406. doi: 10.1038/ni.1671.
- Kayanoki, Y., Kawata, S., Yamasaki, E., Kiso, S., Inoue, S., Tamura, S., Taniguchi, N. and Matsuzawa, Y. (1999) 'Reduced nitric oxide production by L-arginine deficiency in lysinuric protein intolerance exacerbates intravascular coagulation.', *Metabolism: clinical and experimental*, 48(9), pp. 1136–40. Available at: <http://www.ncbi.nlm.nih.gov/pubmed/10484053>.
- Keel, S. B., Doty, R. T., Yang, Z., Quigley, J. G., Chen, J., Kaplan, J., Palis, J. and Abkowitz, J. L. (2008) 'Corrected 25 July 2008; see last page', *Science*, 506(July), pp. 825–829.
- Ko, J. M., Shin, C. H., Yang, S. W., Seong, M. W., Park, S. S. and Song, J. (2012) 'The first Korean case of lysinuric protein intolerance: Presented with short stature and increased somnolence', *Journal of Korean Medical Science*, 27(8), pp. 961–964. doi: 10.3346/jkms.2012.27.8.961.
- Kohyama, M., Ise, W., Edelson, B. T., Wilker, P. R., Hildner, K., Mejia, C., Frazier, W. A., Murphy, T. L. and Murphy, K. M. (2008) 'Role for Spi-C in the development of red pulp macrophages and splenic iron homeostasis', *Nature*. Nature Publishing Group, 457(7226), pp. 318–321. doi: 10.1038/nature07472.

- Kohyama, M., Ise, W., Edelson, B. T., Wilker, P. R., Hildner, K., Mejia, C., Frazier, W. a, Murphy, T. L. and Murphy, K. M. (2009) 'Role for Spi-C in the development of red pulp macrophages and splenic iron homeostasis.', *Nature*. Nature Publishing Group, 457(7227), pp. 318–21. doi: 10.1038/nature07472.
- Kristiansen, M., Graversen, J. H., Jacobsen, C., Sonne, O., Hoffman, H. J., Law, S. K. and Moestrup, S. K. (2001) 'Identification of the haemoglobin scavenger receptor.', *Nature*, 409(6817), pp. 198–201. doi: 10.1038/35051594.
- Kurko, J. (2016) *Molecular patterns behind immunological and metabolic alterations in lysinuric protein intolerance*. University of Turku.
- Kurko, J., Vähä-Mäkilä, M., Tringham, M., Tanner, L., Paavainen-Huhtala, S., Saarinen, M., Näntö-Salonen, K., Simell, O., Niinikoski, H. and Mykkänen, J. (2015) 'Dysfunction in macrophage toll-like receptor signaling caused by an inborn error of cationic amino acid transport', *Molecular Immunology*. Elsevier Ltd, 67(2), pp. 416–425. doi: 10.1016/j.molimm.2015.07.006.
- Lee, J., Ryu, H., Ferrante, R. J., Morris, S. M. and Ratan, R. R. (2003) 'Translational control of inducible nitric oxide synthase expression by arginine can explain the arginine paradox.', *Proceedings of the National Academy of Sciences of the United States of America*, 100(8), pp. 4843–8. doi: 10.1073/pnas.0735876100.
- Litman, G. W., Rast, J. P. and Fugmann, S. D. (2010) 'The origins of vertebrate adaptive immunity', *Nature Reviews Immunology*, 10(8), pp. 543–553. doi: 10.1038/nri2807.
- Lois, C., Hong, E. J., Pease, S., Brown, E. J. and Baltimore, D. (2002) 'Germline Transmission and Tissue-Specific Expression of Transgenes Delivered by Lentiviral Vectors', *Science*, 295(5556), p. 868 LP-872. Available at: <http://science.sciencemag.org/content/295/5556/868.abstract>.
- Lukkarinen, M., Näntö-Salonen, K., Ruuskanen, O., Lauteala, T., Säkö, S., Nuutinen, M. and Simell, O. (1998) 'Varicella and varicella immunity in patients with lysinuric protein intolerance.', *Journal of inherited metabolic disease*, 21(2), pp. 103–11. Available at: <http://www.ncbi.nlm.nih.gov/pubmed/9584261>.
- MacLeod, C. (2009) 'Regulation of cationic amino acid transporter (CAT) gene expression', *Biochemical Society Transactions*, 24, pp. 846–852.
- Mannucci, L., Emma, F., Markert, M., Bachmann, C., Boulat, O., Carrozzo, R., Rizzoni, G. and Dionisi-Vici, C. (2005) 'Increased NO production in lysinuric protein intolerance.', *Journal of inherited metabolic disease*, 28(2), pp. 123–9. doi: 10.1007/s10545-005-5954-x.
- Marro, S., Chiabrando, D., Messana, E., Stolte, J., Turco, E., Tolosano, E. and Muckenthaler, M. U. (2010) 'Heme controls ferroportin1 (FPN1) transcription involving Bach1, Nrf2 and a MARE/ARE sequence motif at position -7007 of the FPN1 promoter', *Haematologica*, 95(8), pp. 1261–1268. doi: 10.3324/haematol.2009.020123.
- Mauhin, W., Habarou, F., Gobin, S., Servais, A., Brassier, A., Grisel, C., Roda, C., Pinto, G., Moshous, D., Ghalim, F., Krug, P., Deltour, N., Pontoizeau, C., Dubois, S., Assoun, M., Galmiche, L., Bonnefont, J., Ottolenghi, C., Blic, J. De, Arnoux, J. and Lonlay, P. De (2017) 'Update on Lysinuric Protein Intolerance , a Multi-faceted Disease Retrospective cohort analysis from birth to adulthood', *Orphanet Journal of Rare Diseases*. Orphanet Journal of Rare Diseases, pp. 1–12. doi: 10.1186/s13023-016-0550-8.
- McGaha, T. L., Huang, L., Lemos, H., Metz, R., Mautino, M., Prendergast, G. C. and Mellor, A. L. (2012) 'Amino acid catabolism: a pivotal regulator of innate and adaptive immunity', *Immunol*

Rev., 249(1), pp. 135–157. doi: 10.1111/j.1600-065X.2012.01149.x.Amino.

McGilvray, I. D., Serghides, L., Kapus, A., Rotstein, O. D. and Kain, K. C. (2000) 'Nonopsonic monocyte/macrophage phagocytosis of Plasmodium falciparum-parasitized erythrocytes: a role for CD36 in malarial clearance', *Blood*, 96(9), pp. 3231–3240. Available at: <http://www.bloodjournal.org/cgi/content/abstract/96/9/3231%0Ahttp://www.bloodjournal.org/content/bloodjournal/96/9/3231.full.pdf>.

Miyanishi, M., Tada, K., Koike, M., Uchiyama, Y., Kitamura, T. and Nagata, S. (2007) 'Identification of Tim4 as a phosphatidylserine receptor', *Nature*, 450(7168), pp. 435–439. doi: 10.1038/nature06307.

Mondanelli, G., Bianchi, R., Pallotta, M. T., Orabona, C., Albin, E., Iacono, A., Belladonna, M. L., Vacca, C., Fallarino, F., Macchiarulo, A., Ugel, S., Bronte, V., Gevi, F., Zolla, L., Verhaar, A., Peppelenbosch, M., Mazza, E. M. C., Biccato, S., Laouar, Y., Santambrogio, L., Puccetti, P., Volpi, C. and Grohmann, U. (2017) 'A Relay Pathway between Arginine and Tryptophan Metabolism Confers Immunosuppressive Properties on Dendritic Cells', *Immunity*. Elsevier Inc., 46(2), pp. 233–244. doi: 10.1016/j.immuni.2017.01.005.

Muckenthaler, M. U., Rivella, S., Hentze, M. W. and Galy, B. (2017) 'A Red Carpet for Iron Metabolism', *Cell*. Elsevier Inc., 168(3), pp. 344–361. doi: 10.1016/j.cell.2016.12.034.

Munn, D. H., Sharma, M. D., Baban, B., Harding, H. P., Zhang, Y., Ron, D. and Mellor, A. L. (2005) 'GCM2 kinase in T cells mediates proliferative arrest and anergy induction in response to indoleamine 2,3-dioxygenase', *Immunity*, 22(5), pp. 633–642. doi: 10.1016/j.immuni.2005.03.013.

Murray, P. J. (2015) 'Amino acid auxotrophy as a system of immunological control nodes.', *Nature immunology*, 17(2), pp. 132–9. doi: 10.1038/ni.3323.

Murray, P. J. and Wynn, T. A. (2011) 'Protective and pathogenic functions of macrophage subsets', *Nature Reviews Immunology*, 11(11), pp. 723–737. doi: 10.1038/nri3073.

Mykkänen, J., Torrents, D., Pineda, M., Camps, M., Yoldi, M. E., Horelli-Kuitunen, N., Huoponen, K., Heinonen, M., Oksanen, J., Simell, O., Savontaus, M. L., Zorzano, a, Palacín, M. and Aula, P. (2000) 'Functional analysis of novel mutations in γ (+)-LAT-1 amino acid transporter gene causing lysinuric protein intolerance (LPI).', *Human molecular genetics*, 9(3), pp. 431–438. doi: ddd043 [pii].

Nairz, M., Schleicher, U., Schroll, A., Sonnweber, T., Theurl, I., Ludwiczek, S., Talasz, H., Brandacher, G., Moser, P. L., Muckenthaler, M. U., Fang, F. C., Bogdan, C. and Weiss, G. (2013) 'Nitric oxide-mediated regulation of ferroportin-1 controls macrophage iron homeostasis and immune function in Salmonella infection.', *The Journal of experimental medicine*, 210(5), pp. 855–73. doi: 10.1084/jem.20121946.

Nairz, M., Schroll, A., Demetz, E., Tancevski, I., Theurl, I. and Weiss, G. (2015) "'Ride on the ferrous wheel" - The cycle of iron in macrophages in health and disease', *Immunobiology*. Elsevier GmbH., 220(2), pp. 280–294. doi: 10.1016/j.imbio.2014.09.010.

Nairz, M., Theurl, I., Swirski, F. K. and Weiss, G. (2017) "'Pumping iron"—how macrophages handle iron at the systemic, microenvironmental, and cellular levels', *Pflügers Archiv European Journal of Physiology*. Pflügers Archiv - European Journal of Physiology, 469(3–4), pp. 397–418. doi: 10.1007/s00424-017-1944-8.

Nakamura, A., Ebina-Shibuya, R., Itoh-Nakadai, A., Muto, A., Shima, H., Saigusa, D., Aoki, J., Ebina, M., Nukiwa, T. and Igarashi, K. (2013) 'Transcription repressor Bach2 is required for

- pulmonary surfactant homeostasis and alveolar macrophage function.’, *The Journal of experimental medicine*, 210(11), pp. 2191–204. doi: 10.1084/jem.20130028.
- Nemeth, E., Rivera, S., Gabayan, V., Keller, C., Taudorf, S., Pedersen, B. K. and Ganz, T. (2004) ‘IL-6 mediates hypoferrremia of inflammation by inducing the synthesis of the iron regulatory hormone hepcidin’, 113(9), pp. 1271–1276. doi: 10.1172/JCI200420945.The.
- Noguchi, A., Nakamura, K., Murayama, K., Yamamoto, S., Komatsu, H., Kizu, R., Takayanagi, M., Okuyama, T., Endo, F., Takasago, Y., Shoji, Y. and Takahashi, T. (2016) ‘Clinical and genetic features of lysinuric protein intolerance in Japan’, *Pediatrics International*, 58(10), pp. 979–983. doi: 10.1111/ped.12946.
- Norio, R., Perheentupa, J., Kekomäki, M. and Visakorpi, J. K. (2008) ‘Lysinuric protein intolerance, an autosomal recessive disease’, *Clinical Genetics*. Blackwell Publishing Ltd, 2(4), pp. 214–222. doi: 10.1111/j.1399-0004.1971.tb00280.x.
- Ogier de Baulny, H., Schiff, M. and Dionisi-Vici, C. (2012a) ‘Lysinuric protein intolerance (LPI): A multi organ disease by far more complex than a classic urea cycle disorder’, *Molecular Genetics and Metabolism*. Elsevier Inc., 106(1), pp. 12–17. doi: 10.1016/j.ymgme.2012.02.010.
- Ogier de Baulny, H., Schiff, M. and Dionisi-Vici, C. (2012b) ‘Lysinuric protein intolerance (LPI): a multi organ disease by far more complex than a classic urea cycle disorder.’, *Molecular genetics and metabolism*. Elsevier Inc., 106(1), pp. 12–7. doi: 10.1016/j.ymgme.2012.02.010.
- Oldenborg, P.-A., Zheleznyak, A., Fang, Y.-F., Lagenaur, C. F., Gresham, H. D. and Lindberg, F. P. (2000) ‘Role of CD47 as a Marker of Self on Red Blood Cells’, *Science*, 288(5473), p. 2051 LP-2054. Available at: <http://science.sciencemag.org/content/288/5473/2051.abstract>.
- Ouederni, M., Khaled, M. Ben, Rekaya, S., Fraj, I. Ben and Mellouli, F. (2017) ‘A nine-month-old-boy with Atypical Hemophagocytic Lymphohistiocytosis’, *Mediterranean Journal of Hematology and Infectious Disease*, (9), pp. 1–8. doi: 10.4084/MJHID.2017.057.
- Palacín, M., Bertran, J., Chillarón, J., Estévez, R. and Zorzano, A. (2004) ‘Lysinuric protein intolerance: Mechanisms of pathophysiology’, *Molecular Genetics and Metabolism*, 81(SUPPL.). doi: 10.1016/j.ymgme.2003.11.015.
- Palacín, M., Borsani, G. and Sebastio, G. (2001) ‘The molecular bases of cystinuria and lysinuric protein intolerance.’, *Current opinion in genetics & development*, 11(3), pp. 328–35. Available at: <http://www.ncbi.nlm.nih.gov/pubmed/11377971>.
- Park, S.-Y., Jung, M.-Y., Kim, H.-J., Lee, S.-J., Kim, S.-Y., Lee, B.-H., Kwon, T.-H., Park, R.-W. and Kim, I.-S. (2008) ‘Rapid cell corpse clearance by stabilin-2, a membrane phosphatidylserine receptor’, *Cell Death and Differentiation*, 15(1), pp. 192–201. doi: 10.1038/sj.cdd.4402242.
- Park, S.-Y., Jung, M.-Y., Lee, S.-J., Kang, K.-B., Gratchev, A., Riabov, V., Kzhyshkowska, J. and Kim, I.-S. (2009) ‘Stabilin-1 mediates phosphatidylserine-dependent clearance of cell corpses in alternatively activated macrophages.’, *Journal of cell science*, 122, pp. 3365–3373. doi: 10.1242/jcs.049569.
- Parto, K., Kallajoki, M., Aho, H. and Simell, O. (1994) ‘Pulmonary Alveolar Proteinosis and Glomerulonephritis in Lysinuric Protein Intolerance: case reports and autopsy findings of four pediatric patients’, *Human Pathology*, 25(4), pp. 400–407.
- Parto, K., Mäki, J., Pelliniemi, L. and Simell, O. (1994) ‘Abnormal Pulmonary Macrophages in Lysinuric Protein Intolerance’, *Arch Pathol Lab Med*, (118), pp. 536–541.
- Parto, K., Svedström, E., Majurin, M. L., Härkönen, R. and Simell, O. (1993) ‘Pulmonary

manifestations in lysinuric protein intolerance .', *Chest*, 104, pp. 1176–1182.

Patel, B. N., Dunn, R. J., Jeong, S. Y., Zhu, Q., Julien, J.-P. and David, S. (2002) 'Ceruloplasmin regulates iron levels in the CNS and prevents free radical injury.', *The Journal of neuroscience*, 22(15), pp. 6578–6586. doi: 20026652.

Perdiguerro, E. G. and Geissmann, F. (2015) 'The development and maintenance of resident macrophages', *Nature Immunology*. Nature Publishing Group, 17(1), pp. 2–8. doi: 10.1038/ni.3341.

Perheentupa, J. and Visakorpi, J. K. (1965) 'Protein intolerance with deficient transport of dibasic amino acids', *The Lancet*, 286(7417), pp. 813–816. doi: 10.1016/S0140-6736(65)92446-3.

Perkins, C. P., Mar, V., Shutter, J. R., Castillo, J. Del, Danilenko, D. M., Medlock, E. S., Ponting, I. L., Graham, M., Stark, K. L., Zuo, Y., Cunningham, J. M. and Bosselman, R. A. (1997) 'Anemia and perinatal death result from loss of the murine ecotropic retrovirus receptor mCAT-1', *Genes and Development*, 11(7), pp. 914–925. doi: 10.1101/gad.11.7.914.

Ploner, A. (2015) 'Heatplus: Heatmaps with row and/or column covariates and colored clusters. R package version 2.18.0'.

Qualls, J. E., Subramanian, C., Rafi, W., Smith, A. M., Balouzian, L., Defreitas, A. A., Shirey, K. A., Reutterer, B., Kernbauer, E., Stockinger, S., Decker, T., Miyairi, I., Vogel, S. N., Salgame, P., Rock, C. O. and Murray, P. J. (2012) 'Sustained generation of nitric oxide and control of mycobacterial infection requires argininosuccinate synthase 1', *Cell Host and Microbe*. Elsevier Inc., 12(3), pp. 313–323. doi: 10.1016/j.chom.2012.07.012.

R Core Team (2016) *R: A language and environment for statistical computing*, R Foundation for Statistical Computing, Vienna, Austria. Available at: <https://www.r-project.org/>.

Reig, N., Chillarón, J., Bartoccioni, P., Fernández, E., Bendahan, A., Zorzano, A., Kanner, B., Palacín, M. and Bertran, J. (2002) 'The light subunit of system bo,+ is fully functional in the absence of the heavy subunit', *EMBO Journal*, 21(18), pp. 4906–4914. doi: 10.1093/emboj/cdf500.

Richir, M. C., Siroen, M. P. C., van Elburg, R. M., Fetter, W. P. F., Quik, F., Nijveldt, R. J., Heij, H. A., Smit, B. J., Teerlink, T. and van Leeuwen, P. A. M. (2007) 'Low plasma concentrations of arginine and asymmetric dimethylarginine in premature infants with necrotizing enterocolitis', *British Journal of Nutrition*. 2007/05/01. Cambridge University Press, 97(5), pp. 906–911. doi: DOI: 10.1017/S0007114507669268.

Ritchie, M. E., Phipson, B., Wu, D., Hu, Y., Law, C. W., Shi, W. and Smyth, G. K. (2015) 'limma powers differential expression analyses for RNA-sequencing and microarray studies.', *Nucleic acids research*. England, 43(7), p. e47. doi: 10.1093/nar/gkv007.

Rotoli, B. M., Bussolati, O., Sala, R., Barilli, A., Talarico, E., Gazzola, G. C. and Dall'Asta, V. (2004) 'INF gamma stimulates arginine transport through system y+L in human monocytes', *FEBS Letters*, 571(1–3), pp. 177–181. doi: 10.1016/j.febslet.2004.06.086.

Rotoli, B. M., Dall'asta, V., Barilli, A., D'Ippolito, R., Tipa, A., Olivieri, D., Gazzola, G. C. and Bussolati, O. (2007) 'Alveolar macrophages from normal subjects lack the NOS-related system y+ for arginine transport.', *American journal of respiratory cell and molecular biology*, 37(1), pp. 105–12. doi: 10.1165/rcmb.2006-0262OC.

Santamaria, F., Brancaccio, G., Parenti, G., Francalanci, P., Squitieri, C., Sebastio, G., Dionisi-Vici, C., D'argenio, P., Andria, G. and Parisi, F. (2004) 'Recurrent fatal pulmonary alveolar

proteinosis after heart-lung transplantation in a child with lysinuric protein intolerance.', *The Journal of pediatrics*, 145(2), pp. 268–72. doi: 10.1016/j.jpeds.2004.04.047.

Santamaria, F., Parenti, G., Guidi, G., Rotondo, A., Grillo, G., Larocca, M. R., Celentano, L., Strisciuglio, P., Sebastio, G. and Andria, G. (1996) 'Early detection of lung involvement in lysinuric protein intolerance: Role of high-resolution computed tomography and radioisotopic methods', *American Journal of Respiratory and Critical Care Medicine*, 153(2), pp. 731–735. doi: 10.1164/ajrccm.153.2.8564125.

Sebastiani, G., Wilkinson, N. and Pantopoulos, K. (2016) 'Pharmacological Targeting of the Hpcidin / Ferroportin Axis', 7(June), pp. 1–11. doi: 10.3389/fphar.2016.00160.

Sebastio, G., Sperandeo, M. P. and Andria, G. (2011) 'Lysinuric protein intolerance: reviewing concepts on a multisystem disease.', *American journal of medical genetics. Part C, Seminars in medical genetics*, 157C(1), pp. 54–62. doi: 10.1002/ajmg.c.30287.

Shima, Y., Maeda, T., Aizawa, S., Tsuboi, I., Kobayashi, D., Kato, R. and Tamai, I. (2006) 'L - arginine import via cationic amino acid transporter CAT1 is essential for both differentiation and proliferation of erythrocytes', *Cell Differentiation*, 107(4), pp. 1352–1356. doi: 10.1182/blood-2005-08-3166.Reprints.

Sin, Y. Y., Ballantyne, L. L., Mukherjee, K., St Amand, T., Kyriakopoulou, L., Schulze, A. and Funk, C. D. (2013) 'Inducible arginase 1 deficiency in mice leads to hyperargininemia and altered amino acid metabolism', *PLoS ONE*, 8(11). doi: 10.1371/journal.pone.0080001.

Sinclair, L. V., Rolf, J., Emslie, E., Shi, Y.-B., Taylor, P. M. and Cantrell, D. A. (2013) 'Control of amino-acid transport by antigen receptors coordinates the metabolic reprogramming essential for T cell differentiation', *Nature Immunology*, 14(5), pp. 500–508. doi: 10.1038/ni.2556.

Smyth, G. K. (2004) 'Linear models and empirical bayes methods for assessing differential expression in microarray experiments.', *Statistical applications in genetics and molecular biology*. Germany, 3, p. Article3. doi: 10.2202/1544-6115.1027.

Smyth, G. K., Michaud, J. and Scott, H. S. (2005) 'Use of within-array replicate spots for assessing differential expression in microarray experiments.', *Bioinformatics (Oxford, England)*. England, 21(9), pp. 2067–2075. doi: 10.1093/bioinformatics/bti270.

Soares, M. P. and Weiss, G. (2015) 'The Iron age of host-microbe interactions', *EMBO reports*, 16(11), pp. 1482–1500. doi: 10.15252/embr.201540558.

Sperandeo, M., Annunziata, P., Bozzato, A., Piccolo, P., Maiuri, L., D'Armiento, M., Ballabio, A., Corso, G., Androa, G., Borsani, G. and Sebastio, G. (2007) 'Slc7a7 disruption causes fetal growth retardation by downregulating Igf1 in the mouse model of lysinuric protein intolerance', *Am J Physiol Cell Physiol*, 293, pp. 191–198. doi: 10.1152/ajpcell.00583.2006.

Sperandeo, M. P., Borsani, G., Incerti, B., Zollo, M., Rossi, E., Zuffardi, O., Castaldo, P., Tagliatela, M., Andria, G. and Sebastio, G. (1998) 'The gene encoding a cationic amino acid transporter (SLC7A4) maps to the region deleted in the velocardiofacial syndrome.', *Genomics*, 49(2), pp. 230–236. doi: 10.1006/geno.1998.5252.

Stanley, E., Lieschke, G. J., Grail, D., Metcalf, D., Hodgson, G., Gall, J. a, Maher, D. W., Cebon, J., Sinickas, V. and Dunn, a R. (1994) 'Granulocyte/macrophage colony-stimulating factor-deficient mice show no major perturbation of hematopoiesis but develop a characteristic pulmonary pathology.', *Proceedings of the National Academy of Sciences of the United States of America*, 91(12), pp. 5592–5596.

Strologo, L. D., Pras, E., Pontesilli, C., Beccia, E., Ricci-Barbini, V., de Sanctis, L., Ponzone, A.,

- Gallucci, M., Bisceglia, L., L., Z., Jimenez-Vidal, M., Font, M., Zorzano, A., Rousaud, F., Nunes, V., Gasparini, P., Palacín, M. and Rizzoni, G. (2002) 'Comparison between SLC3A1 and SLC7A9 Cystinuria Patients and Carriers: A Need for a New Classification', *Journal of the American Society of Nephrology*, 13(10), pp. 2547–2553. doi: 10.1097/01.ASN.0000029586.17680.E5.
- Subramanian, A., Tamayo, P., Mootha, V. K., Mukherjee, S., Ebert, B. L., Gillette, M. A., Paulovich, A., Pomeroy, S. L., Golub, T. R., Lander, E. S. and Mesirov, J. P. (2005) 'Gene set enrichment analysis: a knowledge-based approach for interpreting genome-wide expression profiles.', *Proceedings of the National Academy of Sciences of the United States of America*. United States, 102(43), pp. 15545–15550. doi: 10.1073/pnas.0506580102.
- Suzuki, T., Arumugam, P., Sakagami, T., Lachmann, N., Chalk, C., Sallese, A., Abe, S., Trapnell, C., Carey, B., Moritz, T., Malik, P., Lutzko, C., Wood, R. E. and Trapnell, B. C. (2014) 'Pulmonary macrophage transplantation therapy', *Nature*. Nature Publishing Group, 514(7523), pp. 450–454. doi: 10.1038/nature13807.
- Tanner, L. M., Kurko, J., Tringham, M., Aho, H., Mykkänen, J., Nääntö-Salonen, K., Niinikoski, H. and Lukkarinen, H. (2017) 'Inhaled Sargramostim Induces Resolution of Pulmonary Alveolar Proteinosis in Lysinuric Protein Intolerance', in Morava, E., Baumgartner, M., Patterson, M., Rahman, S., Zschocke, J., and Peters, V. (eds) *JIMD Reports, Volume 34*. Berlin, Heidelberg: Springer Berlin Heidelberg, pp. 97–104. doi: 10.1007/978-3-662-53115-1_15.
- Theurl, I., Hilgendorf, I., Nairz, M., Tymoszyk, P., Haschka, D., Asshoff, M., He, S., Gerhardt, L. M. S., Holderried, T. A. W., Seifert, M., Sopper, S., Fenn, A. M., Anzai, A., Rattik, S., McAlpine, C., Theurl, M., Wieghofer, P., Iwamoto, Y., Weber, G. F., Harder, N. K., Chousterman, B. G., Arvedson, T. L., McKee, M., Wang, F., Lutz, O. M. D., Rezoagli, E., Babitt, J. L., Berra, L., Prinz, M., Nahrendorf, M., Weiss, G., Weissleder, R., Lin, H. Y. and Swirski, F. K. (2016) 'On-demand erythrocyte disposal and iron recycling requires transient macrophages in the liver', *Nature Medicine*. Nature Publishing Group, 22(8), pp. 945–951. doi: 10.1038/nm.4146.
- Theurl, I., Theurl, M., Seifert, M., Mair, S., Nairz, M., Rumpold, H., Zoller, H., Bellmann-Weiler, R., Niederegger, H., Talasz, H. and Weiss, G. (2008) 'Autocrine formation of hepcidin induces iron retention in human monocytes', *Blood*, 111(4), pp. 2392–2399. doi: 10.1182/blood-2007-05-090019.
- Thompson, R. W., Pesce, J. T., Ramalingam, T., Wilson, M. S., White, S., Cheever, A. W., Ricklefs, S. M., Porcella, S. F., Li, L., Ellies, L. G. and Wynn, T. A. (2008) 'Cationic amino acid transporter-2 regulates immunity by modulating arginase activity', *PLoS Pathogens*, 4(3). doi: 10.1371/journal.ppat.1000023.
- Torrents, D., Estévez, R., Pineda, M., Fernández, E., Lloberas, J., Shi, Y., Zorzano, A. and Palacín, M. (1998) 'Identification and Characterization of a Membrane Protein (γ +L Amino Acid Transporter-1) That Associates with 4F2hc to Encode the Amino Acid Transport Activity γ +L', *The Journal of biological chemistry*, 273(49), pp. 32437–32445.
- Torrents, D., Mykkänen, J., Pineda, M., Feliubadaló, L., Estévez, R., de Cid, R., Sanjurjo, P., Zorzano, a, Nunes, V., Huoponen, K., Reinikainen, a, Simell, O., Savontaus, M. L., Aula, P. and Palacín, M. (1999) 'Identification of SLC7A7, encoding γ +LAT-1, as the lysinuric protein intolerance gene.', *Nature genetics*, 21(3), pp. 293–6. doi: 10.1038/6809.
- Trapnell, B., Whitsett, J. and Koh, N. (2003) 'Pulmonary alveolar proteinosis', *New England Journal of Medicine*, 349(26), pp. 2527–2539. Available at: <http://www.nejm.org/doi/full/10.1056/NEJM195806052582301> (Accessed: 8 October 2014).
- Valimahamed-Mitha, S., Berteloot, L., Ducoin, H., Ottolenghi, C., de Lonlay, P. and de Blic, J. (2015) 'Lung involvement in children with lysinuric protein intolerance', *Journal of Inherited*

Metabolic Disease, 38(2), pp. 257–263. doi: 10.1007/s10545-014-9777-5.

Weiss, G., Goossen, B., Doppler, W., Fuchs, D., Pantopoulos, K., Werner-Felmayer, G., Wachter, H. and Hentze, M. W. (1993) 'Translational regulation via iron-responsive elements by the nitric oxide/NO-synthase pathway.', *The EMBO journal*, 12(9), pp. 3651–3657.

Weiss, G., Werner-Felmayer, G., Werner, E. R., Grünewald, K., Wachter, H. and Hentze, M. W. (1994) 'Iron regulates nitric oxide synthase activity by controlling nuclear transcription.', *The Journal of experimental medicine*, 180(3), pp. 969–976. doi: 10.1084/jem.180.3.969.

Wilkinson, N. and Pantopoulos, K. (2014) 'The IRP/IRE system in vivo: Insights from mouse models', *Frontiers in Pharmacology*, 5 JUL(July), pp. 1–15. doi: 10.3389/fphar.2014.00176.

Yeramian, A., Martin, L., Serrat, N., Arpa, L., Soler, C., Bertran, J., McLeod, C., Palacin, M., Modolell, M., Lloberas, J. and Celada, A. (2006) 'Arginine Transport via Cationic Amino Acid Transporter 2 Plays a Critical Regulatory Role in Classical or Alternative Activation of Macrophages', *The Journal of Immunology*, 176(10), pp. 5918–5924. doi: 10.4049/jimmunol.176.10.5918.

Yin, J., Ren, W., Duan, J., Wu, L., Chen, S., Li, T., Yin, Y. and Wu, G. (2014) 'Dietary arginine supplementation enhances intestinal expression of SLC7A7 and SLC7A1 and ameliorates growth depression in mycotoxin-challenged pigs', *Amino Acids*, 46(4), pp. 883–892. doi: 10.1007/s00726-013-1643-5.

Yona, S., Kim, K. W., Wolf, Y., Mildner, A., Varol, D., Breker, M., Strauss-Ayali, D., Viukov, S., Williams, M., Misharin, A., Hume, D. A., Perlman, H., Malissen, B., Zelzer, E. and Jung, S. (2013) 'Fate Mapping Reveals Origins and Dynamics of Monocytes and Tissue Macrophages under Homeostasis', *Immunity*. Elsevier, 38(1), pp. 79–91. doi: 10.1016/j.immuni.2012.12.001.

Yoshida, Y., Machigashira, K., Suehara, M., Arimura, H., Moritoyo, T., Nagamatsu, K. and Osame, M. (1995) 'Immunological abnormality in patients with lysinuric protein intolerance.', *Journal of the neurological sciences*, 134(1–2), pp. 178–82.

Zhang, A.-S. and Enns, C. A. (2009) 'Molecular mechanisms of normal iron homeostasis.', *Hematology. American Society of Hematology. Education Program*, 2009(1), pp. 207–14. doi: 10.1182/asheducation-2009.1.207.

Zhang, G. and Cao, L. (2017) 'New mutations in the *SLC7A7* gene of two chinese sisters with lysinuric protein intolerance', *Pediatric Pulmonology*, 52(11), pp. E94–E96. doi: 10.1002/ppul.23760.